SCIENTIFIC CULTURE
www.sci-cult.com

SCIENTIFIC CULTURE, Vol. 10, No. 1, (2024), pp. 1-58
Open Access. Online & Print

DOI: 10.5281/zenodo.8297692

CAN COMPLEXITY MEASURES WITH HIERARCHICAL CLUSTER ANALYSIS IDENTIFY OVERPAINTED ARTWORK?

Ion Andronache [1], Ioulia Papageorgiou[2], Athena Alexopoulou[3], Dimitrios Makris[3], Maria Bratitsi[4], Helmut Ahammer[5], Marko Radulovic[6], Ioannis Liritzis[7-10*]

[1]Research Center for Integrated Analysis and Territorial Management – CAIMT, Faculty of Geography, University of Bucharest, 4-12 Regina Elisabeta Avenue, Bucharest, 3rd district, 030018, Romania
[2]Department of Statistics Athens University of Economics and Business, Patission 76, 104 34 Athens, Greece
[3]Dept. of Conservation of Antiquities and Works of Art, Faculty of Applied Arts and Culture, ARTICON: Laboratory of Conservation – Promotion of Visual Arts, Books and Archival Material, University of West Attica, 12, Aghiou Spiridonos str., 12210 Egaleo, Athens, Greece
[4]University of the Aegean, Dept. of Mediterranean Studies, 1 Demokratias Str., Rhodes, Greece
[5]GSRC, Division of Biophysics, Medical University of Graz, 8010 Graz, Austria
[6]Department of Experimental Oncology, Institute of Oncology and Radiology of Serbia, Pasterova 14, 11000 Belgrade, Serbia
[7]Laboratory of Yellow River Cultural Heritage, Key Research Institute of Yellow River Civilization and Sustainable Development & Collaborative Innovation Center on Yellow River Civilization, Henan University, Kaifeng 475001, Minglun Road 85, China
[8]European Academy of Sciences & Arts, St. Peter-Bezirk 10, A-5020 Salzburg, Austria
[9]Edinburgh University, School of History, Classics and Archaeology, College of Arts, Humanities & Social Sciences, Dept of Archaeology, Edinburgh EH8 9AG, Scotland
[10]Rhodes University, Dept of Physics & Electronics, Makhanda (Grahamstown) 6140, Eastern Cape, South Africa

Received: 15/12/2022
Accepted: 10/06/2023

Corresponding author: Ioannis Liritzis (liritzis@henu.edu.cn)

ABSTRACT

Exploring the attribution of sub-painted layers in overpainted artworks created with various pigments on canvas/wood has received limited attention. Previously this problem of underpainting inhered limitations. This study addresses the palimpsest-like stratigraphy of such artworks using an innovative and validated statistical approach. To replicate the process, painted and overpainted panels were meticulously constructed following historical recipes for preparation and pigment selection. Spectral data in the near-infrared (NIR) range (400-1000nm) were captured using a multispectral NIR camera, employing reflected light under normal illumination conditions. A total of 45 pigments, representing 45 colors, were employed in the creation of three sets of overpainted layers: upper Egyptian blue, cadmium red, and cadmium yellow. Several parameters influencing the experimental setup were considered, including capturing conditions and imaged areas. A normalization procedure was applied to ensure consistent capturing conditions across all images. The standardized set of spectral images was subjected to appropriate agglomerative hierarchical clustering methods (Average Linkage, Complete Linkage, Ward Linkage, and Ward D2 Linkage), as well as principal component analysis (PCA) with accompanying statistical tests to validate clustering (Silhouette, Box plots, K-means, Wilks). Additionally, complex and entropy measures were employed. By integrating traditional statistical multivariate methods with modern complexity measures, consistent interpretation of the data was achieved. PCA combined with clustering methods enabled referencing of spectral data with the Mahalanobis connection distance, highlighting clusters directly associated with differences in intensity along the NIR range for each panel's segmented spectral cubes. It is non-destructive method and offers a unique data base for future research. The novelty of this study is therefore utilizing the experimental database and applying innovative corroborated mathematical techniques. This approach facilitated the identification of overpainted panels based on their similar NIR spectral characteristics and successfully identified an unknown painted panel within this initial three-color database with highly satisfactory results.

KEYWORDS: near infrared, spectroscopy, algorithm, multispectral, statistical, imaging, hyperspectral, camera, pigments

1. INTRODUCTION

The spectral analysis of painted artworks, utilizing techniques such as multispectral and hyperspectral imaging, has proven valuable in the field of conservation. These non-invasive methods have yielded promising results in areas such as painting analysis, material characterization, and digital documentation for the study and preservation of artworks (Casini et al., 1999; Janssens and Van Grieken, 2004; Rosi et al., 2010; Daniel et al., 2017; Janssens et al., 2017; Rampazzi et al., 2017; Alexopoulou et al., 2019; Bratitsi et al., 2019; Afifi et al., 2020; Albini et al., 2020; Ali et al., 2020; Ashkenazi et al., 2021). Multispectral infrared imaging, a simple and non-invasive technique widely employed in Cultural Heritage analysis, has been extensively studied (Van Asperen de Boer, 1975; Balas et al., 2003; Cristoforetti et al., 2006; Fischer and Kakoulli, 2006; Vilaseca et al., 2006).

Polyspectral cameras, including both multispectral and hyperspectral variants, are commonly used in research, industrial applications, artificial vision, and online multispectral and hyperspectral imaging. Although relatively new to the field of conservation, these methods have already demonstrated promising results in painting analysis, material characterization, and digital documentation (Fischer and Kakoulli, 2006; Cosentino, 2016; Favero et al., 2017; MacDonald et al., 2017; Picollo et al., 2020).

Multispectral cameras capture image data at specific frequencies across the electromagnetic spectrum, utilizing filters or instruments sensitive to specific wavelengths, including those beyond the visible spectrum such as infrared. Spectral imaging enables extraction of additional information that the human eye cannot perceive.

The literature refers to pigments as soluble dye substances or insoluble grains dispersed in powder form within the binding material. Natural dyes can be categorized into three groups: natural pigments from plants, animals, and minerals. (Pigments used in this study are listed in **Table S0 Supplementary**).

Pigments are classified based on their source (organic or inorganic) and their chemical composition and physical properties, including solubility (Degano et al., 2009). Ancient pioneers such as Aristotle, Theophrastus, Claudius Ptolemy, and Pliny the Elder have laid the foundation and recorded past knowledge on pigments, including color mixing techniques (Caley and Richards, 1956; Loeb and Henderson, 1970; Healy, 1999; Adamson, 2006; Katsaros et al., 2009, 2010).

Techniques used for overpainted works of art are being mention (Synchrotron Radiation Based XRF and macro-XRF and Confocal 3D Micro-XRF, IR. See: (Janssens et al., 2017; Bratitsi et al., 2019; Evans et al., 2023). In fact, in irradiated art surfaces the wavelength range is divided into areas where one can see the surface of a work of art or penetrate in depth revealing the hidden secrets. Wavelengths for deeper areas are x-rays and infrared radiation because they penetrate the varnish. In the case of IR the ranges include the areas from deep red at 760nm to the limits of microwaves but only a restrict region of it ranging from 760nm to 2500nm can be used in the art diagnosis. IR is an invisible radiation, characterized by its great penetration ability. Of course, all the above case studies involve transferring the paintings to the synchrotron sources laboratories and that is not always achievable. The limitation of Macro-XRF is that the in mobile detectors the fluorescence radiation is of low energy and is absorbed by the dye. However, all of these scanners required several seconds of space per pixel, limiting their application to very small detail.

Optical Coherence Tomography uses near infrared radiation of 700-1500nm allowing a 3D imaging of layers (Targowski and Iwanicka, 2012) provided information about the thickness of the varnish of an image and signs of a forgery signature in the Portrait. Until recently the only techniques that could examine underlayers were X-Rays and IR, but with many difficulties such as in thicker layers or carbon-based pigments, although nowadays are being used in many conservation studios allowing faster and detailed acquisition.

The exploitation of the fluorescence radiation that emitted by the painting during X-Ray irradiation instead of the absorption was of great importance, as it allows a contrast not being achieved by any other technique. Confocal XRF is the only so far in situ technique being able to investigate under layered paintings.

X-ray does not provide elemental analysis, nor does interpret underlying paint layers in cases of heavy metals painting such as lead or mercury, or in cases of overlapped by thicker layers with highly absorbent elements such as zinc. Very important is the ground layer on which the painting surface is deposited, as its components may act prohibitively for the display of the color elements (such as zinc ground layers) (Alfeld et al., 2011; Noble et al., 2012; Loeff et al., 2012; Alfeld et al., 2013).

However, Falco (Falco, 2009) described a process of modifying a commercial digital camera 8 Mpixel in IR, tested in a work by Lorenzo Lotto, but he has received many criticisms (Stork and Kossolapov, 2011). For observing underlayers, a useful tool is Short Wave IR, i.e. at 1000-2400 nm. Van Asperen de Boer (Van Asperen de Boer, 1975; Van Asperen De Boer, 1968) invented IR-reflectography, and investigated Early Netherlandish Painting.

At any rate, all the case studies refer to underdrawings and not to underpainted layers, and all these methods are non-portable, difficult to use and at an early stage.

With the merging of traditional machine vision and advanced measurement technologies, complex metrology and imaging applications now require a higher number of spectral channels and application-specific spectral filtering options to achieve high inspection throughputs. In this context, reliable and high-fidelity color and multispectral imaging play crucial roles in industrial quality control.

Given the tolerances in creating a painted panel/icon and normalizing the obtained images using the Mu.S.I.S IR camera, the double layered colored pigments data were analyzed using statistical and complexity measures methods.

The present study is a novel concept devised as methodology and sample preparation and aims to determine if a random image/icon has overlays and, if so, identify the underlying color by fitting its spectral cube into the cluster groups formed from the analysis of samples in a simulated database of overpainted panels. For this purpose, three sets were created, one with upper Egyptian blue and the other two with cadmium red and cadmium yellow as the overlying colors, each set comprising 45 underlying colors. Additionally, a set representing the preparation stage was included. Three test measurements were conducted, with spectral values having a ±3% distance from specific measurements.

Statistical processing coupled with complexity measures is the most appropriate methodological manner for studying and analyzing large amounts of data in a scientific and reliable manner. To ensure the correct collection and transformation of data, it is essential to formulate clear and specific research questions and objectives, considering the type of data and corresponding methodologies.

This project introduces the original concept of combining statistical and fractal tools and painstaking prepared overpainted panels following strictly as close as possible traditional painting techniques to classify overpainting icons. The pigments used in this study are those commonly found in Byzantine and post-Byzantine portable icons created using the egg tempera technique, as identified through analysis and bibliographic sources (Hetherington, 1989; Harley, 2001; Eastaugh et al., 2008; Kakabas, 2008; Parpulov et al., 2010; Oltrogge, 2011; Mastrotheodoros and Beltsios, 2022). Previous attempts confined to identification of a single surface color (pigment) via spectroscopy techniques (Raman, FTIR, Multispectral etc.) and / or for underdrawings and support but no determination of the colors contained in the underneath painted layer has been reported.

2. MATERIALS AND METHODS

2.1 The Three simulated Painted Sets Painting panels preparation and the three sets

The construction of painted and overpainted panels followed older recipes as closely as possible in terms of preparation and pigments used, serving as a database. The aim of the project was to study overpainted panels and identify both the upper and underlying pigments, particularly in the case of overpainted icons. Therefore, preparatory panels were created with color overlays to observe the visual behavior of the color layers when overlapped and align with the traditional recipes for making Byzantine portable icons (Fig.S1-S3 and Table S0 **Supplementary**).

(a)


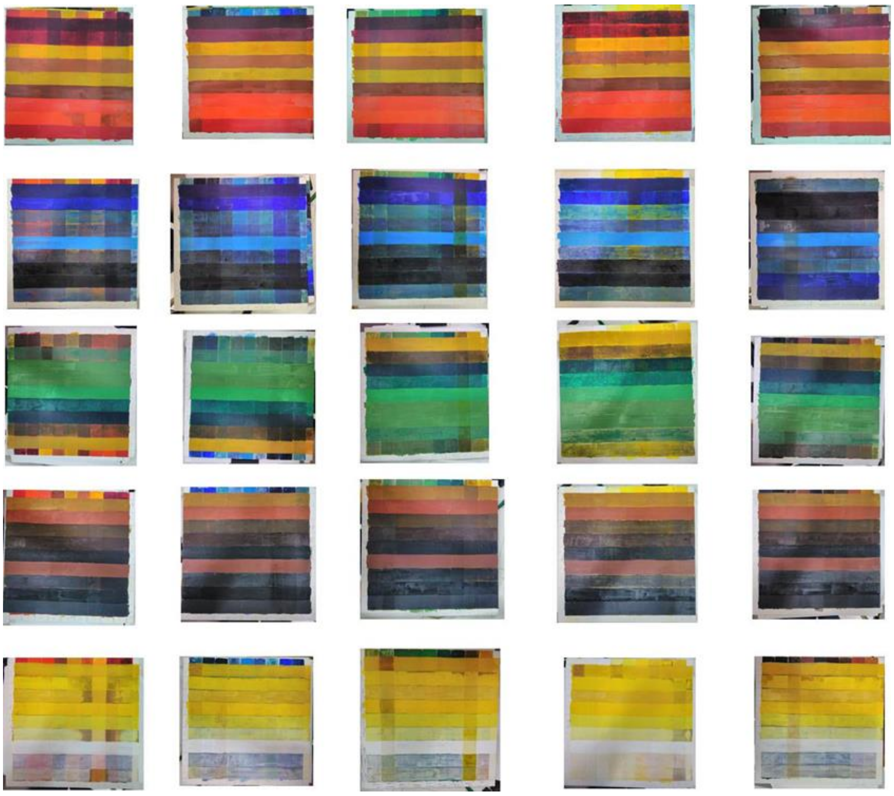

(b)

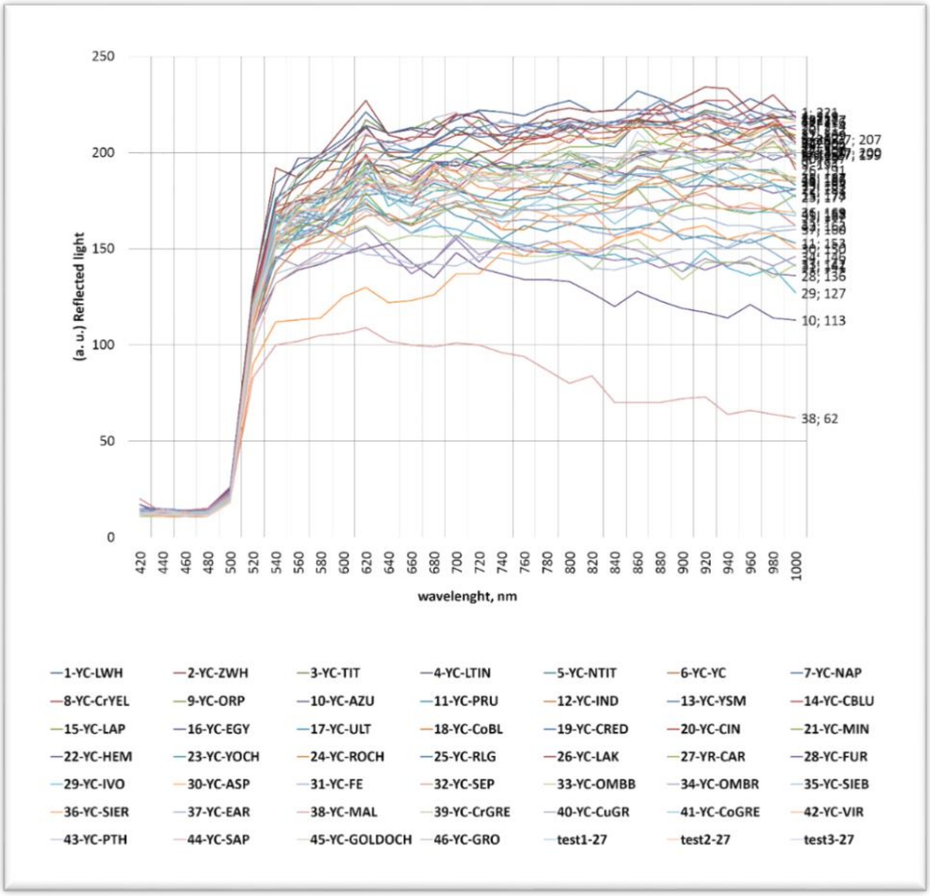

(a. u.) Reflected light
wavelenght, nm
250
200
150
100
50
0
420 440 460 480 500 520 540 560 580 600 620 640 660 680 700 720 740 760 780 800 820 840 860 880 900 920 940 960 980 1000
29; 127
10; 113
38; 62
1-YC-LWH
2-YC-ZWH
3-YC-TIT
4-YC-LTIN
5-YC-NTIT
6-YC-YC
7-YC-NAP
8-YC-CrYEL
9-YC-ORP
10-YC-AZU
11-YC-PRU
12-YC-IND
13-YC-YSM
14-YC-CBLU
15-YC-LAP
16-YC-EGY
17-YC-ULT
18-YC-CoBL
19-YC-CRED
20-YC-CIN
21-YC-MIN
22-YC-HEM
23-YC-YOCH
24-YC-ROCH
25-YC-RLG
26-YC-LAK
27-YR-CAR
28-YC-FUR
29-YC-IVO
30-YC-ASP
31-YC-FE
32-YC-SEP
33-YC-OMBB
34-YC-OMBR
35-YC-SIEB
36-YC-SIER
37-YC-EAR
38-YC-MAL
39-YC-CrGRE
40-YC-CuGR
41-YC-CoGRE
42-YC-VIR
43-YC-PTH
44-YC-SAP
45-YC-GOLDOCH
46-YC-GRO
test1-27
test2-27
test3-27

C) YC

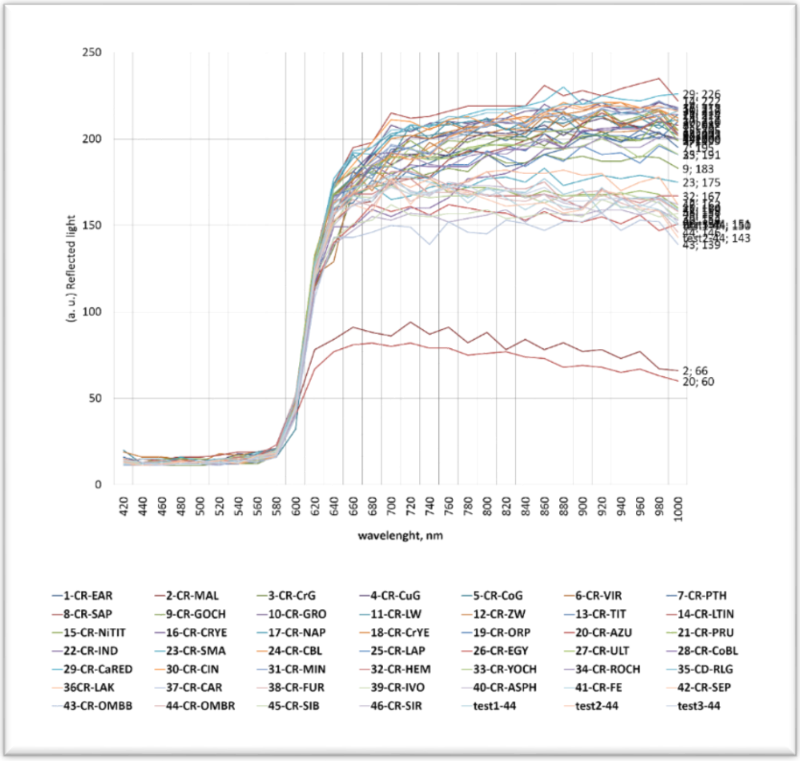

D) RC

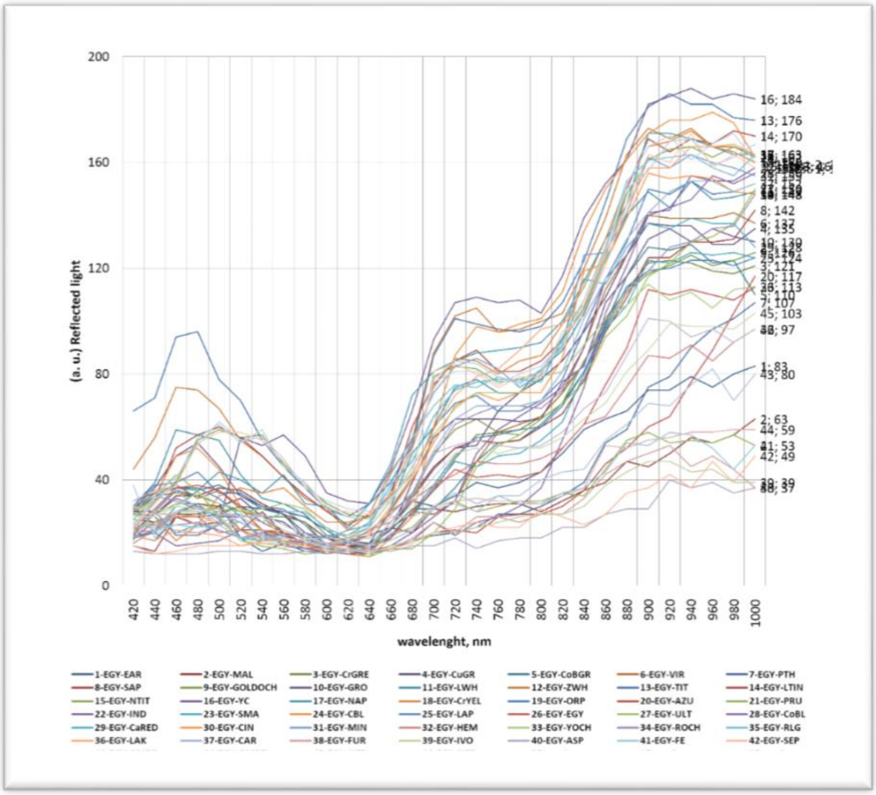

E) EB

Figure 1. Illustration of the generated single and double-layered panels. A) The five Panels displaying single layers arranged in the following horizontal order: 1. green, 2. blue, 3. white and yellow, 4. black and earthy, and 5. red pigments. B) the five Panels showing double layers with overpainting, organized by row of size 30x30 cm and thickness 8 mm with: (Upper)1. red, 2. blue, 3. green, 4. black and earthy, and (lower) 5. white and yellow pigments, C-E are NIR spectra of analyzed samples for upper color of panels C) cadmium yellow, D) cadmium red and E) Egyptian blue.

The panels were prepared with a layer of plaster and rabbit glue adhesive, followed by a drawing and two overpainted layers containing various pigments, creating the painted layers that form the images in real icons.

A total of 135 panel were constructed, consisting of 45 pigments (referred to as colors) covering the same 45 colors, along with 45 single reference colors.

The focus of this investigation is the study of paintings on portable images created with the egg tempera technique. Previous studies have explored the use of multispectral and hyperspectral cameras or x-rays to reveal the underlying design in black and white. However, the ability to determine the colors present in the underlying painting layer remains a primary area of study. Therefore, the objective of this paper is to examine the possibility of predicting the underlying color and investigate how the underlying layer influences the visible color.

Taking into account the tolerances involved in creating a work of art on a painted panel/icon and normalizing the obtained images using the MU.S.I.S NIR camera (see Instrumentation and Method section below), we employed a novel methodology. This approach involves a tentative base of simulated experimental panels applying traditional techniques and a great number of overpainted combinations, statistical analysis using robust hierarchical statistics combined with new application and development of fourteen complexity measures, including fractal dimension, entropies, and Kolmogorov complexity. These methods were applied to all the collected data.

The investigation presented here delves into the analysis of overpainted artworks on canvas/wood, particularly in terms of identifying the sub-painted layer. This palimpsest-like stratigraphy is approached using a novel concept. In fact, the initial step involves untraining-based classification, which establishes a valuable correlation between spectral profiles and the identity of pigment materials based on available a priori knowledge. Building upon this foundation, we selected a list of clustering methods, tests, and complexity algorithms suitable for classifying multidimensional spectral data

2.2 The Three simulated Painted Sets

In this section, we present the first three sets of spectra. Each set corresponds to a specific underlying color: Egyptian blue (Set 1), cadmium red (Set 2), and cadmium yellow (Set 3). **Table S0** (**Supplementary**) shows the 45 pigment selections used as underlying colors, with an additional pigment (46th) representing the corresponding color in the preparation stage without an underlying layer. These three sets are chosen to demonstrate the methodology employed.

For the 45 different samples and the 3 test samples, measurements were taken on 30 variables, corresponding to spectral cube pixels per panel. The arbitrary unit of reflected light represents the calculated spectrum per image pixel in spectral cubes. As a result, the obtained data matrix is a 48-row by 30-column (48x30) matrix, with spectral measurements represented by X_{ij} (i=1, …, 48, j=1, …30), denoting the measured reflected light in arbitrary units (a.u.) for the ith sample at the jth wavelength (nm). (Fig. 1C, D, E).

For these three groups, we measured the Visible Near IR spectra (420-1000 μm), which are provided in **Supplementary Tables S1-S3**. Additionally, we defined three spectra for each set as simulations of "unknown" samples, which closely correspond to the measured ones within ±3% deviation.

For example, for the Egyptian blue as the overlay color, we created three simulated samples based on sample No. 15-EGY-NTIT, which represents titanium nickel yellow as the underlying layer. These simulated samples are labeled as 15test-1, 15test-2, and 15test-3.

Similarly, for the overlying color cadmium red, we generated three simulated samples based on sample No. 44-CR-OMBR, which represents the underlying raw color (ombre) shade. These simulated samples are labeled as test1-44, test2-44, and test3-44.

Finally, for the overlying yellow cadmium color, the simulated samples are based on sample 27-YR-CAR, which represents carmine red as the underlying color. These simulated samples are labeled as test1-27, test2-27, and test3-27.

The data for these three sets and the nine test samples are provided in **Supplementary** Tables S1-S3.

2.3 Spectroscopy Instrumentation & Measurements

The experimental set-up for capturing images across different regions of the spectrum involves using a pair of lamps to illuminate the object, filters to control the passage of radiation at specific wavelengths, and a suitable detector. Additionally, measures are taken during acquisition to correct errors related to the spectral distribution and photometric magnitudes of the light source *('Multispectral Imaging in Reflectance and Photo-induced Luminescence modes: a User Manual', 2013)*. For multispectral imaging, an infrared CCD camera capable of detecting wavelengths up to 1000nm and a high-resolution screen are utilized.

The images were obtained using the Mu.S.I.S. (Multispectral Imaging System) multispectral detector, which is based on infrared reflectography (IRR). This technique takes advantage of the near-infrared and short-wave infrared's ability to penetrate the first surface color layers, allowing the recording of the percentage of reflected radiation using the Kubelka-Munk theory (Delaney et al., 2017).

The hyperspectral detector used is the Mu.S.I.S HS model 2009 (formerly Forthphotonics Hellas S.A., now Dysis), equipped with a CCD 1/200 Progressive Scan sensor (1600 x 1200 pixels, 8 bits, 15 fps) and 30 selectable spectral bands spaced at 20 nm intervals within the range of 400 – 1000 nm for both black and white and color imaging. A micro NIKKOR 60mm, f/2.8D lens was positioned in front of the camera. Tungsten light sources, specifically Philips Argaphoto PF 319 E/44 220V/150W - E27 conical mirror lamps, were used to provide sufficient intensity in both the visible and infrared regions of the spectrum. While LED lamps require special arrangements for multispectral techniques, their use is a subject of ongoing research.

The Mu.S.I.S HS detector has the ability to sequentially store spectral images (spectral cubes) and calculate a full spectrum per image pixel, as well as perform False Color Infrared Imaging. This imaging system is employed for IRR, spectral cube, and FCIR imaging studies of icons, paintings on wood, canvas, paper, manuscripts, ceramics, stone surfaces, wall paintings, and mosaics. The experimental conditions were determined based on specific protocols of Non-Destructive Testing activities by Advanced Research Technologies for Investigation and Conservation (ARTICON Lab), considering optimum brightness, contrast ratio, incident lighting type and quality, and optimal magnification for image analysis. The scanning was performed within a 20 x 20 cm window grid.

Measurements using the Mu.S.I.S HS instrumentation were carried out at the Laboratory of Non-destructive testing of the Department of Conservation of Antiquities and Works of Art, as well as at the ARTICON Lab, University of West Attica under the attention of Prof. A. Alexopoulou.

Infrared radiation has the capability to penetrate paint layers, reflect at the inner interface of the paint layer and substrate, and escape into the air. A suitable detection system collects this non-visible radiation and converts it into a black-and-white visual image (Balas et al., 2003).

Infrared (IR) imaging is particularly valuable for canvas paintings as it reveals features beneath the pictorial layer, such as underdrawings, using reflected illumination with the Mu.S.I.S HS hyperspectral imaging detector at near-infrared wavelengths. Each image acquisition was performed within the spectral range of 420-1000 nm (Alexopoulou et al., 2019).

However, it is crucial to ensure that the captured images and recorded VIR spectra provide visual information that can be optimized and quantified for further study and statistical processing (Wueller and Kejser, 2016).

Unforeseen factors, such as changing conditions throughout the day, heat from the lights during the shooting process, camera age, and reproducibility, can lead to inconsistencies in image uniformity. To address this, daily repeated calibration with the same Mu.S.I.S data was conducted. Consequently, the resulting gray measurement data had to be normalized, meaning they had to be transformed in a way that ensured similar gray scale values across all shots. This normalization process is a usual practice and was achieved using Adobe Photoshop CC-2019 and a script involved converting specific areas of each shot to the same level when measuring the gray tones of the color-checker scale, which was positioned within the frame of the shot and also averaging the profile of a panel due to possible differentiation of thickness by brushing the two overpainted layers (see, **SUPPLEMENTARY:** Standardization of measurements and Calibration).

The spectral range of 400 - 1000 nm (VNIR, VISNIR) used in multispectral (MSI) and hyperspectral imaging (HSI), collectively known as spectral imaging (SI), is non-destructive and non-invasive. These techniques involve capturing images using multiple bandwidths within the visible and near-infrared spectrum (400–1000 nm). Over the past two decades, these methods have been widely applied in various fields, including art conservation and archaeology, for surface inspection and materials identification (Alexopoulou et al., 2019; Fairchild, 2005; Liang, 2012).

As when wavelengths transit from visible to the near-infrared region, greater penetration is achieved, this enables the visualization of features and conditions beneath the surface. Hyperspectral imaging can provide a rich dataset, allowing the detection of objects of interest that are invisible to the human eye and facilitating materials identification based on specific conditions and setups (with the radiation magnitude at 555-560nm serving as the reference magnitude for maximum sensitivity of the human eye in photopic vision (Fairchild, 2005))

The acquisition process involved continuous attempts and trials to minimize changes in conditions as much as possible (refer to Fig. 1 (C-E) for all plots of the three Sets).

2.4 Statistical methods

In the examination of art objects with unknown painting materials, a crucial step is to compare the collected spectra with reference spectra (training set) using spectral similarity metrics, specifically those known to perform well (Balas et al., 2018). Preliminary data analysis plays a vital role in detecting heterogeneity, deviations from normality, presence of outliers, and any underlying data structure. Statistical tools such as Principal Component Analysis (PCA), data transformation, and Mahalanobis distance can be employed for this purpose (Baxter, 2015; Papageorgiou, 2020).

In our application, we successfully detected heterogeneity and underlying structure in the data. The subsequent analysis aimed to identify existing groups. To accomplish this, we implemented cluster analysis, specifically hierarchical methods using four different linkages: Average, Complete, and two modifications of Ward's method. The data were standardized, resulting in a mean of zero and variance of one for each variable, and the Euclidean distance was utilized as a measure of distance. Details about the implementation of Average linkage, Complete linkage, Ward, and Ward-2, along with their corresponding statistical methods, are discussed in the **SUPPLEMENTARY** material (Choice of Statistical Methods).

Additionally, we employed the k-means clustering algorithm to group the painted panels into a predetermined number of clusters based on the results obtained from hierarchical clustering. To assess the quality of the resulting clusters and confirm that similar painted panels belong to the same cluster while dissimilar ones belong to different clusters, we utilized PCA, Silhouette values, Wilks test, and box plots by groups. Through this comprehensive analysis, distinct and clear results were obtained, particularly in relation to the group containing the three created test panels, which exhibited significant dissimilarity from the remaining panels. These findings are supported by the aforementioned indices and coefficients, as detailed below.

2.5 Complexity and Entropy Methods

This study provides a concise description of the parameters and characteristics utilized in the analysis, employing six fractal algorithms, four entropy measures, and four complexity measures. For more detailed information, please refer to the corresponding references. Originally developed and implemented for temporal signals, these algorithms and methods were adapted for analyzing one-dimensional spectral data point values, hence the interchangeability of terms such as "signal" and "spectrum."

The computations were performed using the ComsystanJ plugin package (Ahammer, 2023) (https://comsystan.github.io/comsystanj/) for ImageJ2/Fiji (https://imagej.net/software/fiji/) (Schindelin et al., 2012). The ComsystanJ plugins offer two options for selecting partial signals or adjacent data point values. In this study, we chose the first option, which involves dividing the entire signal (data sequence) into non-overlapping subsequent boxes (windows). For each window, the specific complexity parameter is calculated individually, generating a set of results. Alternatively, the second option entails creating a sub-signal by combining adjacent data points into one box (window), resulting in heavily overlapping boxes and producing as many results as there are data points in the signal. Although this gliding option increases calculation times significantly, the overlap does not necessarily yield superior results.

We provide a brief overview of the 14 complexity and entropy measures utilized in this study: six fractals (Allometric scaling dimension, Higuchi Dimension, Tug of war Dimension, Katz Dimension, Petrosian Dimension, Sevcik Dimension), four Entropy measures (Shannon Entropy, Approximate entropy, Sample Entropy, Permutation entropy) and four other complexity measures (Kolmogorov complexity, Hurst coefficient, Detrended fluctuation analysis DFA, Lyapunov exponent) (See **SUPLEMENTARY** for details).

The results of the applied statistical and 14 measures were applied to support each other and strengthen the findings on a corroborated manner. Both investigate the most appropriate method for clustering and identification of an unknown overpainted panel that matches the experimental data base.

3. RESULTS

The spectral data 〖X〗 ij obtained in the NIR region for the three sets of 49 data strings (45 different data samples, three tests, and one with only the preparatory panel) are subjected to processing using statistical clustering and complexity measures. Statistical analysis of spectral features was conducted using IBM SPSS 27 software and R.

The objective of this analysis is to identify groups within the data and classify each pixel into one of these groups based on its similarity to the remaining spectra that comprise the validation data set. The selection of the optimal classification model or spectrum similarity metric is typically specific to the application at hand. Experimental evaluation of algorithm accuracy is crucial since theoretical research alone cannot determine the best-performing algorithm(s). In contrast to earlier observations using ISODATA (a variant of K-means), unsupervised methods, particularly the K-means variation, have yielded satisfactory results (Balas et al., 2018).

The statistical grouping aims to achieve two outcomes: a) clusters of reflected spectra that exhibit similarity across different pigment combinations of overpainted panels, and b) the probability of matching the three tests with the expected real sample, allowing for a tolerance of ±3% (the three test data strings for the three sets are provided in the **SUPPLEMENTARY**).

3.1 Statistical analysis

SET 1: EGYPTIAN BLUE AS OVERPAINTING

In this section, we present the steps of the statistical analysis conducted on Set 1 (for additional data, refer to **Supplementary** Statistical analysis of Set 1). Similar analyses have been performed on the other two Sets. Standardization was applied to the data, resulting in a mean value of zero and standard deviation of one. Preliminary analysis of Set 1 did not reveal any outliers nor normally distributed variables. Consequently, we proceeded with distribution-free cluster analysis methods, specifically hierarchical and k-means approaches. Our focus was on the group that includes the three test data strings. Below, we provide a detailed overview of these methods and the resulting number of groups.

Fig. 2A depicts the dendrogram generated using Ward's method for hierarchical clustering. The leftmost group, highlighted in red, comprises the 15test-1, 15test-2, and 15test-3 samples (identified as 47, 48, and 49, respectively, in **Supplementary Table S1**) that were created. This cluster correctly includes No. 15, featuring Egyptian blue above and nickel titanium yellow below. Additionally, it encompasses six more samples with Egyptian blue as the upper layer and underlying colors, namely: No. 12 (zinc white), No. 13 (titanium white), No. 16 (cadmium yellow), No. 17 (yellow Naples), and No. 18 (chrome yellow), which are characterized by yellowish and whitish hues associated with titanium yellow pigments.

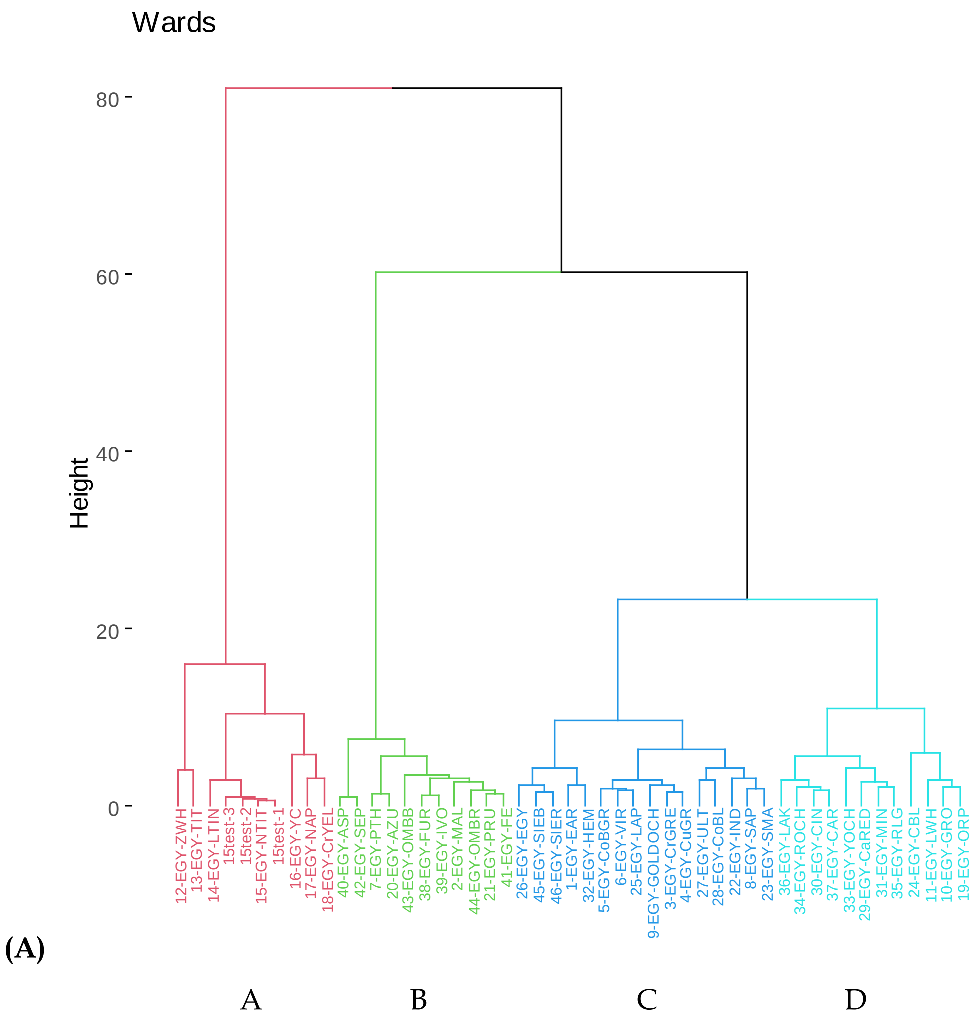

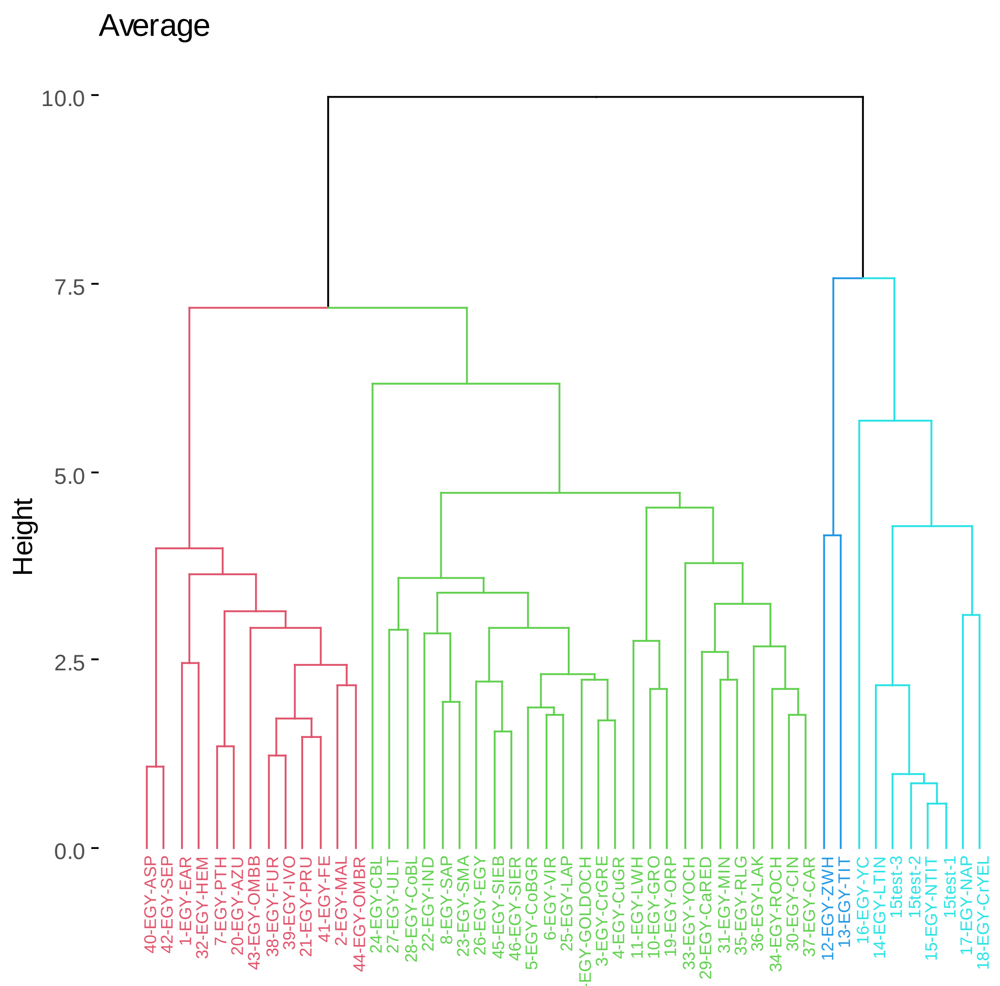

(B)

AL-A **AL-B** **AL-C** **AL-D**

Figure 2. A) ward with four colored groups; notice the three tests with the "unknown" (15-EGY-NTIT) in the left red group. B) average linkage gives four colored groups (AL-A to AL-D); with particularly separated ones the No 12 και 13 (in blue).

The cluster analysis performed in this study provides valuable insights into the influence of underlying colors on the overpainted upper layer, which, in this case, is Egyptian blue. The created groups reveal distinct characteristics within the dataset. Group A (left, red) includes zinc and titanium whites, lead tin, nickel titanium, cadmium, Naples and chromium yellows, along with the three tests. Group B (green) consists of three blacks, sepia and iron browns, umbers (raw and baked), phthalo and malachite greens, and azurite and Prussian blues. Group C (blue) can be further divided into two subgroups, predominantly featuring earth greens, chrome, copper, cobalt, viridian and sap greens, golden ochre, as well as indigo blue, enamel, lapis, Egyptian, ultramarine and cobalt, red hematite, and raw and baked sienna. Finally, group D (green-blue) mainly encompasses red colors such as cadmium, cinnabar, minion, realgar, and lake, along with two ochres (red and yellow), lead white, yellow with arsenic (orpiment), cerulean blue, and the single color directly in preparation (ground). Therefore, the groups can be categorized into very light colors, very dark colors, blues and greens, and reds, including the preparation color.

Next, the average linkage method (Fig. 2B) was applied, resulting in four groups with the following observations:

The fourth group (AL-D) is of particular interest as it includes the three tests characterized by the color blue. Within this group, colors No12 (zinc white) and No13 (titanium white) serve as underpainted colors with Egyptian blue as the overpainted upper layer (AL-C). These two colors are separated from the remaining group, which aligns with the Ward method. However, the other two groups, AL-A and AL-B, differ from the previous analysis. Group AL-A comprises earth greens, malachite and phthalic greens, azurite and Prussian blues, hematite red, three blacks, sepia and iron browns, and both baked and raw umbers. On the other hand, group AL-B, the largest group, includes chrome, copper, cobalt, viridian, and sap greens, golden ochre, the single color with the preparation below, lead white, yellow orpiment, both sienna, and almost all blues and reds, excluding those belonging to group AL-A (azurite, Prussian, and hematite).

The complete linkage method yields the same sample composition as the average linkage method (see **SUPPLEMENTARY** complete linkage set 1, Fig S4). The silhouette scores for each group, including 15 test samples per method (15test 1, 15test 2, and 15test 3), as well as the mean values for average and complete linkage and Ward, demonstrate comparability (refer to **SUPPLEMENTARY** Silhouette scores for Set 1, **Figs.S5, S6**).

Set 1: Boxplots of the groups

Based on the principal components (below) and using the 1st component which represents 71% of the total, which is very satisfactory, the box plots for the 3 groups per method are shown below (Fig. 3). The group that we are interested in is the group with the highest scores in all graphs and is very clearly distinct with large differences, i.e. it presents particular characteristics of tightness from the other clusters. This is in agreement with the conclusions from silhouette values.

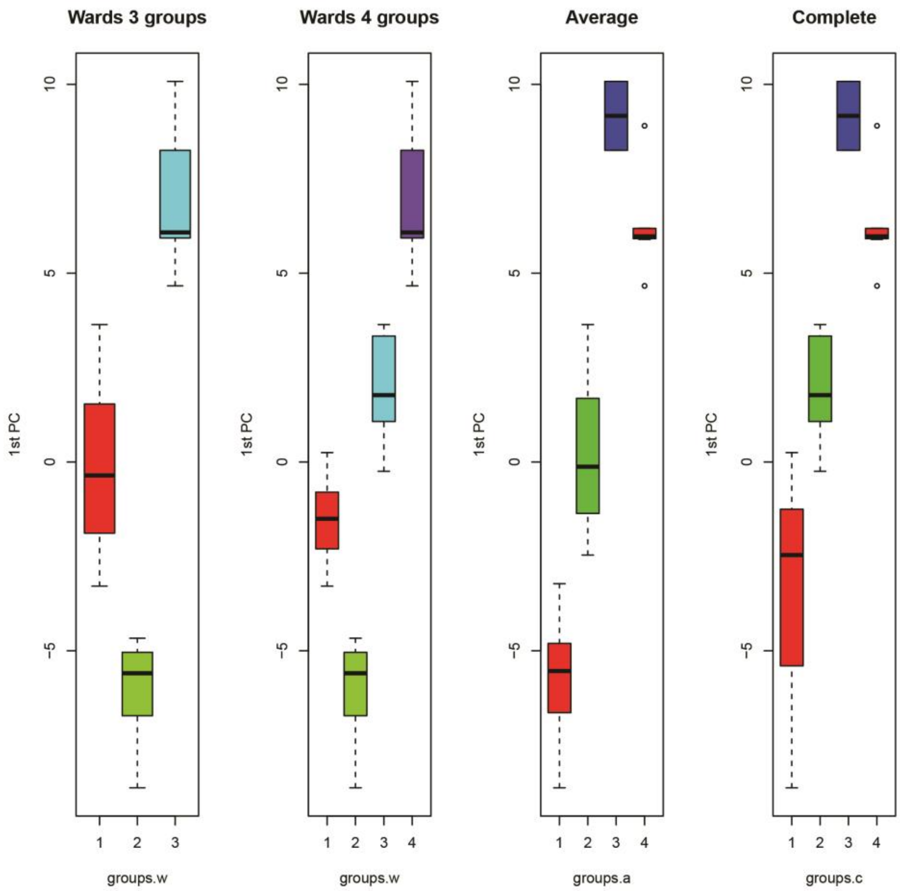

Figure 3. Box plot for the Ward with 3 and 4 clusters and for average και complete linkage. The First principal component (-10 to +10) with the lower (25%) and higher (75%) quartiles for each cluster of interest per method.

Note the median per each cluster and method as a line inside each box with the box being between the lower and upper quartiles. Thus, the box plots identify the middle 50% of the respective cluster data, the median, and the extreme points.

The 2 samples (No 12: zinc white and No 13: titanium white), which belong to a differentiated group and are separated in some methods (average and complete), are those with slightly smaller variable response scores (red color). The 8 samples that include the 3 tests are in any case a distinct set characterized by the large value of the score; these are: 15test-1, 15test-2, 15-test3, 16-EGY-YC, 15-EGY-LTIN, 17-EGY-NAP and 18-EGY-CrYEL.

Set 1: Principal Component Analysis (PCA)

In order to get a visual representation of the clustering results, we make use of the PCA scores, a projection method that will allow us to work with a lower dimension than the actual which is 30. The first 2 principal components represent 84% of the information of the data which is a very satisfactory percentage. (See **Supplementary PCA of Set 1, Fig S7**). Overall, all five groupings (presented in Fig.S18) exhibit a clear separation among groups confirming that the suggested grouping is meaningful. It appears that the first component is adequate to explain the variability of the data points.

In the PCA graph that follows with the labels of the data, (**Supplementary in Fig.S7, S8**) it is clearly seen how extremely close (enclosed in the blue box) to sample 15 are the 3 tests, which are almost indistinguishable since they are the on top of the other.

We have next implemented unsupervised K-means method, which classifies objects into a predetermined number of groups so that objects belonging to the same group are as uniform as possible (i.e., high intra-class similarity), while objects in different groups are as different as possible (Hartigan & Wong, 1979). (**Fig S9, Supplementary).** The k-means method in the present study with k=4, has resulted to four groups with the group of interest to contain exactly the same samples as in Ward's. (**Fig S10 Supplementary**).

Next is the Wilks value it is notified that the lowest value is given by K-means but the highest by Wards (**SUPPLEMENTARY Wilks Set 1**).

SET 2: RED CADMIUM AS OVERPAINTING

Next comes the second set of colors with cadmium red as the dominant overpainted color. In this case, sample No. 44 was chosen at random with the cadmium red overlay and raw umbra shadow underlying. Three tests named test1-44, test2-44 and test3-44 were created, the distances of their spectral values from the corresponding measured ones are ±3%, just as it was done in the previous group with Egyptian blue as the overpainted, when they were created the dendrograms for standardized data, concerning four methods, whose groupings are shown in Fig.5 below for Average Linkage (and in **Supplementary Statistical Analysis Set 2** for Complete Linkage, Ward Linkage; Ward D2 gives same result; Figs. S11, S12).

The samples test1-44, test2-44 and test3-44 are grouped with the corresponding sample 44-CR-OMBR (refers to the cadmium red overlay and raw umber overlay), while at the same time some other samples belong to the same group. All dendrograms consent on the group containing the 3 test samples. There are 16 samples in total in this group and one can distinguish a small subdivision for some of them.

Following is the division for the dendrograms, for the Average Linkage methods into 4 groups (Fig. 4), and similar ones for the Complete linkage and Ward The group which includes the tests is highlighted in cyan (see, **SUPPLEMENTARY Statistical analysis Set 2, Fig S11, S12).**

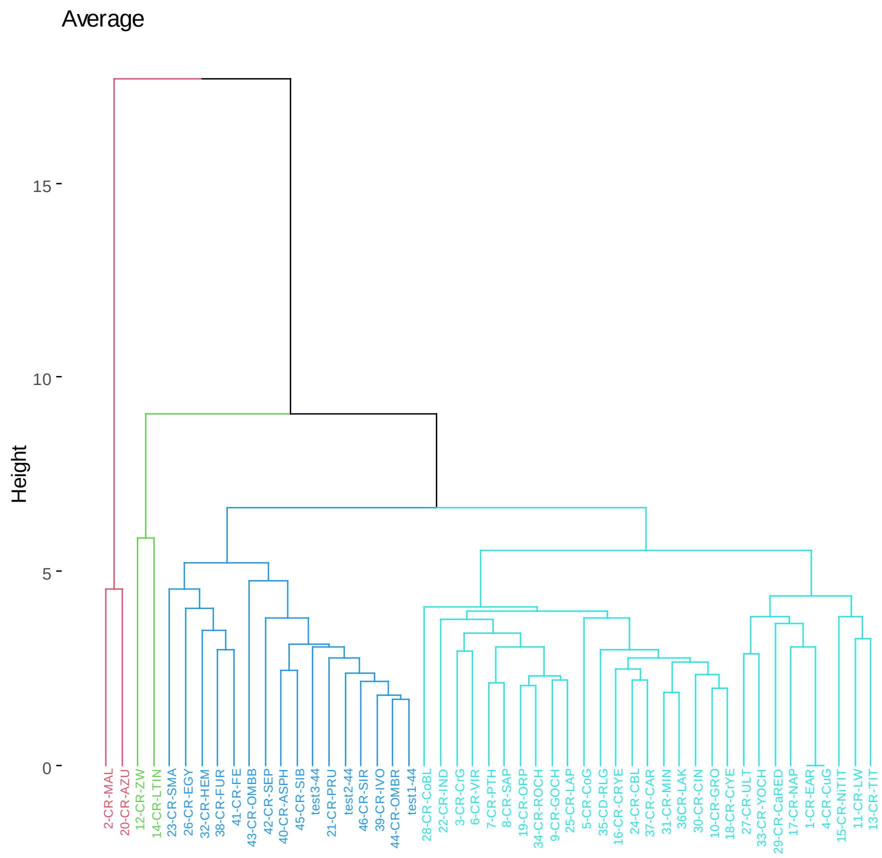

Figure 4. The four groups in average linkage

If the correlation tables for the previous 4 grouping methods are constructed, they show absolute agreement regarding the group of these 16 samples. This group includes the samples: "21-CR-PRU", "23-CR-SMA", "26-CR- EGY", "32-CR-HEM", "38-CR-FUR", "39-CR-IVO", "40-CR-ASPH", "41-CR-FE", "42-CR-SEP", "43-CR-OMBB", "44-CR-OMBR", "45-CR-SIB", "46-CR-SIR", "test1-44", "test2-44" and "test3-44". These are the blue enamel, Egyptian, Prussian, hematite red, the three blacks and all the earthy ones, which make up the iron and sepia browns, raw and baked ombres and sienna.

The 2 subgroups that can be distinguished in all the dendrograms (Fig. 4 and Fig.**S11, S12 SUPPLEMENTARY)** are: "21-CR-PRU", "39-CR-IVO", "40-CR-ASPH" "42-CR-SEP", "43-CR-OMBB", "44-CR-OMBR", "45-CR-SIB", "46-CR-SIR", "test1-44", "test2- 44", "test3-44" and "23-CR-SMA", "26-CR-EGY", "32-CR-HEM", "38-CR-FUR", "41-CR-FE". That is, the Prussian and Egyptian blue, Hematite red, Furnace black and iron brown are distinguished.

The Adjusted Rand index that measures concordance between the methods in terms of the result is very satisfactory (maximum value for complete agreement is 1), as shown in the values: Average with Complete: 0.9617714, Average with Wards: 1, Average with Wards D2: 1, Wards with Wards D2: 1. Compatible results are obtained and by Silhouette values (See **SUPPLEMENTARY Silhouette Set 2, Fig. S13)**

In Fig. 5 below are included the box plots of the different methods that were used and they concern the order Ward, Average and Complete Linkage (see also **SUPPLEMENTARY Fig.S14**). Based on the principal components and using the 1st principal component which represents the 63% of the total variability, the box plots for the groups suggested by hierarchical methods.

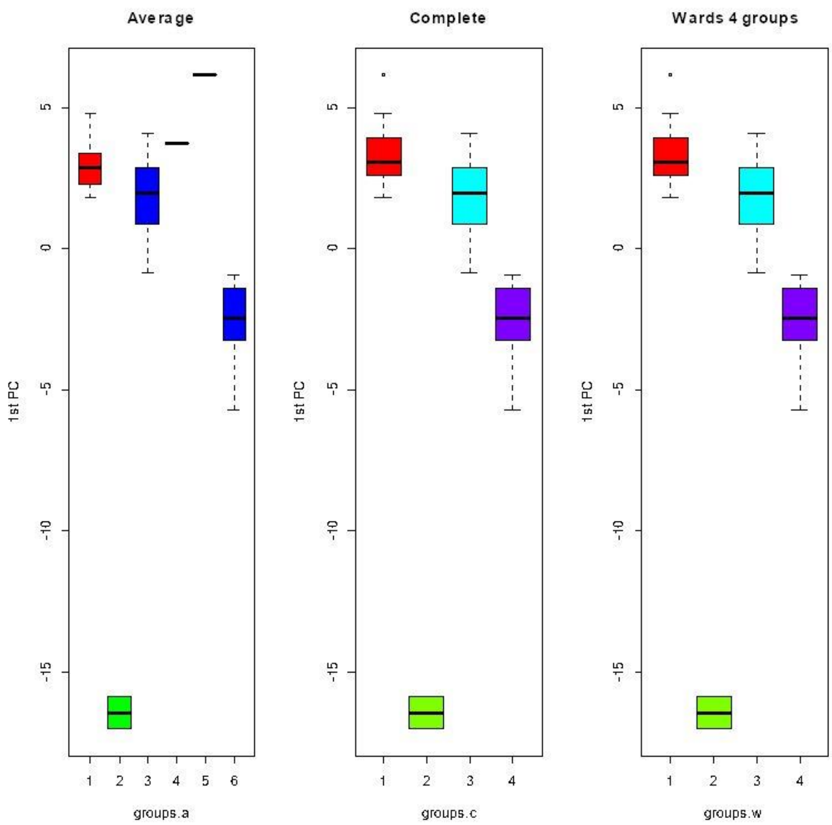

Figure 5. Box plot for: Average 6 groups, Complete with 4 groups and Wards with 4 groups.

Validation tests were carried out with several methods, for which the following interpretation is derived: the group with tests 1, 2 and 3 that interests us and which for the *Complete Linkage* method is the 4th in the row with the purple color (Fig. 5), has values less than average in variables of spectral wavelength values in nm "620", "640", "660", "680", "700", "720", "740", "760", "780", "800", "820 ", "840", "860", "880", "900", "920", "940", "960" and "980", referring to the spectrum areas. Even smaller values in the variables have those observed in group 2, which in Fig. 5 is depicted in green and which consists of only 2 samples, "2-CR-MAL" and "20-CR-AZU" and refer to green malachite and azurite blue as underlying colors and which are very different from all others in the above areas of the spectrum. The average values of the 4 groups are given in **Supplementary Table S4.**

The PCA plots has shown also that the two principal components represent 84% of the information of the data which is a very satisfactory percentage (see the plots of the groups located in Fig. 6A. The group we are interested in truly contains the tests 1, 2 and 3, which are the samples in the center with No 4 for the Wards and Complete linkage methods and No 6 for the Average linkage. It is definitely a distinct group from the rest and the grouping methods are confirmed here as well.

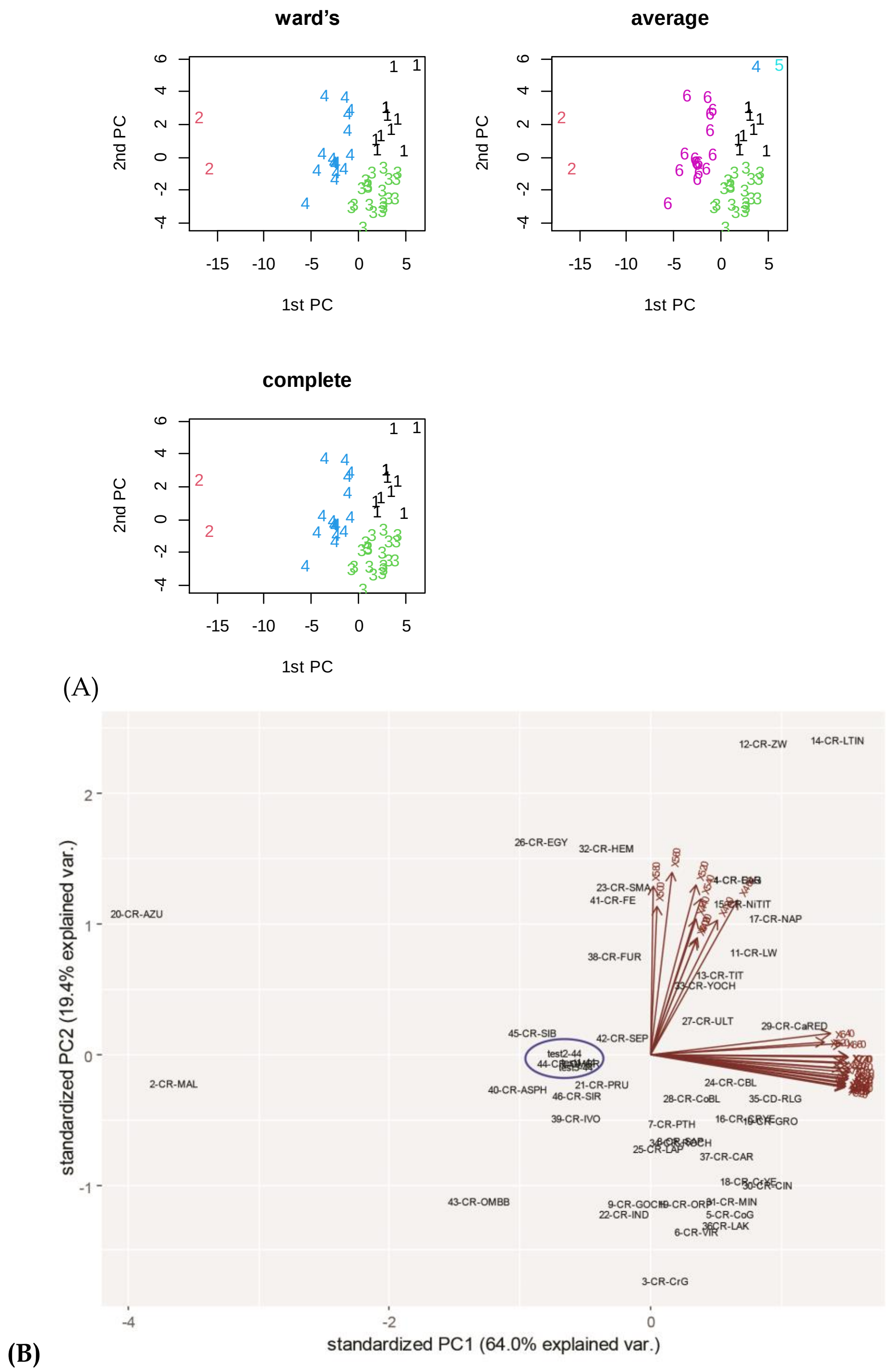

Figure 6. A) PCA groups from Ward, Average linkage and Complete linkage, B) Biplot showing the structure of the loadings from PCA for Comp 1 and 2. The large positive loadings of lower group of variables 520-1000nm on component 1 that is the most spectral part of spectra have a strong influence in this component. The upper group of vectors loadings close to 0 indicate that the variable of respective wavelength 400-520nm has a weak influence on the component. Note two extreme outliers far left, and the respective samples around the loadings (see also alternative supportive plot in Fig. S15 SUPPLEMENTARY).

In the PCA graph that follows in Fig.6B with the labels of the data, it is clearly seen how extremely close (enclosed in the blue ellipse) to sample 44 are the 3 tests, which are almost indistinguishable since they are on top of each other, while it can also be seen why 2 sub-groups were proposed in the central group, those with a negative 2nd principal component 44, 45, test1, test2, test3, 21, 40, 46, 39, 43 and those with a positive , the 26, 32, 23, 41, 38. Next the clustering for data set with k-means algorithm gives exactly the same clustering that includes all 3 tests, just like with dendrograms. (**SUPPLEMENTARY Fig. S16).** The calculated Adjusted Rand index between the three resulting groups of the heirarchical methods and the k-means ranges between 0.83 and 0.96, indicating a very good agreement.

SET 3: CADMIUM YELLOW OVERPAINTING

This section presents the final set of data (Set 3) in the experimental procedure aimed at demonstrating the grouping of tests with their corresponding measured samples. In this particular case, cadmium yellow was chosen as the upper color, encompassing various underlying colors as well as the three tests created for this purpose. Sample No. 27-YC-CAR, randomly selected, represents the combination of cadmium yellow and carmine red as the underlying colors. Three tests, named test1-27, test2-27, and test3-27, were created, with their spectral values showing a deviation of ±3% from the corresponding measured values. Dendrograms were constructed for the standardized data using four methods. Additionally, sample No. 46 represents a single color with a preparatory (ground) background.

Figure 8A illustrates the dendrogram created using the Average Linkage method (also refer to Fig S35). Notably, sample No. 38-YC-MAL, which features an underlying red malachite color, appears to be significantly distant from all other samples, indicating a possible outlier. This observation is further supported by PCA analysis and the calculation of Mahalanobis distance for this sample (refer to **Supplementary** Statistical analysis of set 3, PCA, **Fig.S17**).

Sample 38, characterized by a yellow upper color, exhibits an extreme position and deviates from the average values of Set 3 starting from 520 nm, with a significant difference observed after 840 nm. It appears that the green (malachite) underlying pigment exhibits its distinct infrared absorption compared to other colors. The presence of outliers adversely affects most clustering techniques; therefore, we exclude this sample from further analysis.

We repeat the analysis for the remaining 48 samples and hierarchical clustering for the three linkages (the Wards D2 is similar to Wards) lead to dendrograms presented in Figure 8B (see also **SUPPLEMENTARY Fig.S18, S19**). A first comment concerns the fact that in all methods, the 3 test samples are grouped with the corresponding sample from which they were created, that of No 27.

The 3 test samples "test1-27", "test2-27" and "test3-27" are grouped (right part of green group) with the samples 24 -YC-ROCH", 45-YC-GOLDOCH, "27-YR-CAR. This subgroup relates to the next (left) one comprised by "9-YC-ORP", "12-YC-IND", "16-YC-EGY", "21-YC-MIN", "23-YC-YOCH", ", "26-YC-LAK", ", "39-YC-CrGRE", "40-YC-CuGR", "42-YC-VIR", "44-YC -SAP", This group is augmented with samples "13-YC-YSM", "15-YC-LAP", "17-YC-ULT", "18-YC-CoBL", "22-YC-HEM", "32-YC-SEP", "35-YC-SIEB", "36-YC-SIER", "37-YC-EAR" and "41-YC-CoGRE" for Complete and Average Linkage.

In fact, examining the underlie colors of upper yellow cadmium, to which these samples pertain, the first sub-group includes the carmine, lacquer, orpiment, and minion reds, the Indian and Egyptian blues, the three red ochres, yellow and gold, and the greens of chrome, copper, viridian and sap. The second subgroup concerns blue enamel, lapis lazuli, ultramarine, cobalt, hematite red, earth and cobalt greens, raw and baked sienna and sepia brown. The three colors that work differently in the Complete method are Egyptian Blue, Chrome Green, and Copper (regarding numerical and labels referred to samples see Fig. 8B but also Tables S2-S4 **SUPPLEMENTARY**).

Below are the box plots of the groups that concern us and can be seen in Fig.9 and are shown in bright green in the average and wards method and blue in Complete. In all cases one can conclude that the suggested groups are well separated.

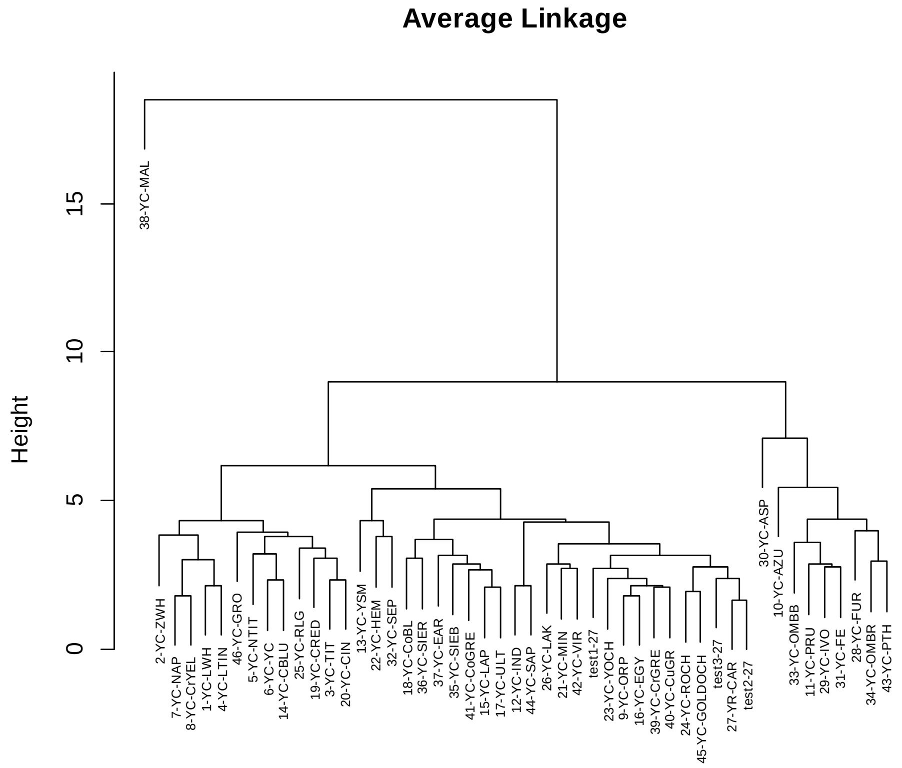

(A)

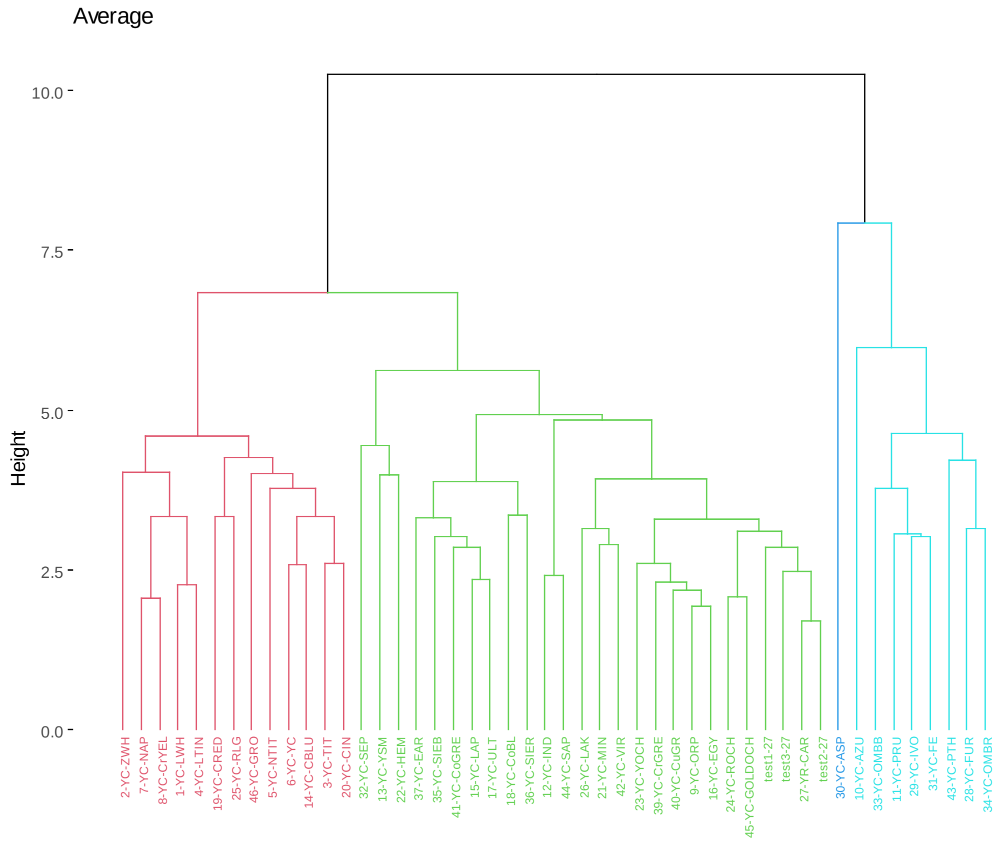

(B)

Figure 8. A) Dendrograms for Average Linkage, B) alternative presentation of average Linkage in 4 colored groups excluding No 38.

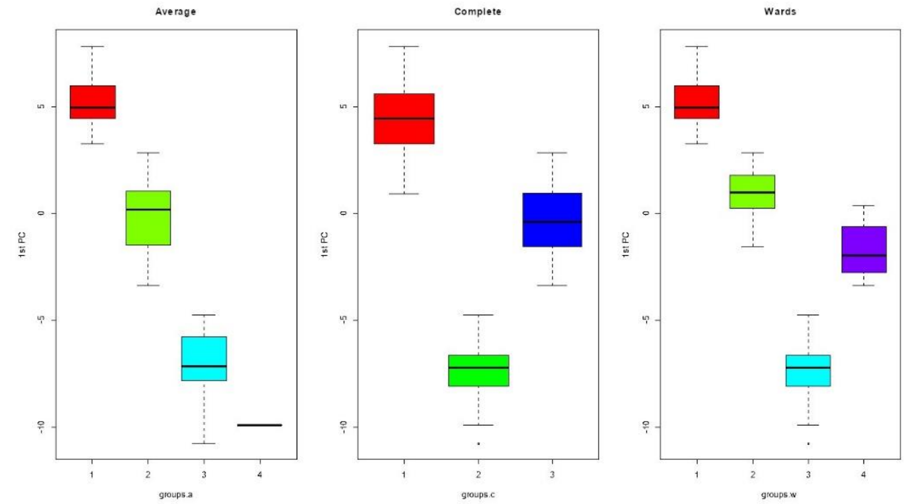

Figure 9. Box plot of average και complete and Ward's linkage.

The grouping of all samples of the set 3 is also confirmed by the Silhouette values for each group per method as well as their average value and a graphical representation of the clustering results using PCA as a projection method (see **Supplementary Fig. S20 and S21**).

A biplot of the samples in the first two principal components (the 2 first explain 83% of the total variability) is shown in Figure 10, where it appears that the test samples are indeed very close to No 27 and all that belong to the same group. The 3 test samples that concern us are enclosed in the blue circle (see also **SUPPLEMENTARY Fig.S22)**, a biplot on the first two PCs with the distinct position of the 3 tests.

Finally, the k-Means method below also agrees with the group containing the 3 tests close to the expected No 27 (see **SUPPLEMENTARY Fig.S23**).

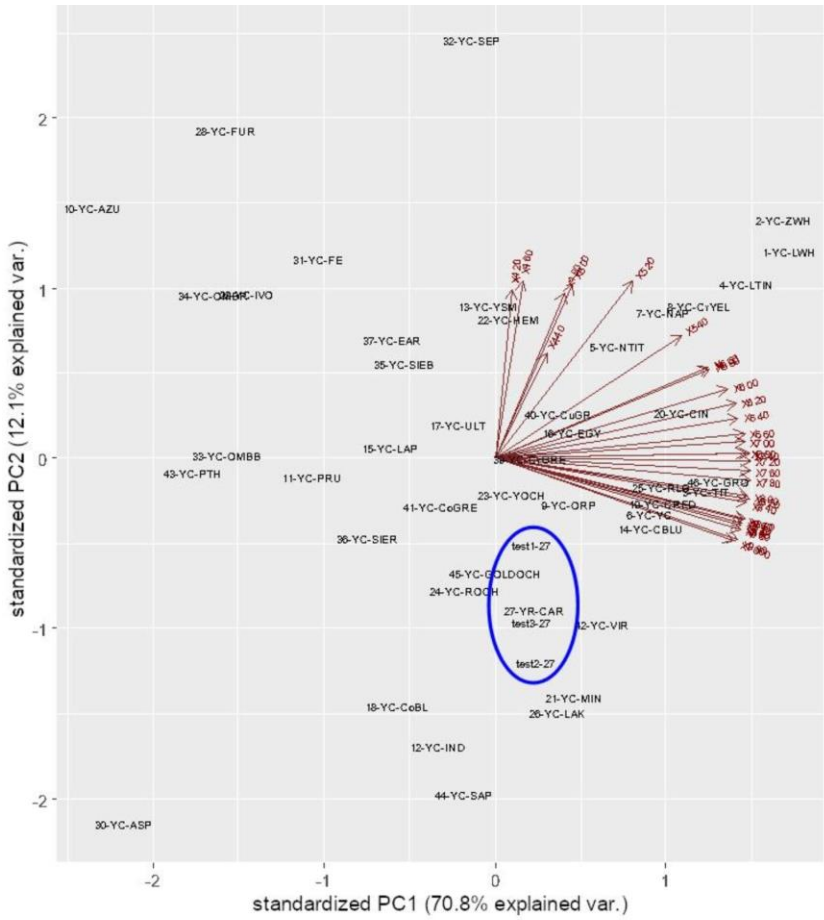

Figure 10. A biplot on the first two PCs. The 3 tests are enclosed in the blue circle

3.2 COMPLEXITY ANALYSIS

In the analysis of spectral measurements for the three sets, complexity measures were utilized and applied to the entire dataset. The previously mentioned fourteen (14) complexity measures were calculated, yielding the following results.

The measurements were conducted on both the original data and the pre-processed data, which underwent interpolation and subsequent boxing. The following figures display the plots generated from these measurements for each of the three-color sets (Set 1, Set 2, and Set 3). The plots illustrate the complex indices per standardization, with and without interpolation.

To expand the set of "wavelength" values from 420 to 1000 nm, we performed linear interpolation on the "near IR values." Linear interpolation assumes a linear change in y for a given change in x. We employed the INDEX and MATCH functions in Excel to achieve the interpolation. The original 30 "x" values spanned from 420 to 1000 nm with a 20 nm increment. By reducing the increment of the "x" data sequence, we expanded it to 183 data points. Subsequently, appropriate Excel formulas were used to calculate interpolated "y" data for each "x" value.

In the plots, the three test samples and the measured sample are indicated by two red circles. An arbitrarily drawn red horizontal line denotes the position of the four samples of interest (the three tests and the measured sample) that align with the respective index in relation to the other samples in the sets. In these plots, the three tests are always plotted at the far right as the three last points, while the measured sample shifts its position. Plots without red circles or lines indicate a lack of alignment and corresponding index matching.

Representative figures of the most suitable algorithms are presented in Fig. 11 for Set 1 (with upper pigment Egyptian blue, 1A-1E), Fig. 11 for Set 2 (with red cadmium upper color, 1F-1J), and Fig. 11 (1K, 1L) for Set 3 (with yellow cadmium upper color). All other plots that did not meet the desired criteria are provided in the **SUPPLEMENTARY** Complex Analysis indices plots to ensure reproducibility and evidence of proof for researchers.

When analyzing cadmium yellow, the three tests in the Allometric Scaling Dimension (without interpolation) are close to each other but slightly distant from the measured sample. This pattern is also observed in the Shannon Entropy dimension, both with and without interpolation. However, in the Tug of War dimension, although the three tests are close to each other, they are significantly distant from the measured sample.

For cadmium red, both in the Allometric Scaling Dimension (with and without interpolation), all three tests and the corresponding measured sample are very close to each other. However, in the case of interpolation, this dimension makes it easier to identify the real sample compared to other colors. Similar results are observed in the Hurst coefficient without interpolation. In the Tug of War dimension, the three tests are close to each other but quite far from the measured sample. The same applies to the Lyapunov exponent with interpolation, but their position in the database plot, along with a few other samples including the "unknown" sample, can potentially provide a more accurate identification of the measured sample.

Regarding Egyptian blue, in the Allometric Scaling Dimension (with and without interpolation), the three tests are very close to each other and also very close to the measured sample. Particularly, the three tests of sample 15-EGY-NTIT (nickel-titanium) in the original data overlap with seven others, which differ from the red line within the standard deviation of the three tests. These samples are 13-EGY-TIT, 14-EGY-LTIN, 15-EGY-NTIT, 25-EGY-LAP, 27-EGY-ULT, 28-EGY-CoBL, 30-EGY-CIN, and 43-EGY-OMBR. However, in the interpolated data, the closest samples are 1-EGY-EAR, 8-EGY-SAP, 14-EGY-LTIN, 15-EGY-LTIT, 21-EGY-PRU, and 22-EGY-IND. In the Higuchi Dimension, the three tests are very close to each other but relatively distant from the measured sample. Without interpolation, they are further away from the measured sample compared to the other two tests. Both Sample Entropy (with and without interpolation) and Shannon Entropy (without interpolation) show the three tests and the measured sample to be very close to each other. However, in Shannon Entropy (without interpolation), the three tests are very distant from the measured sample. Similar observations are made for the Higuchi Dimension. In the Katz dimension with subsequent boxes, the three tests are close to each other and also to the measured sample, but they are farther away in the case of interpolation. The Sevcik dimension yields good results in all cases, and in the interpolated data, Sample Entropy performs well. The Detrended Fluctuation analysis for the Egyptian Blue without interpolation also provides satisfactory results. The Kolmogorov complexity with ZLIB compression demonstrates close values between the three tests and sample No. 15, but within a 3% error, it includes a larger number of possible sample data (18) compared to other methods. The Kolmogorov complexity with GZIB compression includes slightly fewer possible samples. The results of all other indices for the three sets are not compatible and are rejected (refer to **Supplementary** material Figs S24-S61 and at the end p.56 the computing steps of the complexity measures indices).

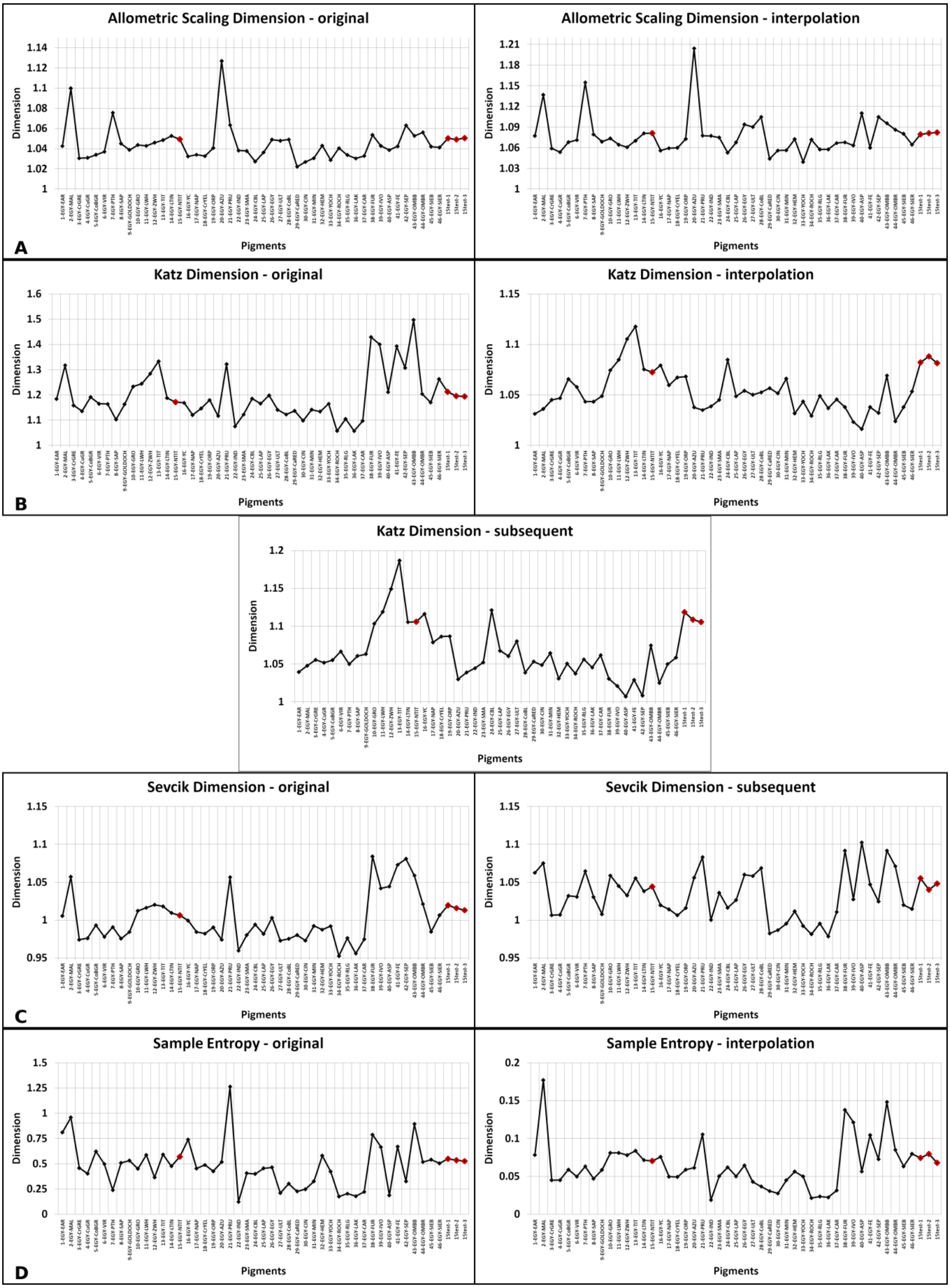
Allometric Scaling Dimension - original
Allometric Scaling Dimension - interpolation
A
Katz Dimension - original
Katz Dimension - interpolation
B
Katz Dimension - subsequent
Sevcik Dimension - original
Sevcik Dimension - subsequent
C
Sample Entropy - original
Sample Entropy - interpolation
D
Dimension
Pigments

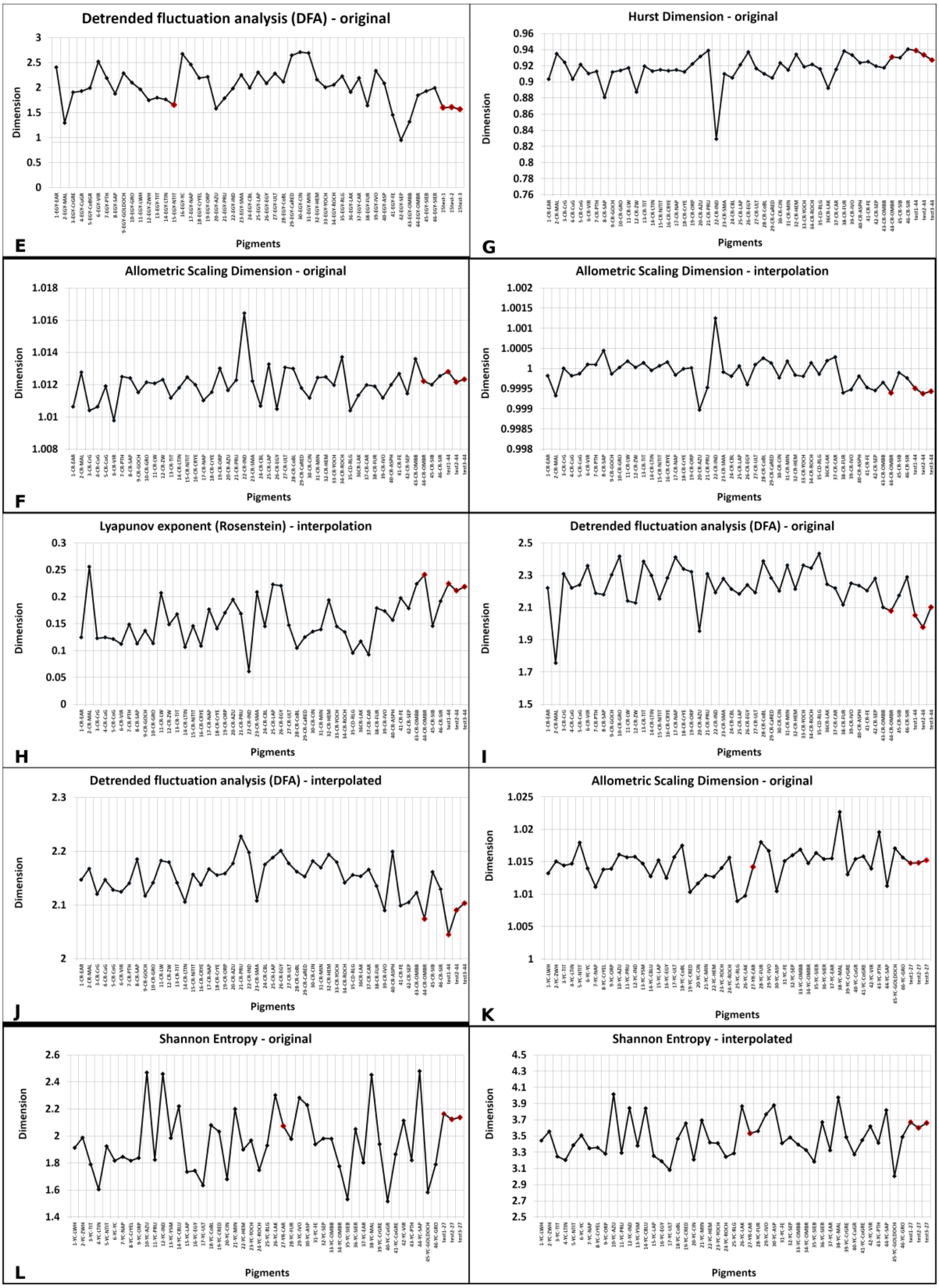

Figure 11. Egyptian blue surface color. Complexity measures for the original and interpolated data. A) Allometric Scaling Dimension without and with interpolation, B) Katz Dimension without and with interpolation and with subsequent boxes. Tests Correspond to: original, interpolation and Subsequent boxes; C) Sevcik Dimension without interpolation and with subsequent boxes; D) Sample Entropy without and with interpolation, (E) Detrended fluctuation analysis (DFA), original data. Red marks the three tests and the measured "unknown". Red Cadmium: F) Allometric Scaling Dimension without and with interpolation; G) Hurst coefficient without interpolation; H) Lyapunov with interpolation, I) Detrended fluctuation analysis, original, J) Detrended fluctuation Analysis interpolated; Cadmium yellow: K) Allometric without interpolation, L) Shannon entropy without and with interpolation

In general, the most suitable complex dimension for all three cases is the Allometric Scaling Dimension. However, the three tests are slightly distant (~5%) from the corresponding measured sample and the few mentioned above, as illustrated in Figures 11-12 with red circles and lines.

Overall, analyzing short data (original data) versus long data (interpolated) using fractal, entropy, and complexity measures can yield similar but not identical results.

4. DISCUSSION OF THE RESULTS

The present investigation demonstrates the effective separation of painted surfaces based on their color appearance as a result of the artist's technique. In each painting (icons in the present study) the artist processes the pigments used on a specially prepared support and substrate in order to reproduce the perception of color in accordance with his technique and color visual sense. The wide use of inorganic and organic pigments ultimately produces the effect we recognize in a painted image. The color surfaces vary so that a wide spectrum of colors exists. In addition, several times the original painted surfaces are overpainted. Of particular interest is the artistic rendering of color in the work. Which means that it is interesting to investigate the pigments used in a painted layer and also the combined visual effect in painted works. In the present investigation, for the first time, we construct a wide variety of color surfaces on panels as a data base and demonstrate that NIR spectral emissions can be grouped into similar or closest colors by applying statistical hierarchical clustering with accompanying group validity tests, which results are combined by the applied complexity and entropy measures.

In this way, the spectral cube of a painting in the spectral range 420-1000 nm can be identified with the closest sample of the painting surface data base (plain or overpainted) and the color or the combination of pigments that render the color can be identified.

This concept has been applied to three sets of 135 painted panels and were thoroughly processed, out of 2070 experimentally home-made painted panels.

The statistical analysis for this set led to quite clear results regarding the group containing the 3 tests generated, as it is very different from the rest generated, and this is supported in many ways by statistical tests.

The **1st set** with Egyptian blue as the surface color: The three tests clearly group together with 15-EGY-NTIT which is the metric they were created from, but also with four pigments: titanium zinc white, lead tin yellow, Naples and chromium; however, zinc and titanium white could be considered as forming a separate cluster. It is of interest the obtained result which revealed an increased probability of locating the unknown color among many in the database, and it is limited to the correct sample or at most one more (Table S1). Thus, for the Set 1 the 3 tests (random values within 3% of 15-EGY-NTIT) of original and interpolated strings together with the No 15-EGY-NTIT are a common aspect in both *statistical groupings* concerning the cluster with those colors that group together with the 3 tests and the "unknown" No 15 sample, and those groups from *Allometric, Katz, Sevcic and Sample entropy*. In all five methods used the three tests, group together with the No 15 (as should be expected) as a common entry and the No 14. This way applying these methods and making a simple clustering any unknown color should correspond between a choice of two to be the right one. In fact, the No 14-EGY-LTIN is next in resemblance being close to No 15 on the two colors used as underlie the nickel-titanium and lead tin, both being yellow pigments. However, we believe that when a sample is present in all methods of original and interpolated data this should be attributed to the unknown; in our case the No 15 that is the anticipated too. The use of interpolated string data only strengthens the result in the Allometry and statistics (dendrograms and PCA) including also the No 14-EGY-LTIN. Hence the combination of fractal and statistical results increases the probability of locating the unknown overpainted panel among many in the database.

The **2nd set** with red cadmium red surface color: The three tests (44-test1, 2, 3) clearly group together with 44-CR-OMBR (ombre raw) which is the metric they were created from, but also with underlie pigments of sienna raw (a yellowish brown), ivory (a pale white) and Prussian (bluish) could be considered as forming a separate cluster ("21-CR-PRU", "39-CR-IVO", "40-CR-ASPH", "42-CR-SEP", "43-CR-OMBB", "44-CR-OMBR", "45-CR-SIB", "46-CR-SIR", "test1-44", "test2-44", "test3-44"). In this set with red surface color the *Allometric Scaling Dimension,* the *Hurst coefficient* without interpolation, the *Tug of war* dimension, and the *Lyapunov exponent* with interpolation seem to approach a highly probable result giving to the three tests a number of probable colors. (See Table 1B). However, applying the 4 methods most appropriate for red upper surface all pinpoint as common the No 44 which is the right one.

Table 1. A) Egyptian blue. The samples (noted in x) of respective methods closest to No 15 and others within < 3% variation, including the three tests. Note the No 14-EGY-LTIN is next in resemblance being close to No 15. Both these two colors have used as underlie the nickel-titanium and lead tin, both being yellow pigments. At any rate, only the sample present in all methods of original and interpolated data should be attributed to the unknown, in our case the No 15, that is the anticipated too. B) Red chromium and C) Yellow chromium the surface color. The red cross represents the „unknown" sample which lies also within ±3% of the three tests and other samples per method.

(A)

Sample No	**Staτ.**	**All. O.**	**All. I.**	**Katz O.**	**Katz I.**	**Katz S.**	**Sev. O.**	**Sev. I.**	**SampEn. O.**	**SampEn. I.**	**DFA O.**	**KC – ZLIB O.**
1			X	X								
2												
3												
4												
5				X								X
6									X			X
7												X
8			X									X
9												
10					X	X				X		
11					X	X		X		X		X
12	X							X		X		X
13	X	X						X	X			X
14	X	X	X	X	X	X	X	X		X		X
15	**X**	**X**	**X**	**X**	**X**	**X**	**X**	**X**	**X**	**X**	**X**	**X**
16	X			X	X	X	X			X		X
17	X											X
18	X											X
19				X					X			
20								X				
21			X								X	
22			X									
23												
24				X	X	X						
25				X								X
26		X		X								
27		X										X
28		X										X
29												
30												
31									X			X
32												
33												
34												X
35												
36												
37												
38		X									X	
39												
40				X								
41				X				X				
42					X					X	X	
43		X										
44							X		X			
45										X		X
46										X		

(B & C)

	3b red								3c yellow			
Sample No	**Statistics**	**All. O.**	**All. I.**	**Hurst O.**	**Lyap I.**	**DFA O.**	**DFA. I.**		**Statistics**	**All. I.**	**Sha. O.**	**Sha. I.**
1												
2		X	X	X	X					X		X
3				X						X		
4										X		
5		X										
6										X		
7		X										
8		X										
9									X			
10		X										
11		X			X							
12		X										
13										X		
14												
15		X								X		
16		X							X			
17												
18											X	
19												X
20				X								
21	X	X	X	X							X	
22												
23		X			X				X	X		
24									X			
25					X							
26				X	X							
27									X	X	X	X
28												X
29												
30												
31		X								X		
32		X		X								
33		X										
34										X		
35												
36											X	X
37		X										
38		X	X	X		X	X					
39	X		X	X					X			X
40	X	X					X		X			
41		X	X				X					
42	X		X							X	X	X
43	X				X	X						
44	X	X	X	X	X	X	X					
45	X	X		X					X			
46	X	X								X		

The **3rd set** with yellow cadmium as surface color: The three tests (27-test1, 2, 3) clearly group together with 27-YR-CAR (carmine) which is the metric they were created from, but also with underlie pigments of 45-YC-GoldOCHRE, 24-YC-ROCHRE (red ochre), 9-YC-ORPm(orpiment), 23-YC-YOCH (yellow ochre), 16-YC-EGY (Egyptian blue), 39-YC-CrORE (chromium green), and 40-YC-CuGR (copper green), which could be considered as forming a separate cluster. The 3 methods applied (statistical, Allometric dimension and Shannon) indicate as common color No 27 which is the anticipated.

Table 1C gives the groups of various methods for yellow surface color within which the three tests fall in relation to No.27.

In the complexity measures some of the different processing methods gave respectively the anticipated result for 8 of them: the *Allometric Scaling Dimension* and the *Sample Entropy*, the *Katz dimension* with Subsequent boxes and the *Sevcik* dimension also gives a good result in all its cases, and in the interpolated the *Sample entropy*. Due to the algorithmic characteristics that process the data it is found that specific complexity measures identify the right panel of a particular-colored surface, even beyond the single layer with underlie a ground preparatory. These measures together with statistical elaboration provide a common color which as it is found is the right data set. That is an unknown overpainted panel can be identified with success.

5. CONCLUSION

Spectral data measured by a multispectral NIR camera in the range 400-1000nm and in 30 equally spaced spectral cubes were processed by statistical hierarchical methods and fractal algorithms and complexity measures. Overpainted artworks of two painted layers made in the laboratory and following traditional techniques during Byzantine times created a data base in total 45 pigments (named as colors), covering the same 45 colors hence producing 2025 combinations plus 45 single colors that act as reference points; a total of 2070 plates, were constructed. It was shown that present methodology enhanced the previous ones by identifying icons with overpainted layers using Mu.S.I.S NIR camera and analyzing the spectral data by a new concept. The novelty of this study is therefore suitable for implementation in many panel and mural painting.

Such a multispectral overpainted artworks using various pigments on canvas/wood have not been investigated in depth concerning possible attribution of a sub-painted layer. This palimpsest-like painted panels have been approached here with the novel corroborated statistical concept and fractal algorithms. Three sets each one with three different upper pigment/colors; Egyptian blue, red (cadmium), and yellow (cadmium) respectively, were fully exploited.

A detailed statistical clustering supported by statistical tests (average, complete and ward linkage, K-means, Wilks test, Silhouettes, PCA) was applied. The resulted clusters of overpainted panels with certain pigments were supported by statistical tests. Three to five groups of overpainted panels were found for the three sets.

In addition, a thorough investigation by fractal, complexity and entropy algorithms were applied on three processing data (original, interpolated, subsequent boxes). The three tests (created by a metric sample by random process but within a 3% variation per each of the 30 data values) were compared with the metric sample and the analysis have proved this anticipating matching. The matching unavoidably included some other overpainted two pigment layers test panels. This result may be explained as due to the variable painted surfaces by the non-uniform painting of the artist, and uneven surfaces and this uncertainty needs a further future investigation. Allometric method followed by the Sample Entropy, the Katz dimension, the Sevcik dimension, the Shannon, the DFA and the Sample entropy excluding the majority of the nine algorithms were found appropriate to use. The convergence of all these algorithms to the same or may be additional sample, is a criterion of attributing to that sample the "unknown". Thus, the methodology and methods of complexity in coordination with the hierarchical clustering can be used in the future (work in progress) for similar investigations of overlapping paintings. Hence, an unknown painted work can be compared to our present data base applying the respective methods per surface color and may identify the probable color which proved to be the anticipated one.

Acknowledgements: I.L. is thankful for support of the Sino-Hellenic Academic Project (www.huaxiahellas.com) from Key Research Institute of Yellow River Civilization and Sustainable Development & Collaborative Innovation Center on Yellow River Civilization of Henan Province, Henan University, Kaifeng, China. I.A. was supported by a grant from the Ministry of Research, Innovation and Digitization, CNCS/CCCDI-UEFISCDI, project number PN-III-P2-2.1-SOL-2021-0084. M.B was funded by State Scholarships Foundation (IKY). We thank the two anonymous referees for constructive comments. We thank Prof. I. Karapanagiotis, Aristotle University of Thessaloniki, and Prof .M-P. Colombini, Universita di Pisa, for very useful suggestions. Last, but not least, IL thanks Prof Karl Ziemelis Chief Physical Sciences Editor at Nature for his encouraging recommendations about the niche application of present analysis strategy.

Author Contributions: I.L., A.A., D.M.: led project design, the coordination of the project and contracting; M.B., made the technical preparation of the panels under the supervision of Prof. Athena Alexopoulou and for collection of Mu.S.I.S IR camera readings and the normalization readings guided by Prof. I.Liritzis and provided respective text description; I.L., I.P., I.A., H.A, M.R., led data processing and analysis. I.P., made the statistical analysis; I.A., made the fractal and complexity analysis; A.A., D.M., and I.L., provided instrumentation concepts and contributed to the identification of study outcomes; I.L., Conceived the statistical and complexity methodology and processing and wrote the drafting of the manuscript; I.L., A.A., I.P., I.A., contributed to the corrected and redrafting of the manuscript; I.L., A.A., I.P., I.A, D.M., were involved in the interpretation of the results, and the critical review, and all senior authors involved in the approval of the manuscript. The present project of the team was part of an ongoing PhD and was initiated during December 2022. According to the rules of department at least one publication should be made with the consent of the three-member supervising committee (IL, AA, DM). During the writing of this article the exact contribution of each co-author is described above, with the prohibitive restriction of I.A. and I.P. as the analytical statistical and complexity procedure used exclusively for this article and not as part of a doctoral thesis.

REFERENCES

Adamson, P. (2006). Vision, light and color in al-kindī, Ptolemy and the ancient commentators. *Arabic Sciences and Philosophy*, Vol. 16/2, 207–236. https://doi.org/10.1017/S0957423906000312

Afifi, H. A. M., Etman, M. A., Abdrabbo, H. A. M., & Kamal, H. M. (2020). Typological study and non-destructive analytical approaches used for dating a polychrome gilded wooden statuette at the grand Egyptian museum. *Scientific Culture*, Vol. 6/3, 69–83. https://doi.org/10.5281/ZENODO.4007568

Ahammer, H. (2023). *ComsystanJ* (2.1.0) [Java]. Medical University of Graz. https://comsystan.github.io/comsystanj

Albini, M., Ridolfi, S., Giuliani, C., Pascucci, M., Staccioli, M. P., and Riccucci, C. (2020). Multi-Spectroscopic Approach for the Non-invasive Characterization of Paintings on Metal Surfaces. *Frontiers in Chemistry*, Vol. 8, 289. https://doi.org/10.3389/fchem.2020.00289

Alexopoulou, A., Kaminari, A. A., and Moutsatsou, A. (2019). Multispectral and Hyperspectral Studies on Greek Monuments, Archaeological Objects and Paintings on Different Substrates. Achievements and Limitations. In A. Moropoulou, M. Korres, A. Georgopoulos, C. Spyrakos, and C. Mouzakis (Eds.), *Transdisciplinary Multispectral Modeling and Cooperation for the Preservation of Cultural Heritage* (Vol. 962, pp. 443–461). Springer International Publishing. https://doi.org/10.1007/978-3-030-12960-6_31

Alfeld, M., Janssens, K., Dik, J., de Nolf, W., and van der Snickt, G. (2011). Optimization of mobile scanning macro-XRF systems for the in situ investigation of historical paintings. *J. Anal. At. Spectrom.*, Vol. 26/5, 899–909. https://doi.org/10.1039/C0JA00257G

Alfeld, M., Snickt, G., Vanmeert, F., Janssens, K., Dik, J., Appel, K., Loeff, L., Chavannes, M., Meedendorp, T., and Hendriks, E. (2013). Scanning XRF investigation of a Flower Still Life and its underlying composition from the collection of the Kröller–Müller Museum. *Applied Physics A*, Vol. 111/1, 165–175. https://doi.org/10.1007/s00339-012-7526-x

Ali, M. F., Darwish, S. S., and El Sheikha, A. M. (2020). Multispectral analysis and investigation of overlapping layer cartonnage fragments from Egyptian museum, Cairo. *Scientific Culture*, Vol. 6/3, 69–83. https://doi.org/10.5281/ZENODO.3956805

Ashkenazi, D., Shnabel, R., Lichtenberger, A., and Tal, O. (2021). Chemical Composition and Microstructure Analysis of Plaster and Pigments Retrieved from a Decorated House Wall at Seleucid Tell Iẓṭabba (Nysa-Scythopolis, Beth She'an, Israel). *Mediterranean Archaeology and Archaeometry*, Vol. 21/3. https://doi.org/10.5281/ZENODO.5598239

Balas, C., Epitropou, G., Tsapras, A., and Hadjinicolaou, N. (2018). Hyperspectral imaging and spectral classification for pigment identification and mapping in paintings by El Greco and his workshop. *Multimedia Tools and Applications*, Vol. 77/8, 9737–9751. https://doi.org/10.1007/s11042-017-5564-2

Balas, C., Papadakis, V., Papadakis, N., Papadakis, A., Vazgiouraki, E., and Themelis, G. (2003). A novel hyper-spectral imaging apparatus for the non-destructive analysis of objects of artistic and historic value. *Journal of Cultural Heritage*, Vol. 4, 330–337. https://doi.org/10.1016/S1296-2074(02)01216-5

Baxter, M. J. (2015). *Exploratory multivariate analysis in archaeology*. Percheron Press, a division of Eliot Werner Publications, Inc.

Bratitsi, M., Liritzis, I., Alexopoulou, A., and Makris, D. (2019). Visualising underpainted layers via spectroscopic techniques: A brief review of case studies. *Scientific Culture*, Vol. 5/3, 55–68. https://doi.org/10.5281/ZENODO.3340112

Caley, E. R., and Richards, J. F. (1956). *Theophrastus on stones: Introduction, greek text, english translation, and commentary*. Ohio State University.

Casini, A., Lotti, F., Picollo, M., Stefani, L., and Buzzegoli, E. (1999). Image Spectroscopy Mapping Technique for Non-Invasive Analysis of Paintings. *Studies in Conservation*, Vol. 44/1, 39. https://doi.org/10.2307/1506694

Cosentino, A. (2016). Transmittance spectroscopy and transmitted multispectral imaging to map covered paints. *Conservar Património*, Vol. 24, 37–45. https://doi.org/10.14568/cp2015021

Cristoforetti, G., Legnaioli, S., Palleschi, V., Salvetti, A., and Tognoni, E. (2006). Optical chemical sensors for cultural heritage. In F. Baldini, A. N. Chester, J. Homola, and S. Martellucci (Eds.), *Optical Chemical Sensors* (Vol. 224, pp. 515–526). Springer Netherlands. https://doi.org/10.1007/1-4020-4611-1_25

Daniel, F., Mounier, A., Pérez-Arantegui, J., Pardos, C., Prieto-Taboada, N., Fdez-Ortiz De Vallejuelo, S., and Castro, K. (2017). Comparison between non-invasive methods used on paintings by Goya and his contemporaries: Hyperspectral imaging vs. point-by-point spectroscopic analysis. *Analytical and Bioanalytical Chemistry*, Vol. 409/16, 4047–4056. https://doi.org/10.1007/s00216-017-0351-5

Degano, I., Ribechini, E., Modugno, F., and Colombini, M. P. (2009). Analytical Methods for the Characterization of Organic Dyes in Artworks and in Historical Textiles. *Applied Spectroscopy Reviews*, Vol. 44/5, 363–410. https://doi.org/10.1080/05704920902937876

Delaney, J. K., Dooley, K. A., Radpour, R., and Kakoulli, I. (2017). Macroscale multimodal imaging reveals ancient painting production technology and the vogue in Greco-Roman Egypt. *Scientific Reports*, Vol. 7/1, 15509. https://doi.org/10.1038/s41598-017-15743-5

Dyer, J., Verri, G., and Cupitt, J. (Directors). (2013). *'Multispectral Imaging in Reflectance and Photo-induced Luminescence modes: A User Manual.'* European CHARISMA Project.

Eastaugh, N., Walsh, V., Chaplin, T., and Siddall, R. (2008). *Pigment compendium: A dictionary and optical microscopy of historical pigments: Vol. (Author)* (2è ed). Butterworth-Heinemann.

Evans, E. H., Pisonero, J., Smith, C. M. M., and Taylor, R. N. (2023). Atomic spectrometry update: Review of advances in atomic spectrometry and related techniques. *Journal of Analytical Atomic Spectrometry*, Vol. 38/5, 974–999. https://doi.org/10.1039/D3JA90013D

Fairchild, M. D. (2005). *Color appearance models* (2nd ed). J. Wiley.

Falco, C. M. (2009). Invited Article: High resolution digital camera for infrared reflectography. *Review of Scientific Instruments*, Vol. 80/7, 071301. https://doi.org/10.1063/1.3174431

Favero, P. A., Mass, J., Delaney, J. K., Woll, A. R., Hull, A. M., Dooley, K. A., and Finnefrock, A. C. (2017). Reflectance imaging spectroscopy and synchrotron radiation X-ray fluorescence mapping used in a technical study of The Blue Room by Pablo Picasso. *Heritage Science*, Vol. 5/1, 13. https://doi.org/10.1186/s40494-017-0126-5

Fischer, C., and Kakoulli, I. (2006). Multispectral and hyperspectral imaging technologies in conservation: Current research and potential applications. *Studies in Conservation*, Vol. 51, 3–16. https://doi.org/10.1179/sic.2006.51.Supplement-1.3

Harley, R. D. (2001). *Artists' pigments c.1600-1835: A study in English documentary sources* (2nd rev. ed). Archetype Publ.

Healy, J. F. (1999). *Pliny the Elder on science and technology*. Oxford University Press.

Hetherington, P. (1989). *The "Painter's manual" of Dionysius of Fourna: An English translation [from the Greek] with commentary of cod. gr. 708 in the Saltykov-Shchedrin State Public Library, Leningrad*. Sagittarius Press ; Oakwood Publications.

Janssens, K. H. A., and Van Grieken, R. E. (2004). *Non-destructive microanalysis of cultural heritage materials*. Elsevier.

Janssens, K., Van Der Snickt, G., Vanmeert, F., Legrand, S., Nuyts, G., Alfeld, M., Monico, L., Anaf, W., De Nolf, W., Vermeulen, M., Verbeeck, J., and De Wael, K. (2017). Non-Invasive and Non-Destructive Examination of Artistic Pigments, Paints, and Paintings by Means of X-Ray Methods. In R. Mazzeo (Ed.), *Analytical Chemistry for Cultural Heritage* (pp. 77–128). Springer International Publishing. https://doi.org/10.1007/978-3-319-52804-5_3

Kakabas, G. (2008). *Dionysios of Fourna (c. 1670 - c. 1745): Artistic creation and literary description*. Alexandros Press.

Katsaros, T., Liritzis, I., and Laskaris, N. (2010). Identification of Theophrastus' pigments egyptios yanos and psimythion from archaeological excavations: A case study. *ArchéoSciences*, Vol. 34, 69–80. https://doi.org/10.4000/archeosciences.2632

Katsaros, Th., Liritzis, I., and Laskaris, N. (2009). Is White Pigmnet On Appeles Palette A TiO2 Rich Kaolin? New Analytical Results On The Case of Melian—Earth. *Mediterranean Archaeology and Archaeometry*, *9*, 29–35.

Liang, H. (2012). Advances in multispectral and hyperspectral imaging for archaeology and art conservation. *Applied Physics A*, Vol. 106/2, 309–323. https://doi.org/10.1007/s00339-011-6689-1

Loeb, J., and Henderson, J. (1970, January 1). *Aristotle, "On Colours."* Loeb Classical Library. https://www.loebclassics.com/view/aristotle-colours/1936/pb_LCL307.5.xml

Loeff, L. S. V. der, Alfeld, M., Meedendorp, T., Dik, J., Hendriks, E., Snickt, G. V. der, Janssens, K., and Chavannes, M. (2012). *Rehabilitation of a Flower Still Life in the Kroller-Muller Museum and a lost Antwerp painting by Van Gogh* (L. van Tilborgh, D. van Halsema, J. House, and G. Weisberg, Eds.; pp. 33–53). WBOOKS.

MacDonald, L. W., Vitorino, T., Picollo, M., Pillay, R., Obarzanowski, M., Sobczyk, J., Nascimento, S., and Linhares, J. (2017). Assessment of multispectral and hyperspectral imaging systems for digitisation of a Russian icon. *Heritage Science*, Vol. 5/1, 41. https://doi.org/10.1186/s40494-017-0154-1

Mastrotheodoros, G.P., and Beltsios, K.G. (2022). Recipes for pigment manufacturing in greek post-byzantine painting manuals. *Scientific Culture*, Vol. 8/1, 147–159. https://doi.org/10.5281/ZENODO.5772478

Noble, P., Loon, A. van, Alfeld, M., Janssens, K., and Dik, J. (2012). Rembrandt and/ or studio, Saul and David, c.1655: Revealing the curtain using cross-section analyses and X-ray fluorescence imaging. *Techne*, Vol. 35, 36–45.

Oltrogge, D. (2011). Byzantine recipes and book illumination. *Revista de Historia Da Arte*, *No. Especial*, 53–61.

Papageorgiou, I. (2020). Ceramic investigation: How to perform statistical analyses. *Archaeological and Anthropological Sciences*, Vol. 12/9, 210. https://doi.org/10.1007/s12520-020-01142-x

Parpulov, G. R., Dolgikh, I. V., and Cowe, P. (2010). A Byzantine Text on the Technique of Icon Painting. *Dumbarton Oaks Papers*, Vol. 64, 201–216. JSTOR. http://www.jstor.org/stable/41480886

Picollo, M., Cucci, C., Casini, A., and Stefani, L. (2020). Hyper-Spectral Imaging Technique in the Cultural Heritage Field: New Possible Scenarios. *Sensors*, Vol. 20/10, 2843. https://doi.org/10.3390/s20102843

Rampazzi, L., Brunello, V., Corti, C., and Lissoni, E. (2017). Non-invasive techniques for revealing the palette of the Romantic painter Francesco Hayez. *Spectrochimica Acta Part A: Molecular and Biomolecular Spectroscopy*, Vol. 176, 142–154. https://doi.org/10.1016/j.saa.2017.01.011

Rosi, F., Miliani, C., Clementi, C., Kahrim, K., Presciutti, F., Vagnini, M., Manuali, V., Daveri, A., Cartechini, L., Brunetti, B. G., and Sgamellotti, A. (2010). An integrated spectroscopic approach for the non-invasive study of modern art materials and techniques. *Applied Physics A*, Vol. 100/3, 613–624. https://doi.org/10.1007/s00339-010-5744-7

Schindelin, J., Arganda-Carreras, I., Frise, E., Kaynig, V., Longair, M., Pietzsch, T., Preibisch, S., Rueden, C., Saalfeld, S., Schmid, B., Tinevez, J.-Y., White, D. J., Hartenstein, V., Eliceiri, K., Tomancak, P., and Cardona, A. (2012). Fiji: An open-source platform for biological-image analysis. *Nature Methods*, Vol. 9/7, 676–682. https://doi.org/10.1038/nmeth.2019

Stork, D. G., and Kossolapov, A. J. (2011). X-ray image analysis of Lorenzo Lotto's Husband and wife. *Proc. SPIE 7869, Computer Vision and Image Analysis of Art II*, 78690L, 1–10. https://doi.org/10.1117/12.873191

Targowski, P., and Iwanicka, M. (2012). Optical Coherence Tomography: Its role in the non-invasive structural examination and conservation of cultural heritage objects—a review. *Applied Physics A*, Vol. 106/2, 265–277. https://doi.org/10.1007/s00339-011-6687-3

Van Asperen De Boer, J. R. J. (1968). Infrared Reflectography: A Method for the Examination of Paintings. *Applied Optics*, Vol. 7/9, 1711. https://doi.org/10.1364/AO.7.001711

van Asperen de Boer, J. R. J. (1975). An introduction to the scientific examination of paintings. *Nederlands Kunsthistorisch Jaarboek (NKJ) / Netherlands Yearbook for History of Art*, Vol. 26, 1–40. JSTOR. https://doi.org/10.1163/22145966-90000688

Vilaseca, M., Pujol, J., Arjona, M., and De Lasarte, M. (2006). Multispectral system for reflectance reconstruction in the near-infrared region. *Applied Optics*, Vol. 45/18, 4241. https://doi.org/10.1364/AO.45.004241

Wueller, D., and Kejser, U. B. (2016). *Standardization of Image Quality Analysis – ISO 19264*. https://doi.org/10.2352/issn.2168-3204.2016.1.0.111.

SUPPLEMENTARY MATERIAL

INTRODUCTION

Pigments are classified based on their source (organic or inorganic) and their chemical composition and physical properties, including solubility (Degano et al., 2009). Ancient pioneers such as Aristotle, Theophrastus, Claudius Ptolemy, and Pliny the Elder have laid the foundation and recorded past knowledge on pigments, including color mixing techniques (Adamson, 2006; Caley and Richards, 1956; Loeb and Henderson, 1970; Healy, 1999; Katsaros et al., 2009, 2010).

Extensive analysis of Byzantine and post-Byzantine icon cases, in pigments and stratigraphy, has been conducted using various techniques such as XRF, SEM/EDX, μRaman, FTIR, HPLC, and earlier versions of multispectral imaging systems (Daniilia et al., 2008; Valianou et al., 2011; Iordanidis et al., 2013; Gehad et al., 2015; Alexopoulou and Kaminari, 2008; Janssens et al., 2017; Khasawneh and Elserogy, 2019; Karydis et al., 2019; Mastrotheodoros and Beltsios, 2022; Lazidou et al., 2018; Karapanagiotis et al., 2013; Sotiropoulou et al., 2010; Karapanagiotis et al., 2007). Previous studies have employed MU.S.I.S system and its earlier versions, combining a hyperspectral camera with innovative electro-optic tunable filters, alongside spectral analysis and classification algorithms. The Maximum Likelihood algorithm demonstrated excellent performance in identifying and differentiating single pigments with similar hues but different chemical compositions, achieving accuracies ranging from 80.3% to 99.7% when used to analyze materials used by El Greco and his workshop (Balas et al., 2018; Theodoropoulou and Tsairis, 2000).

Legnaioli et al. (Legnaioli et al., 2013a, 2013b) explored the application of various Blind Source Separation algorithms with a multispectral camera (Chroma C4) to enhance hidden patterns and retrieve hidden information in paintings. They also employed a simpler method known as the "false-colors" technique, which involved selecting three channels from the multispectral set and superimposing them to create a false-color image, combining infrared, red, blue, and green channels.

Underdrawings can be better examined in paintings before 16th-century, as they contain highly reflective grounds with black carbon-based underdrawings that absorb strongly the infrared. Also, the availability of the detectors is now wide and of course extends to multi-spectral and hyper-spectral imaging (Daniilia et al., 2008; Valianou et al., 2011; Iordanidis et al., 2013; Gehad et al., 2015; Alexopoulou and Kaminari, 2008; Janssens et al., 2017; Khasawneh and Elserogy, 2019; Karydis et al., 2019; Mastrotheodoros and Beltsios, 2022).

Given the tolerances in creating a painted panel/icon and normalizing the obtained images using the Mu.S.I.S IR camera, the double layered colored pigments data were analyzed using statistical and complexity measures methods.

The present study is for first time devised as methodology and sample preparation and aims to determine if a random image/icon has overlays and, if so, identify the underlying color by fitting its spectral cube into the cluster groups formed from the analysis of samples in a simulated database of overpainted panels. For this purpose, three sets were created, one with upper Egyptian blue and the other two with cadmium red and cadmium yellow as the overlying colors, each set comprising 45 underlying colors. Additionally, a set representing the preparation stage was included. Three test measurements were conducted, with spectral values having a ±3% distance from specific measurements.

The objective of this analysis is to identify groups within the data and classify each pixel into one of these groups based on its similarity to the remaining spectra that comprise the validation data set. The selection of the optimal classification model or spectrum similarity metric is typically specific to the application at hand. Experimental evaluation of algorithm accuracy is crucial since theoretical research alone cannot determine the best-performing algorithm(s). In contrast to earlier observations using ISODATA (a variant of K-means), unsupervised methods, particularly the K-means variation, have yielded satisfactory results (Balas et al., 2018).

Because wall murals and portable icons were functional artifacts of devotion, they were overpainted anytime they were damaged and no longer recognizable. In rare cases, complete paintings were repainted with previous iconographies at the desire of the owner or because various eras enforced different norms. The issue of overpainting with meticulous experimental set up of two layered painted panels involves particular sample preparation, taking measurements in near IR by a standardized camera of the spectral data (400-1000μm) analyzed and collecting many spectral data from applied statistical hierarchical techniques and complexity measures. Below additional data and information is given beyond the material in the main article.

Sample preparation

It was important for the samples to adhere to the standards of creating experimental paintings for infrared detection (Moutsatsou & Alexopoulou 2014, p.3-9) and also align with the traditional recipes for making Byzantine portable icons using the egg tempera technique, while including the pigments commonly used by Byzantine and post-Byzantine hagiographers (Taylor, 1979) (see Table S0). Note that e.g. titanium white, zinc white have been only scarcely reported in the byzantine and post-byzantine palette (Biligi-Genc et al, 2023; Mastrotheodoros et al., 2023; Eastaugh et al., 2008)

TABLE S0 The pigments (colors) used for the painted layers.

White	Black	Yellow	Red	Blue	Green	Earthen
White lead	Carbon black	Yellow lead tin	Cadmium red	Blue azurite	Earth green	Golden ochres
Zinc white	Black ivory	Nickel titanium yellow	Red cinnabar	Blue of Prussia	Malachite Green	Ochres yellow
Titanium White	Black asphalt	Cadmium yellow	Red minion	Indigo blue	Chrome Green	Time red
		Naples Yellow	Red hematite	Blue Enamel	Copper green	Ombre raw
		Chrome yellow	Red realgar	Cerulean Blue	Cobalt Green	Ombra baked
		Yellow Orpiment	Red Lake	Blue Lapis Lazulli	Viridian Green	Sienna raw
			Carmine red	Egyptian blue	Phthalate green	Baked Sienna
				Ultramarine blue	Green Sap	Sepia brown
				Cobalt blue		Iron brown

The experimental samples comprised a total of 30 panels made from marine plywood, prepared with plaster and the adhesive substance rabbit glue, and divided into 81 squares each (Dardes and Rothe, 1998; Berns, 2005). The organic medium used was egg yolk, as required by the traditional egg tempera technique, while a multispectral study was also conducted (Arroyo et al., 2008). The panel plates were 30x30 cm in size and 8 mm thick. The wood panels were lightly sanded initially to smoothen imperfections, ensuring the use of fine sandpaper to prevent the removal of wood fibers. There was a total of 30 panel plates, 5 of which consisted of 45 single colors/layers directly on the preparation layer (see Fig. S1), while the remaining 25 panels contained overpainted layers with 81 overpainted stripes or small squares (refer to Fig. 1a-d of main article). The materials chosen for the preparatory drafts represented the five most common pigments used in traditional hagiography and were also selected based on the researchers' previous work on prototype construction (Walmsley et al., 1994; Saunders et al., 2006).

These panel are in total of 30. The 5 of them consist of 45 single colors/layers (5 panels by 9 stripes of single pigments per panel) directly on the preparation layer (see Fig.S1).

Data derivation and description

The data of these three sets and the 9 test samples are given in Tables S1-S3.

Figure S1. The 5 panels with single layer pigments on the preparation with: 1. green, 2. blue 3. white and yellow, 4. black and earthy and 5. red pigments are shown in order.

CALIBRATION, CAMERA SETTING AND STANDARDIZATION

Calibration

Reflectance spectra calculations that are independent of ambient light conditions were achieved through calibration. An experimental procedure was conducted to determine the camera's error and highlight the significance of standardization in data measurements (see below). Subsequently, measurements were taken at the same points using the corresponding normalized image (as described below) to observe the resulting differences and demonstrate the efficacy of the normalization process.

The camera produced a spectral cube through a series of 30 shots covering the spectrum range of 420-1000 nm with 20 nm intervals. This spectral cube was loaded into the camera program, allowing for both graphical representation and numerical data of the spectrum.

Standardization of measurements

The photos were continuous after several trials and attempts so that there was, as much as possible, no change in the setting and capturing conditions. At the beginning of the shooting process, an initial photo was taken that is to scale on gray photographic paper and that will act as a reference card. The settings made for the reference card capture, which became the standard for all subsequent captures and aided in the normalization involved measuring the color checker's grayscale gradation reading to be the next gradation equal to twice the previous reading. In order to do this, through the histogram option of the photoshop image editor, the gray scale was measured for each square of the gray scale of the color checker scale, where each one was almost twice the size of the previous one, from the black to white, while the value in the area in the spectralon should not exceed 250 which is the value of white, thus it is avoided the shot to be overexposed.

Many tests were done that related to changing the possibilities provided by the program and related to brightness, luminance, hue, saturation, chroma, lightness (Yu-Ichi, 1980), where through their changes an attempt was made to find out what exactly we should focus on in order to have the right result.

Camera's error evaluation

The purpose of using the MUSES-9 HS imaging sensor was to offer the capability of altering the spatial resolution through pixel binning. The device is capable of supporting extensible spatial resolutions between 8 and 2 megapixels.

An experimental procedure is performed to find the camera's error, but also to demonstrate the importance of standardization for the data measurements.

A measurement was then carried out at the same points but this time on the corresponding normalized image as described above, in order to see the resulting difference and prove the power of the normalization process.

Supplementary Table S1: The numerical data of spectra for the samples with an underlying color of Egyptian blue. The last three refer to the 3 tests and correspond to the measured No. 15 with titanium nickel yellow as the background as No 47, 48, 49.

LOWER COLOR	UPPER COLOR	CODE No	420	440	460	480	500	520	540	560	580	600	620	640	660	680	700	720	740	760	780	800	820	840	860	880	900	920	940	960	980	1000
earth	EGYPTIAN BLUE	1-EGY-EAR	19	17	26	26	27	30	29	28	26	21	16	19	22	32	30	34	39	37	39	43	50	59	63	66	74	74	79	75	80	83
malachite	EGYPTIAN BLUE	2-EGY-MAL	21	27	34	34	37	36	31	27	24	18	15	14	22	20	29	28	30	31	31	28	32	36	39	47	45	50	56	54	57	63
Cr green	EGYPTIAN BLUE	3-EGY-CrGRE	29	23	27	27	28	30	26	20	16	14	13	16	22	27	36	48	57	58	59	64	73	84	101	112	122	123	122	119	118	121
Cu green	EGYPTIAN BLUE	4-EGY-CuGR	25	24	26	27	30	33	26	24	18	15	15	16	22	33	44	52	53	66	73	78	85	96	109	125	137	136	136	129	129	135
cobalt green	EGYPTIAN BLUE	5-EGY-CoBGR	29	35	37	36	38	34	29	27	18	18	16	15	21	29	29	37	47	54	55	61	69	81	99	117	128	127	129	122	123	110
viridian	EGYPTIAN BLUE	6-EGY-VIR	32	35	38	33	36	29	21	20	16	12	14	15	18	28	27	32	47	58	61	64	73	90	112	125	140	139	139	139	141	137
pthalo	EGYPTIAN BLUE	7-EGY-PTH	19	28	36	34	31	18	13	16	13	13	13	12	14	17	19	20	22	27	27	30	34	39	54	59	75	79	90	97	101	107
sap	EGYPTIAN BLUE	8-EGY-SAP	15	13	26	23	24	21	28	20	18	16	15	15	24	34	45	52	55	54	55	60	65	78	96	109	124	124	130	130	131	142
gold ochre	EGYPTIAN BLUE	9-EGY-GOLDOCH	27	34	35	34	31	28	26	26	24	15	16	16	28	34	50	59	63	58	57	63	69	85	97	111	118	121	125	121	123	126
ground	EGYPTIAN BLUE	10-EGY-GRO	29	37	49	54	45	34	30	27	20	16	17	16	21	39	56	63	63	63	62	63	77	83	107	117	131	135	130	135	132	130
lead white	EGYPTIAN BLUE	11-EGY-LWH	30	39	59	57	55	42	33	31	27	19	17	19	30	50	60	75	78	73	73	82	89	103	123	140	149	143	153	146	147	149
zinc white	EGYPTIAN BLUE	12-EGY-ZWH	44	56	75	74	67	55	49	41	33	29	21	27	43	55	88	102	105	96	97	100	103	120	139	163	173	169	173	166	166	163
titan	EGYPTIAN BLUE	13-EGY-TIT	66	71	94	96	78	70	55	45	37	29	26	31	39	53	87	101	99	97	96	98	107	123	145	169	181	186	182	182	177	176
lead tin	EGYPTIAN BLUE	14-EGY-LTIN	22	32	52	57	60	56	49	41	34	28	23	27	34	60	76	85	89	81	81	85	93	105	124	150	169	164	169	167	172	170
nickel titan	EGYPTIAN BLUE	15-EGY-NTIT	22	32	39	55	59	56	57	46	38	31	27	26	34	42	79	83	82	77	78	81	93	105	124	148	161	165	166	162	166	162
cad yellow	EGYPTIAN BLUE	16-EGY-YC	28	28	19	19	23	56	53	57	49	35	32	31	44	66	93	107	109	107	108	103	117	139	152	161	182	185	188	184	186	184
naples	EGYPTIAN BLUE	17-EGY-NAP	18	21	30	36	43	40	35	42	31	30	22	31	46	72	81	85	88	89	90	92	100	115	131	144	171	171	169	166	163	163
Cr yellow	EGYPTIAN BLUE	18-EGY-CrYEL	28	26	17	23	34	37	35	37	30	24	24	26	34	52	75	86	85	80	85	87	99	113	131	152	166	168	172	166	164	160
orpiment	EGYPTIAN BLUE	19-EGY-ORP	30	38	39	43	35	35	30	29	23	15	14	16	29	41	60	69	72	66	66	70	78	97	116	130	150	148	153	148	149	148
azurite	EGYPTIAN BLUE	20-EGY-AZU	18	24	27	31	30	21	21	19	16	13	12	12	15	17	20	21	20	26	27	27	30	36	46	52	60	64	77	89	103	117
prussian	EGYPTIAN BLUE	21-EGY-PRU	20	27	31	31	29	21	21	17	16	13	14	15	19	22	30	32	28	30	32	32	35	34	44	55	58	54	55	54	57	53
indigo	EGYPTIAN BLUE	22-EGY-IND	19	20	15	16	17	21	16	15	15	12	14	13	15	20	26	32	50	59	64	69	75	90	116	125	141	142	155	153	153	158
smalt	EGYPTIAN BLUE	23-EGY-SMA	18	20	28	31	25	18	17	17	14	13	13	14	18	26	37	47	45	49	50	55	62	80	97	106	123	122	126	125	126	124
cerulean blue	EGYPTIAN BLUE	24-EGY-CBL	29	34	49	52	44	30	20	19	14	13	12	11	18	26	60	87	98	96	99	101	111	134	150	161	171	176	176	179	175	162
lapis	EGYPTIAN BLUE	25-EGY-LAP	28	34	37	37	33	26	17	20	15	15	13	13	19	28	38	49	56	57	59	60	68	81	98	113	119	120	123	123	121	124
aigyptian	EGYPTIAN BLUE	26-EGY-EGY	22	29	37	38	36	30	24	20	16	13	13	14	18	28	36	44	41	42	41	43	52	61	76	90	112	110	112	110	108	113
ultramarin	EGYPTIAN BLUE	27-EGY-ULT	25	34	42	36	26	17	15	14	12	13	13	11	14	14	20	29	45	53	57	63	69	77	94	102	117	122	130	132	137	150
cobalt blue	EGYPTIAN BLUE	28-EGY-CoBL	23	27	33	30	26	26	21	15	14	13	12	13	14	17	24	19	24	26	30	37	55	75	103	121	140	143	146	155	152	156
cad red	EGYPTIAN BLUE	29-EGY-CaRED	27	26	20	23	21	18	20	16	17	19	19	24	38	47	64	74	77	78	78	77	93	116	114	128	137	135	139	137	137	128
cinnabar	EGYPTIAN BLUE	30-EGY-CIN	21	24	26	27	23	18	19	16	18	16	18	20	28	40	54	68	73	70	73	73	86	119	122	139	156	154	155	154	149	148
minio	EGYPTIAN BLUE	31-EGY-MIN	21	34	32	29	27	24	19	19	20	18	21	23	36	55	73	83	86	82	75	80	91	125	126	141	162	158	163	160	158	155
aimatite	EGYPTIAN BLUE	32-EGY-HEM	16	21	26	26	20	21	18	17	16	15	16	21	24	32	38	42	47	46	46	48	52	61	64	75	87	86	91	85	92	97
yellow ochre	EGYPTIAN BLUE	33-EGY-YOCH	25	23	28	29	29	28	29	31	29	21	19	22	32	45	57	67	73	73	73	79	81	91	101	106	114	108	111	105	112	113
red ochre	EGYPTIAN BLUE	34-EGY-ROCH	20	21	23	24	21	18	20	17	17	16	16	21	27	35	49	61	65	68	68	67	74	84	100	112	119	128	130	135	136	148
realgar	EGYPTIAN BLUE	35-EGY-RLG	22	23	28	28	27	27	24	28	28	22	18	22	42	56	68	76	75	79	77	81	94	108	128	153	161	162	163	158	155	163
lake	EGYPTIAN BLUE	36-EGY-LAK	19	17	21	20	19	15	17	17	15	15	15	19	30	41	59	72	79	82	89	97	99	106	126	144	158	158	166	166	167	163
carmine	EGYPTIAN BLUE	37-EGY-CAR	17	28	20	20	23	24	19	16	16	16	16	15	22	35	51	63	68	68	68	70	81	101	116	131	141	149	153	153	149	152
furnace	EGYPTIAN BLUE	38-EGY-FUR	23	22	28	28	24	21	16	16	16	15	14	13	14	18	24	20	26	26	24	27	27	33	42	47	50	53	45	49	44	37
ivory	EGYPTIAN BLUE	39-EGY-IVO	30	28	30	29	27	17	16	16	15	13	14	12	15	17	20	20	22	24	26	27	27	30	38	43	47	47	43	44	39	39
asphalt	EGYPTIAN BLUE	40-EGY-ASP	13	12	12	12	13	13	12	12	13	12	13	14	13	15	15	18	14	17	18	18	22	22	27	29	29	40	37	39	35	37
Fe	EGYPTIAN BLUE	41-EGY-FE	24	21	23	22	23	18	18	18	17	15	17	15	17	21	30	35	31	34	31	31	35	37	43	54	53	58	57	52	44	53
sepia	EGYPTIAN BLUE	42-EGY-SEP	15	12	13	15	15	15	16	15	15	13	13	13	14	16	20	22	24	22	22	29	26	23	27	35	37	42	37	47	39	49
ombre burnt	EGYPTIAN BLUE	43-EGY-OMBB	38	18	28	28	24	26	26	18	17	14	14	12	20	21	29	31	28	34	34	40	43	44	55	61	69	68	76	82	70	80
ombre raw	EGYPTIAN BLUE	44-EGY-OMBR	23	27	27	23	27	26	21	21	18	18	18	18	26	26	30	32	33	32	32	31	34	37	53	52	55	56	58	58	59	59
siena burnt	EGYPTIAN BLUE	45-EGY-SIEB	26	26	30	35	31	29	26	21	18	16	17	15	22	31	41	50	52	50	52	52	56	63	69	81	89	99	98	98	97	103
siena raw	EGYPTIAN BLUE	46-EGY-SIER	32	36	36	29	28	26	27	23	19	16	17	15	24	33	50	53	55	53	52	53	58	67	73	87	101	100	94	97	92	97
		15test-1	23	31	40	56	61	54	59	45	39	30	26	25	33	43	78	85	84	79	76	82	90	108	127	150	157	168	169	159	162	167
		15test-2	21	33	38	54	58	58	55	47	38	29	28	27	35	41	81	84	80	75	79	79	96	102	121	144	163	160	171	158	163	158
		15test-3	22	34	41	53	62	55	56	48	37	32	29	28	32	43	77	81	81	76	80	83	92	104	123	152	166	170	161	167	171	160

Supplementary Table S2: the numerical data of spectra for the samples with underlying color cadmium red. The last three refer to the 3 tests and correspond to the measured No. 44 with the underlying raw ombre shadow.

LOWER COLOR	UPPER COLOR	CODE No	420	440	460	480	500	520	540	560	580	600	620	640	660	680	700	720	740	760	780	800	820	840	860	880	900	920	940	960	980	1000
earth	cad red	1-CR-EAR	15	13	14	14	13	14	18	17	23	51	130	168	176	192	185	191	192	190	200	204	203	205	208	202	209	212	209	207	203	200
malachite	cad red	2-CR-MAL	11	12	11	12	12	12	13	13	17	44	78	84	91	88	86	94	87	91	82	88	78	84	78	82	77	78	73	77	67	66
Cr green	cad red	3-CR-CrG	12	12	11	11	11	12	12	12	17	39	114	137	168	173	191	191	189	190	192	197	201	201	196	204	200	204	199	199	203	199
Cu green	cad red	4-CR-CuG	15	13	14	14	13	14	18	17	23	51	130	168	176	192	185	191	192	190	200	204	203	205	208	202	209	212	209	207	203	200
cobalt green	cad red	5-CR-CoG	11	12	12	13	12	13	13	14	16	32	129	168	178	190	202	202	202	204	202	209	206	201	210	209	213	213	207	207	208	202
viridian	cad red	6-CR-VIR	11	12	12	13	12	12	12	13	16	39	121	129	177	183	175	186	198	192	202	202	202	203	213	207	213	213	208	212	216	203
pthalo	cad red	7-CR-PTH	15	12	12	14	12	12	13	14	17	45	122	160	163	176	173	183	186	191	194	191	184	186	191	194	201	202	198	202	204	195
sap	cad red	8-CR-SAP	14	12	12	13	12	12	15	14	17	42	123	152	162	164	177	177	178	188	193	192	195	199	203	194	209	215	210	206	210	208
gold ochre	cad red	9-CR-GOCH	11	13	12	12	12	12	12	13	16	39	120	156	167	172	174	177	180	183	181	191	186	186	191	188	190	187	187	190	189	183
ground	cad red	10-CR-GRO	13	13	13	13	12	13	14	14	18	42	127	173	181	192	208	204	209	210	209	211	212	216	217	217	223	219	217	218	221	217
lead white	cad red	11-CR-LW	20	12	14	15	13	14	14	16	20	44	122	171	191	179	189	208	200	210	206	212	205	207	205	213	203	202	207	212	206	214
zinc white	cad red	12-CR-ZW	19	16	16	15	13	18	17	19	20	45	125	174	181	170	186	201	206	209	205	203	206	205	204	216	207	204	204	205	212	205
titan	cad red	13-CR-TIT	16	13	13	14	13	15	15	17	19	41	116	155	181	177	194	195	200	203	204	203	199	204	206	204	204	201	198	205	200	210
lead tin	cad red	14-CR-LTIN	13	15	15	16	16	17	19	19	21	49	131	174	195	198	215	212	213	216	219	219	219	219	231	225	228	225	229	232	235	222
nickel titan	cad red	15-CR-NiTIT	15	13	15	15	15	14	15	16	20	46	129	168	177	181	192	199	192	199	198	202	200	199	204	205	207	217	210	213	217	205
cad yellow	cad red	16-CR-CRYE	12	12	13	13	13	14	12	15	17	45	118	164	176	191	192	201	200	202	208	210	209	209	220	214	216	221	215	215	221	218
naples	cad red	17-CR-NAP	15	13	14	13	13	15	16	19	20	49	128	174	189	195	203	205	208	208	210	211	205	210	217	215	212	213	215	214	209	211
Cr yellow	cad red	18-CR-CrYE	13	12	13	12	12	12	14	14	16	41	128	167	176	188	200	202	200	204	207	207	211	213	212	214	216	219	221	215	217	212
orpiment	cad red	19-CR-ORP	11	12	12	12	12	12	13	14	16	41	116	167	171	185	192	195	188	189	191	197	196	193	203	197	202	202	202	200	201	200
azurite	cad red	20-CR-AZU	13	12	12	12	14	13	14	17	21	40	67	77	81	82	80	82	79	79	75	76	77	74	73	68	69	68	65	67	63	60
prussian	cad red	21-CR-PRU	12	13	12	12	12	12	13	15	19	48	127	160	168	180	180	183	177	169	172	172	170	166	170	167	168	168	168	170	168	160
indigo	cad red	22-CR-IND	12	11	12	12	12	11	14	14	16	41	115	149	149	159	155	160	160	166	177	178	180	185	194	195	204	206	207	211	214	214
smalt	cad red	23-CR-SMA	12	13	13	16	14	15	15	18	21	43	120	156	167	173	165	167	172	174	172	177	178	175	183	173	176	179	177	179	177	175
cerulean blue	cad red	24-CR-CBL	13	13	13	13	13	12	13	15	19	47	125	163	169	184	190	188	195	201	206	207	212	206	214	215	210	217	207	211	213	202
lapis	cad red	25-CR-LAP	12	13	12	12	12	12	12	15	17	45	122	162	172	183	184	180	177	185	185	193	189	184	191	187	196	191	192	186	196	191
aigyptian	cad red	26-CR-EGY	12	15	14	13	14	14	16	17	23	48	115	140	150	162	158	161	156	162	160	158	157	153	158	153	152	155	151	156	147	151
ultramarin	cad red	27-CR-ULT	13	12	13	12	14	12	16	16	19	52	133	168	172	184	189	190	188	189	195	197	196	197	200	197	202	202	201	199	212	199
cobalt blue	cad red	28-CR-CoBL	11	12	14	14	12	12	14	14	17	51	121	159	170	185	179	185	184	184	184	190	194	194	199	195	205	205	206	206	212	203
cad red	cad red	29-CR-CaRED	13	13	14	13	12	13	15	16	20	52	127	177	192	191	201	208	207	211	214	217	217	219	222	230	220	225	223	222	225	226
cinnabar	cad red	30-CR-CIN	12	13	12	12	12	12	13	13	17	47	130	172	185	198	211	210	205	211	213	208	216	209	215	221	218	221	221	218	217	210
minio	cad red	31-CR-MIN	11	12	12	12	12	12	13	13	18	45	119	164	178	187	196	194	191	202	206	207	212	207	216	211	213	217	215	217	222	216
aimatite	cad red	32-CR-HEM	15	13	14	14	13	15	16	17	23	50	125	156	168	168	174	177	168	172	170	167	167	167	168	165	160	171	166	163	167	167
yellow ochre	cad red	33-CR-YOCH	14	13	13	13	13	14	17	16	18	47	127	171	183	185	184	195	189	195	194	196	197	196	195	194	196	200	196	189	197	191
red ochre	cad red	34-CR-ROCH	13	13	12	13	12	12	13	14	18	40	117	166	174	185	192	190	185	184	190	192	191	197	200	195	195	201	195	195	201	200
realgar	cad red	35-CD-RLG	11	12	12	13	13	14	14	15	19	46	129	172	193	195	205	206	208	213	212	215	215	218	217	220	220	221	218	218	212	216
lake	cad red	36CR-LAK	12	11	12	12	12	12	12	14	17	43	125	158	173	173	192	188	190	201	205	208	211	212	215	219	217	219	219	218	219	216
carmine	cad red	37-CR-CAR	11	13	12	12	13	12	13	15	17	44	122	156	170	180	197	194	192	200	203	209	210	208	213	214	211	218	214	215	218	218
furnace	cad red	38-CR-FUR	13	13	14	13	13	14	13	16	20	52	123	164	168	173	181	181	178	173	175	181	171	171	175	164	169	170	166	165	165	158
ivory	cad red	39-CR-IVO	12	12	12	12	12	13	13	14	18	44	123	151	167	166	173	168	166	167	167	172	170	167	163	167	167	167	169	166	163	154
asphalt	cad red	40-CR-ASPH	12	13	11	13	12	13	13	15	18	42	112	139	147	155	153	157	156	152	154	156	159	152	160	156	156	159	159	156	159	153
Fe	cad red	41-CR-FE	12	15	15	12	13	15	15	17	19	50	122	162	172	174	179	178	175	172	166	171	170	169	177	168	171	157	165	166	166	159
sepia	cad red	42-CR-SEP	15	12	12	14	12	14	15	16	16	46	118	156	169	172	177	172	177	171	176	181	182	180	180	182	179	180	170	175	178	162
ombre burnt	cad red	43-CR-OMBB	11	11	11	12	12	11	14	13	16	39	108	143	143	146	150	149	139	152	146	145	153	151	147	152	152	157	147	153	152	139
ombre raw	cad red	44-CR-OMBR	13	12	12	12	13	13	13	16	18	44	123	157	165	161	175	164	169	169	168	168	165	164	168	159	160	168	163	159	159	146
siena burnt	cad red	45-CR-SIB	14	12	12	13	13	13	13	15	20	44	119	142	151	153	162	156	155	157	157	159	154	155	157	157	155	165	161	159	155	157
siena raw	cad red	46-CR-SIR	12	12	12	13	13	13	13	15	17	40	121	150	162	166	176	170	167	175	173	173	172	166	168	163	161	157	166	161	166	162
		test1-44	12	12	13	12	12	13	13	16	19	45	126	160	167	164	179	169	169	173	163	172	166	159	165	161	159	172	160	162	159	150
		test2-44	13	11	12	13	13	14	12	17	18	43	122	153	162	158	177	162	174	170	169	165	161	162	163	157	159	170	168	160	158	143
		test3-44	14	13	11	12	14	12	14	15	17	44	120	158	161	166	172	168	168	172	173	167	170	168	172	164	164	165	166	157	164	151

Supplementary Table S3: the numerical data of spectra for the samples with underlying color cadmium yellow. The last three refer to the 3 tests and correspond to the measured No. 27 with the underlying red carmine.

LOWER COLOR	UPPER COLOR	CODE NO	420	440	460	480	500	520	540	560	580	600	620	640	660	680	700	720	740	760	780	800	820	840	860	880	900	920	940	960	980	1000
lead white	cad yellow	1-YC-LWH	13	15	13	15	25	129	184	193	199	207	221	210	213	212	217	222	221	219	224	227	221	222	232	228	223	226	222	228	223	221
zinc white	cad yellow	2-YC-ZWH	17	12	13	15	26	127	192	187	199	213	227	209	206	213	220	218	213	214	221	223	221	222	222	222	228	234	233	222	230	218
titan	cad yellow	3-YC-TIT	12	12	13	13	22	116	162	188	196	195	217	210	212	217	209	217	204	206	217	210	216	210	218	214	216	222	220	214	219	217
lead tin	cad yellow	4-YC-LTIN	15	15	13	14	23	125	174	197	197	205	214	210	212	209	219	221	210	214	216	218	215	216	220	220	222	218	217	222	218	219
nickel titan	cad yellow	5-YC-NTIT	14	14	13	12	22	121	176	184	195	201	214	198	197	195	193	199	191	192	193	191	194	192	200	201	203	210	204	206	212	198
cad yellow	cad yellow	6-YC-YC	14	12	12	12	22	117	167	177	190	192	203	199	195	205	212	206	200	204	205	209	207	208	217	209	210	215	205	210	216	205
naples	cad yellow	7-YC-NAP	14	14	13	15	26	123	161	174	174	189	197	196	198	206	212	208	209	211	208	214	205	203	216	216	213	209	213	208	215	205
Cr yellow	cad yellow	8-YC-CrYEL	14	14	13	15	25	119	173	183	187	202	213	200	200	204	209	210	209	207	208	213	212	216	217	216	216	220	215	216	218	207
orpiment	cad yellow	9-YC-ORP	12	12	12	13	22	116	163	171	181	181	192	189	194	197	203	199	192	192	194	200	194	192	200	195	198	195	197	198	206	194
azurite	cad yellow	10-YC-AZU	17	13	14	12	23	107	132	139	142	147	150	153	143	135	148	140	137	134	134	133	127	120	128	123	119	117	114	121	114	113
prussian	cad yellow	11-YC-PRU	12	13	12	12	20	110	152	155	159	167	173	166	162	175	167	164	155	162	159	163	161	160	161	164	155	157	155	153	157	153
indigo	cad yellow	12-YC-IND	11	12	12	12	21	106	138	151	154	160	167	168	162	167	172	170	167	177	179	190	186	184	193	191	205	201	204	200	208	209
smalt	cad yellow	13-YC-YSM	14	15	14	13	24	117	161	170	166	176	178	179	176	184	180	177	175	182	182	183	184	183	192	190	192	188	195	191	191	183
cerulean blue	cad yellow	14-YC-CBLU	15	13	12	12	23	119	169	175	179	182	199	182	183	195	190	200	202	211	213	218	214	214	217	225	221	227	227	217	220	205
lapis	cad yellow	15-YC-LAP	13	13	12	12	23	115	154	161	165	162	179	166	163	169	172	175	173	170	170	173	173	174	181	167	172	173	170	168	171	178
aigyptian	cad yellow	16-YC-EGY	12	13	12	13	24	123	163	173	176	181	194	193	187	195	195	192	195	192	193	191	196	190	198	201	200	202	200	201	196	200
ultramarin	cad yellow	17-YC-ULT	12	13	12	12	23	119	164	168	174	181	190	176	174	180	181	177	175	176	177	175	180	178	182	182	174	187	181	181	183	181
cobalt blue	cad yellow	18-YC-CoBL	11	11	11	11	19	112	155	162	162	169	174	164	166	172	174	167	160	160	167	167	168	172	183	184	187	190	192	191	189	187
cad red	cad yellow	19-YC-CRED	14	12	14	14	21	120	158	164	161	173	190	202	200	205	213	213	204	215	212	216	215	216	220	227	217	221	218	215	222	217
cinnabar	cad yellow	20-YC-CIN	13	12	13	14	23	124	172	175	176	184	209	205	208	208	220	212	206	208	209	215	210	211	213	213	212	218	214	212	215	212
minio	cad yellow	21-YC-MIN	11	12	13	12	20	104	151	160	166	176	195	191	188	199	200	192	193	194	199	203	203	205	216	204	211	209	211	209	214	209
aimatite	cad yellow	22-YC-HEM	17	12	14	13	21	117	163	167	165	176	189	191	185	194	193	196	192	190	191	189	185	190	188	187	182	183	182	183	179	181
yellow ochre	cad yellow	23-YC-YOCH	12	12	12	13	21	114	168	161	176	181	198	172	179	190	197	194	188	195	192	195	193	188	189	189	183	188	185	189	184	177
red ochre	cad yellow	24-YC-ROCH	12	11	12	12	19	110	155	164	168	185	187	181	179	193	190	182	180	182	185	183	178	176	183	188	177	181	185	180	186	185
realgar	cad yellow	25-YC-RLG	12	14	14	13	23	117	143	158	171	195	204	206	201	204	203	213	216	214	213	214	212	216	215	214	218	213	209	220	212	214
lake	cad yellow	26-YC-LAK	12	12	12	12	23	106	145	151	158	173	184	177	172	192	181	191	197	205	209	205	214	213	213	222	208	209	204	212	214	191
carmine	cad yellow	27-YR-CAR	12	13	12	12	19	116	153	169	172	177	186	183	183	190	186	190	188	189	184	199	192	192	206	205	202	196	196	201	203	201
furnace	cad yellow	28-YC-FUR	13	12	14	15	26	120	153	156	161	156	161	149	137	144	155	143	154	149	148	149	146	144	145	140	143	139	143	142	137	136
ivory	cad yellow	29-YC-IVO	13	13	13	12	22	116	143	159	160	165	176	166	158	162	160	156	154	152	149	147	146	147	142	145	138	149	140	136	140	127
asphalt	cad yellow	30-YC-ASP	13	12	11	13	19	90	112	113	114	125	130	122	123	126	137	137	148	146	152	154	148	155	159	154	160	162	155	158	158	150
Fe	cad yellow	31-YC-FE	15	14	13	13	21	120	158	157	163	166	171	166	158	165	155	167	164	165	164	164	159	157	161	160	157	155	150	155	148	141
sepia	cad yellow	32-YC-SEP	20	13	14	15	24	123	164	173	181	190	198	181	179	186	184	174	182	181	180	175	176	171	172	175	176	179	172	171	171	162
ombre burnt	cad yellow	33-YC-OMBB	11	11	12	11	21	118	150	156	157	158	162	154	157	156	157	155	153	146	146	148	139	151	155	145	134	143	143	143	135	142
ombre raw	cad yellow	34-YC-OMBR	12	14	13	14	24	116	146	141	148	147	153	143	140	144	157	147	151	151	154	149	147	152	149	145	138	145	141	146	141	146
siena burnt	cad yellow	35-YC-SIEB	11	13	13	14	22	113	165	163	168	169	185	177	172	176	179	172	167	172	173	168	172	163	171	169	175	171	171	169	169	167
siena raw	cad yellow	36-YC-SIER	13	11	12	12	19	112	158	150	162	153	183	182	179	174	183	175	160	171	168	162	169	156	158	165	176	171	171	174	170	169
earth	cad yellow	37-YC-EAR	15	12	12	14	20	118	157	168	170	180	180	182	173	170	175	173	170	170	170	172	168	169	172	170	165	166	162	162	159	160
malachite	cad yellow	38-YC-MAL	12	12	12	13	21	83	100	102	105	106	109	102	100	99	101	100	96	94	87	80	84	70	70	70	72	73	64	66	64	62
Cr green	cad yellow	39-YC-CrGRE	14	12	12	13	21	121	161	172	177	179	191	187	182	182	180	187	187	189	193	201	195	191	197	192	193	196	197	191	190	185
Cu green	cad yellow	40-YC-CuGR	14	13	12	14	23	117	163	178	177	188	183	184	181	187	196	185	186	196	196	196	198	197	197	200	200	197	201	195	199	197
cobalt green	cad yellow	41-YC-CoGRE	13	12	12	13	20	116	165	165	167	168	181	177	166	166	173	169	166	171	177	181	185	181	189	189	193	195	191	184	184	168
viridian	cad yellow	42-YC-VIR	12	11	12	13	22	114	151	170	171	191	197	196	189	187	196	188	189	192	200	207	208	206	215	212	216	217	217	208	215	216
pthalo	cad yellow	43-YC-PTH	12	14	13	13	20	106	137	141	143	153	147	146	142	142	141	146	145	142	144	147	140	139	142	147	150	150	151	158	161	162
sap	cad yellow	44-YC-SAP	12	13	12	12	21	99	132	140	146	160	170	162	167	174	178	190	181	190	191	194	191	190	201	201	203	210	207	207	209	204
gold ochre	cad yellow	45-YC-GOLDOCH	12	12	12	11	19	113	158	178	178	184	193	185	180	180	186	186	184	189	189	190	188	184	186	182	185	190	183	184	192	186
ground	cad yellow	46-YC-GRO	11	15	13	12	22	114	171	189	199	201	210	203	206	218	221	209	217	213	210	211	218	214	223	219	222	218	220	214	222	217
		test1-27	12	12	13	13	20	118	150	174	167	172	190	180	178	185	182	196	191	188	180	200	198	195	204	200	198	197	192	205	198	207
		test2-27	11	14	12	11	18	113	156	170	170	179	182	188	180	192	191	190	189	184	190	193	190	197	200	209	206	200	201	200	205	199
		test3-27	13	12	11	12	19	119	154	165	177	182	191	178	186	195	185	188	183	187	189	192	191	187	211	199	200	192	195	197	208	200

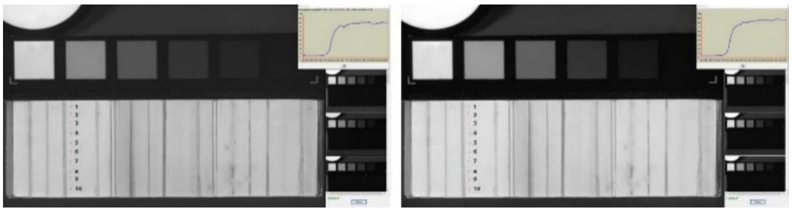

Figure S2. The ten points that spectrum was measured before (left) and after (right) the standardization.

It was observed that at different points in the same square area there is a slight difference in the resulting spectrum values, so this resulting error should be measured. Ten different spots were taken in an area of color that does not naturally contain the preparatory layer, the measurements were taken, and a print screen was made of them to record the difference (Fig.S2).

In the preparatory drafts in every square 5 such preparatory drafts were made. The first with charcoal, the second with graphite, the third with oven black in egg tempera (because in the preliminary drawing -anthivolo- they used fumo which is oven black), the fourth engraved and the fifth raw sienna in egg tempera (Fairchild, 2005).

Then the pigments of different colors were applied. First the first layer parallel to the lines of the drafts, so that they do not drift and especially the charcoal and vertically the overpainting was drawn. The 5 panels were left alone, without overlays, as they were the reference samples. It should be noted here that the IR readings were taken initially on the whole square that included all drafts, eventually this was revealed during the panel preparation and the way near IR readings were taken and the spectra analyzed were extracted from a sub-area of square where no draft was there to avoid confusion in the interaction of IR with the drafts. Moreover, this preparation is preliminary and no control of the uniform brushing is secured. The impact of different drafted preparatory material on spectra as well as the camera conditions and settings in taking the readings is planned for a near future investigation.

The binding material used with pigments was egg, vinegar, and water. The pigments were mixed with the egg mixture in a mortar in order to achieve as much uniformity as possible in relation to the grains of each, but also for complete homogenization. Fig.S3 give representative spectra for the three Sets.

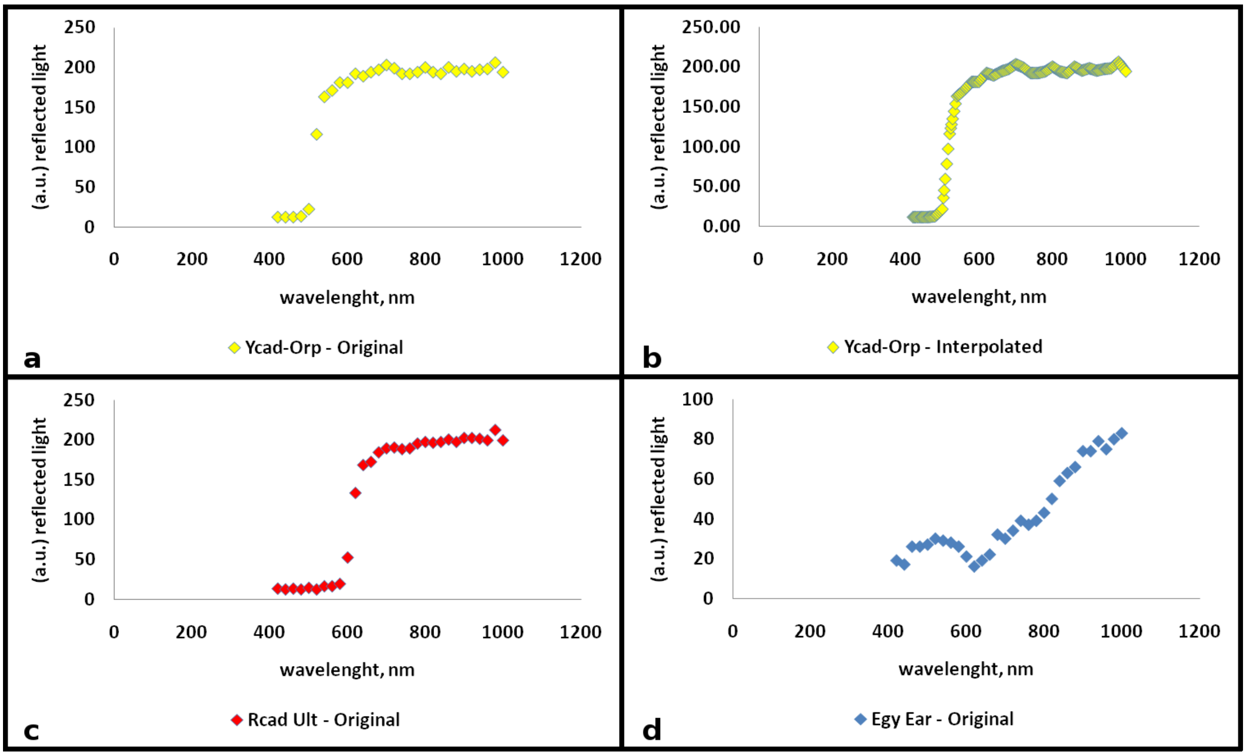

Figure S3. NIR spectra for a) cadmium yellow with orpiment underlie, b) same with a for interpolated values, c) red cadmium with ultramarine and d) Egyptian blue with earth (for data see Tables S1-S3).

THE COMPLEXITY MEASURES

A. Fractals

1. Allometric scaling dimension

Several downscaled and aggregated sub-signals of the input signal were calculated. For all sub-signals, the corresponding mean values and standard deviations were plotted on a double logarithmic graph. The slope of the linear regression provided an estimate of the fractal dimension (West et al., 1999). This is the first time implemented as software in solving a problem.

2. Higuchi Dimension

Lengths of sub-signals (constructed by taking points at different distances) were computed and plotted on a double logarithmic plot as a function of the distance variable. The slope of the linear regression revealed the Higuchi dimension (Higuchi, 1988).

3. Tug of war Dimension

Hash functions with data points inside a radius were constructed by summing up prime number polynomials. Even hash functions were counted and the slope of a double logarithmic plot were taken as an estimate of the fractal dimension (Wong et al., 2005).

4. Katz Dimension

An estimate of the fractal dimension was computed with the average Euclidean distance between successive data points and the maximal Euclidean distance to the first data point (Katz, 1988).

5. Petrosian Dimension

Data point values were binarized by thresholding with the signal's mean. Then, the number of changes in the binary sequence were computed in order to get an estimate of the fractal dimension (Petrosian, 1995).

6. Sevcik Dimension

The signals were linearly transformed to normalized spaces. The lengths of the transformed signals and the spacing variable gave directly an estimate of the fractal dimension (Sevcik, 2010).

Four Entropy measures

1. Shannon Entropy

The probability distributions of all data point values gave a direct entropy value (Shannon, 1948; Zenil, 2020).

2. Approximate entropy

Sub-patterns of the signal were extracted and corresponding similarities, defined by the sub-patterns differences smaller than a give value, gave this entropy measure (Richman and Moorman, 2000).

3. Sample Entropy

A normalized version of the Approximate entropy eliminating self matches (Richman and Moorman, 2000).

4. Permutation entropy

Sub-samples of the signal were extracted and several permutated versions generated. All these permutated sub-samples were compared to the ranked version of the sub-sample and a probability distribution yielded an entropy value (Bandt and Pompe, 2002).

B. Four Other complexity measures

1. Kolmogorov complexity

The Kolmogorov complexity or algorithmic complexity cannot be computed directly as it is a theoretical concept of finding the Bytes used for the shortest computer program to generate an object or a result. But it can be estimated by applying compression algorithms. The Bytes of the compressed data values were taken as this estimate of KC. The common compression algorithms ZLIB and GZIB were used (Zenil, 2020).

2. Hurst coefficient

The power spectrums of the signals were computed and depending on the slope a decision was made if signals were fractional Gaussian noise fGn or fractional Brownian motion fBM. Then the Hurst coefficient was computed with a dispersional analysis for fGn or are scaled windowed variance analysis for fBm (Eke et al., 2000).

3. Detrended fluctuation analysis DFA

Fluctuation functions for several window widths were computed and the residuals determined. The average variance of the detrended signals for a given window width was double logarithmically plotted an the slope gave the scaling exponent (Peng et al., 1994).

4. Lyapunov exponent

Attractors with varying embedding dimensions and delays (in our case wavelengths) were constructed. The nearest neighbour of each point of the series was taken to define minimal distances. The slope of a linear interpolation in a double logarithmic plot of these minimal distances as function of wavelengths gave the value for the largest Lyapunov exponent (Rosenstein et al., 1993).

CHOICE OF STATISTICAL METHODS

The choose of linkage clustering methods to perform the hierarchical clustering we need a Method of minimal sum-of-squares, the Proximity between two clusters to be the summed square in their joint cluster, and a Method of minimal increase of variance and of minimal variance.

The average and complete linkage perform well on cleanly separated globular clusters, but have mixed results otherwise; and Ward is the most effective method for noisy data.

Investigating with different methods is done to evaluate the results with methods that can process the type of data present. The hierarchical clustering used here is generally recommended for small object sample sizes (not thousands) as in the present case. In any case, a more exclusive procedure of proving similarity with some measure of similarity between hierarchical classifications, we refer to "comparison of dendrograms" and "comparison of hierarchical classifications" which we approached with tests (PCA, K means, Box plots, Silhouette, Wilks texts).

It is generally known that it is not recommended to visually compare dendrograms (to choose the method that gives the strongest partition), obtained by different cumulative methods. Since no answer will be given about the "best" method. Each method has its own "default" dendrogram appearance: Dendrograms will consistently differ even when the data has no group structure or random group structure. In this case we can, however, compare dendrograms produced by the same method but on different data.

But in the Ward method it is not correct to decide directly on the number of clusters (ie where to cut the dendrogram to show groups). In Ward, the tree plot shows the increase in the cumulative, not the mean, coefficient of collectivity. and the consequence is that since the later clusters are larger than the number of points, the later groups appear deceptively "better" in the dendrogram. The difficulty of normalizing the Ward dendrogram led us to examine the groups with other statistical tests such as box plot techniques, silhouette values for each group, the K-means method, which classifies the objects into a predetermined number of groups, the Wilks test, and the graphs in PCA with emphasis on the 1st and 2nd components recommended.

An update to the dendrogram problem of Wards method showed that different clustering software might produce different transformed clustering coefficients for Ward's method. Therefore, their dendrograms will look somewhat different, despite the fact that the clustering history and results are the same. For example, SPSS does not take the root of hypermetric coefficients, but accumulates them in the output.

Average-linkage is where the distance between each pair of samples (observations) in each cluster are added up and divided by the number of pairs to get an average inter-cluster distance; *Complete-linkage* (farthest neighbor) is where distance is measured between the farthest pair of samples in two clusters. This method usually produces tighter clusters than single-linkage, but these tight clusters can end up very close together; and *Ward's* clustering which is based on analysis of variance in the group of samples to estimate distances and minimize variability (Gauch and Whittaker, 1981). In the Ward method, the grouping is not done by distance, at least in a direct way. Specifically, it is based on the total sum of squares and which compound will cause less such quantity (Papageorgiou, 2020). Average-linkage and complete-linkage are the two most popular distance metrics in hierarchical clustering.

Distance is taken into account implicitly because the sum of squares is calculated each time using the distance of the samples from the center of the group that will be formed in each hypothesized union. Hence the interpretation of the dendrogram in this case must be done accordingly. Indeed, another tradition (found in some R packages, for example) is to take the root (so called "*Ward-2" implementations*) and not to cumulate. Such differences affect only the general shape/looks of the dendrogram, not the clustering results.

But the image of the dendrogram might influence the decision about the number of clusters. The moral is that it would be safe not to rely on one dendrogram in any method at all, unless we know exactly what these coefficients are out of our program and how to interpret them correctly. One more reason we included the other three methods in our hierarchical homogenization with the ongoing discussion that follows.

PCA was applied for data reduction, commonly used in archaeometry studies to highlight the presence of compositional groups between the artefacts. The initial dimensionality of the data sets, equal to the number of spectral cubes per 20 nm (N), is reduced to n, representing the number of Principal Components (PCs) used. PCs are then calculated as eigenvectors of the covariance matrix of the transformed data, whose eigenvalues represent the variance of the data along with the eigenvector directions.

Box plots were used to show distributions of numeric data values, in order to compare them between multiple groups obtained by linkage and ward methods. The boxplot presents the five sample statistics - the minimum, the lower quartile, the median, the upper quartile and the maximum score.

STATISTICAL ANALYSIS OF SET 1

Complete Linkage-Set 1 (Fig S4)

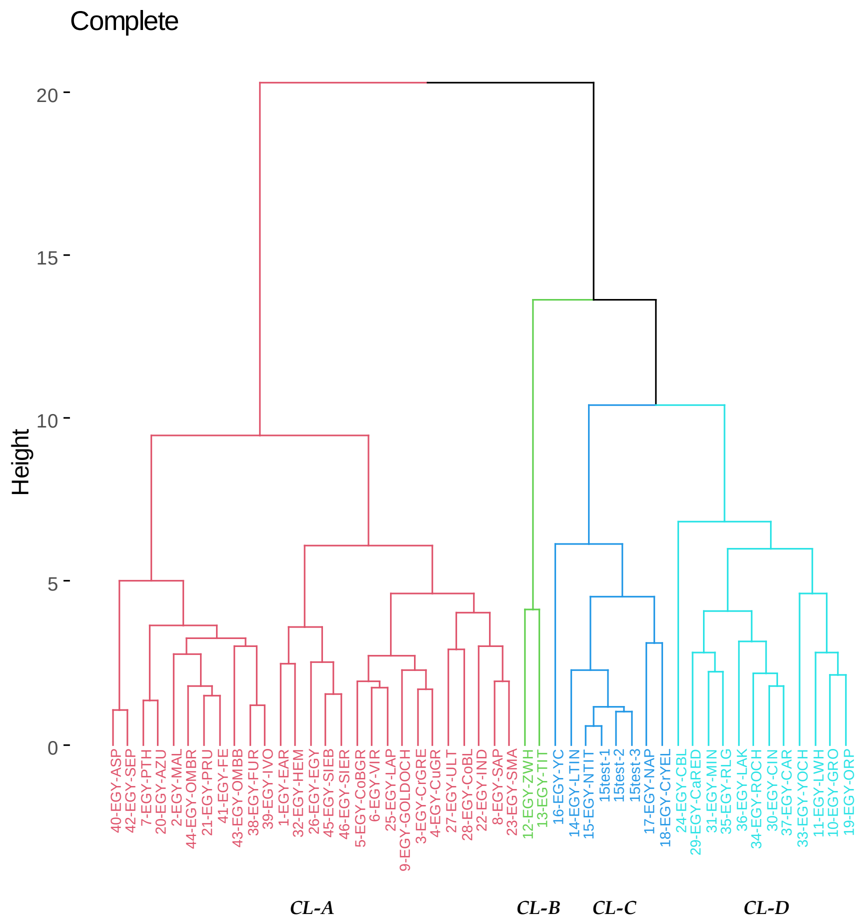

Figure S4: Grouping by complete linkage groups (CL-A to CL-D) again with the two samples, the underpainted No 12: zinc white and No 13: titanium white to form a very distinct group.

The Egyptian blues with underpainted No 12: zinc white and No 13: titanium white belong to a differentiated group from that with the rest containing all three tests. And the other two groups that are formed are also different here and are as follows: the first which is the largest includes the earth greens, chromium, copper, copper, cobalt, viridian, phthalo, sap, the golden ochre, blue azurite, Prussian, indigo, enamel, lapis, Egyptian, ultramarine and cobalt, red hematite and the whole table of blacks and earths. The latter group includes lead white, yellow orpiment, cerulean blue, and all reds except hematite which are in the former group.

Silhouette scores for Set 1

The silhouette scores for average and complete linkage are shown in Fig. S5 and the *Ward* with three and four groups in Fig. S6. This metric examines how similar the objects within a group are (cohesion) and how dissimilar the objects of different groups are (separation). Its value ranges from -1 to +1, where a high value indicates that the object matches the objects in its group fairly well and does not match the objects in the other groups at all. Negative value for a sample would indicate that it does not fit with the rest of the group that belongs to. For the group of interest, we see that the silhouette value ranges from 0.31 with Ward's method to 0.50 with Average method. However, all values are comparable.

PCA of Set 1

Figure S7 the graphs of the groups we find in the first 2 principal components.

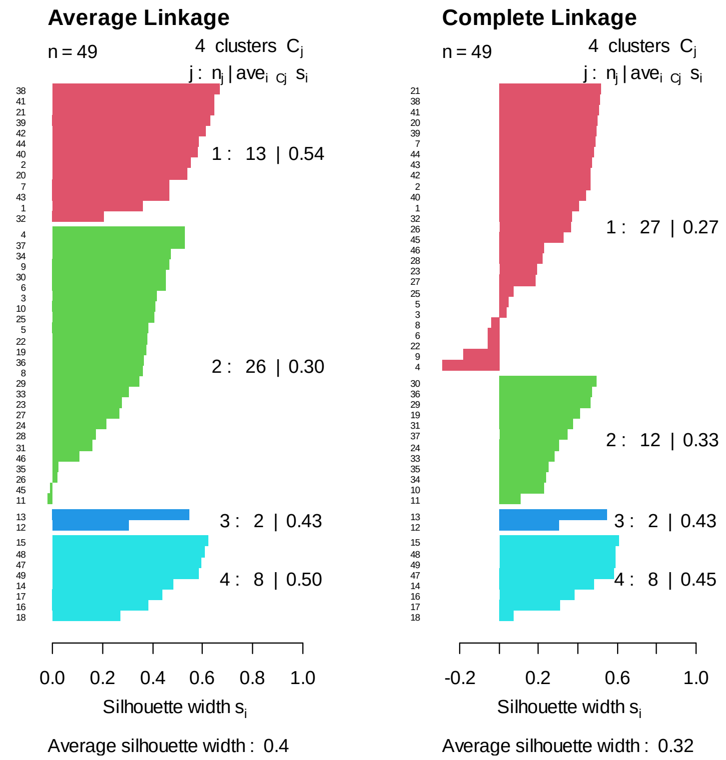

Figure S5: Silhouettes of average and complete linkage

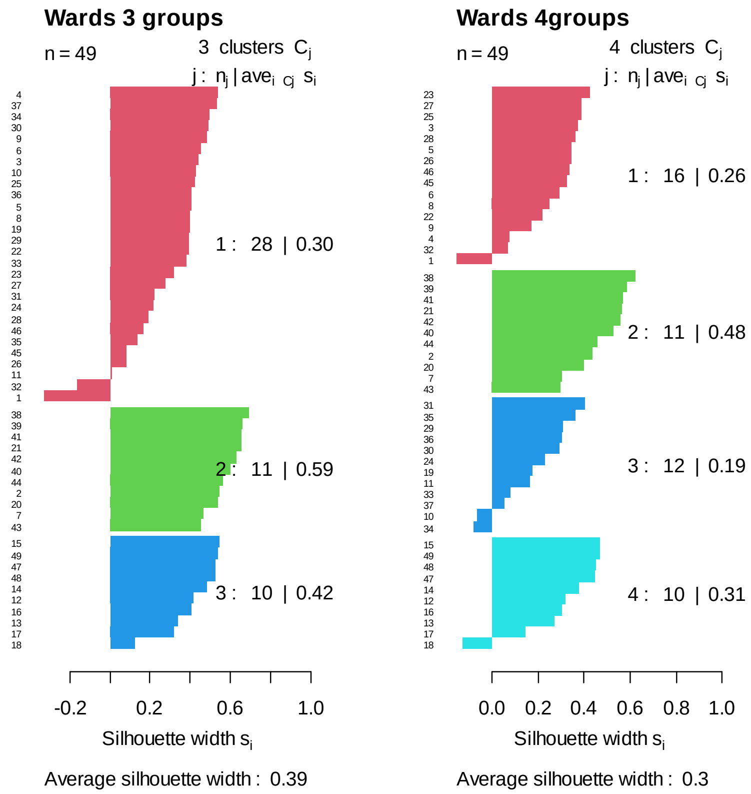

Figure S6: Plots of Silhouettes scores for the Ward & Ward-2 with 3 groups (average ~0.40) and 4 groups (average 0.30) respectively. Silhouette identifies two particular samples forming a seemingly "outlier" little cluster

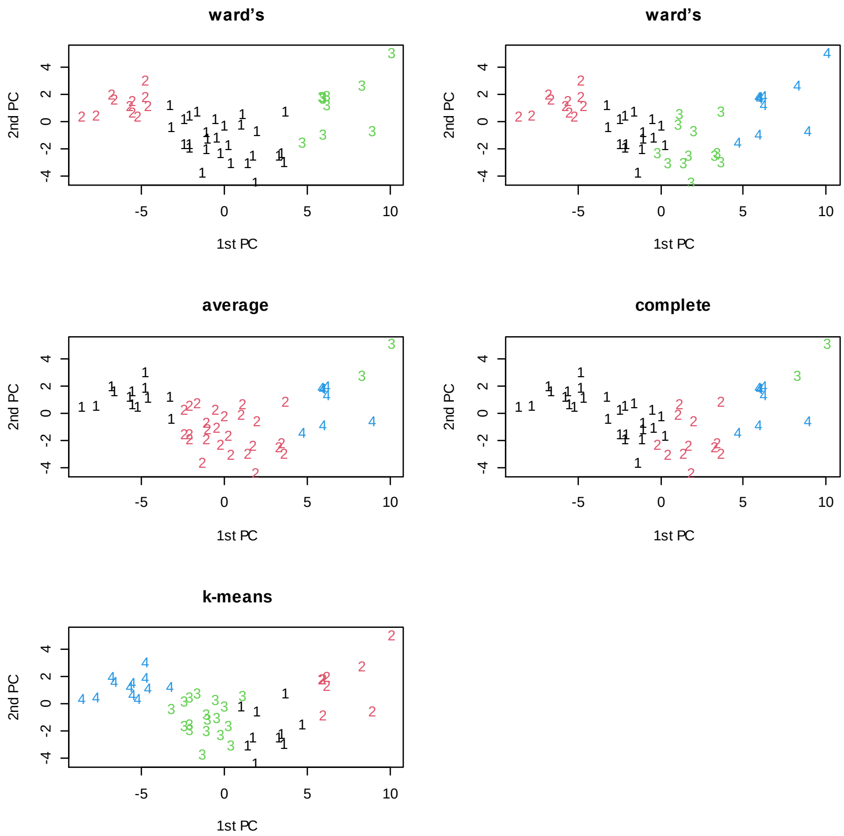

Figure S7: Score plots of PCA for each method (average and complete linkage, k-means and ward (left) and ward-2 (right)

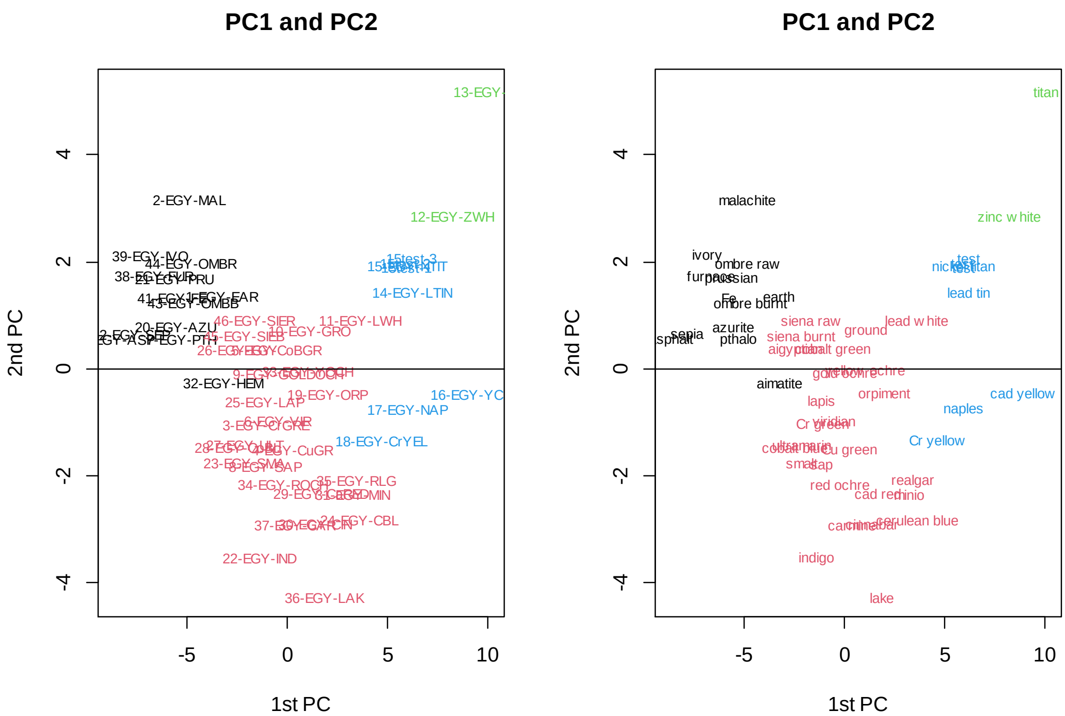

Figure S8: Left: PCA score plots of the samples on the first two principal components. The color in sample points is according to grouping suggested from the Average Linkage. Right: The same plot when using as label for the sample points the lower underpainted color.

Overall, all five groupings presented in Fig. S4 exhibit a clear separation among groups confirming that the suggested grouping is meaningful. It appears that the first component is adequate to explain the variability of the data points. The group we are interested in scores high in the first PCA component as mentioned before and is indeed located on the right in every plot of Fig.S7. Namely, is the group with green color for the first plot, blue color for the 2nd, 3rd and 4th and red color (Fig.S5, S6) and for the k-means plot (Fig.S8, S10).

In the PCA graph that follows with the labels of the data, Fig.S8, S9 it is clearly seen how extremely close (enclosed in the blue box) to sample 15 are the 3 tests, which are almost indistinguishable since they are the on top of the other. In Fig.S8 the 2 subplots are the same plot, but using as a label the upper color (left graph) and the lower color (right graph). The sample points for both graphs are colored with accordance to the Average clustering group.

The noteworthy that the samples test 1, test 2 and test 3 samples are extremely close to 14-EGY-LTIN and 15-EGY-NTIT, i.e. to the yellow lead tin and of course to the yellow nickel titanium that we are interested in as it is the measured based on which the 3 tests were made. The two samples that are separated from this group with some methods, i.e. No 12 zinc white and No 13 titan, score high in PC1, but score also high in PC2 (which represents the 12% of the initial data variation) and this the special characteristic of these two samples compared to the remaining group of interest.

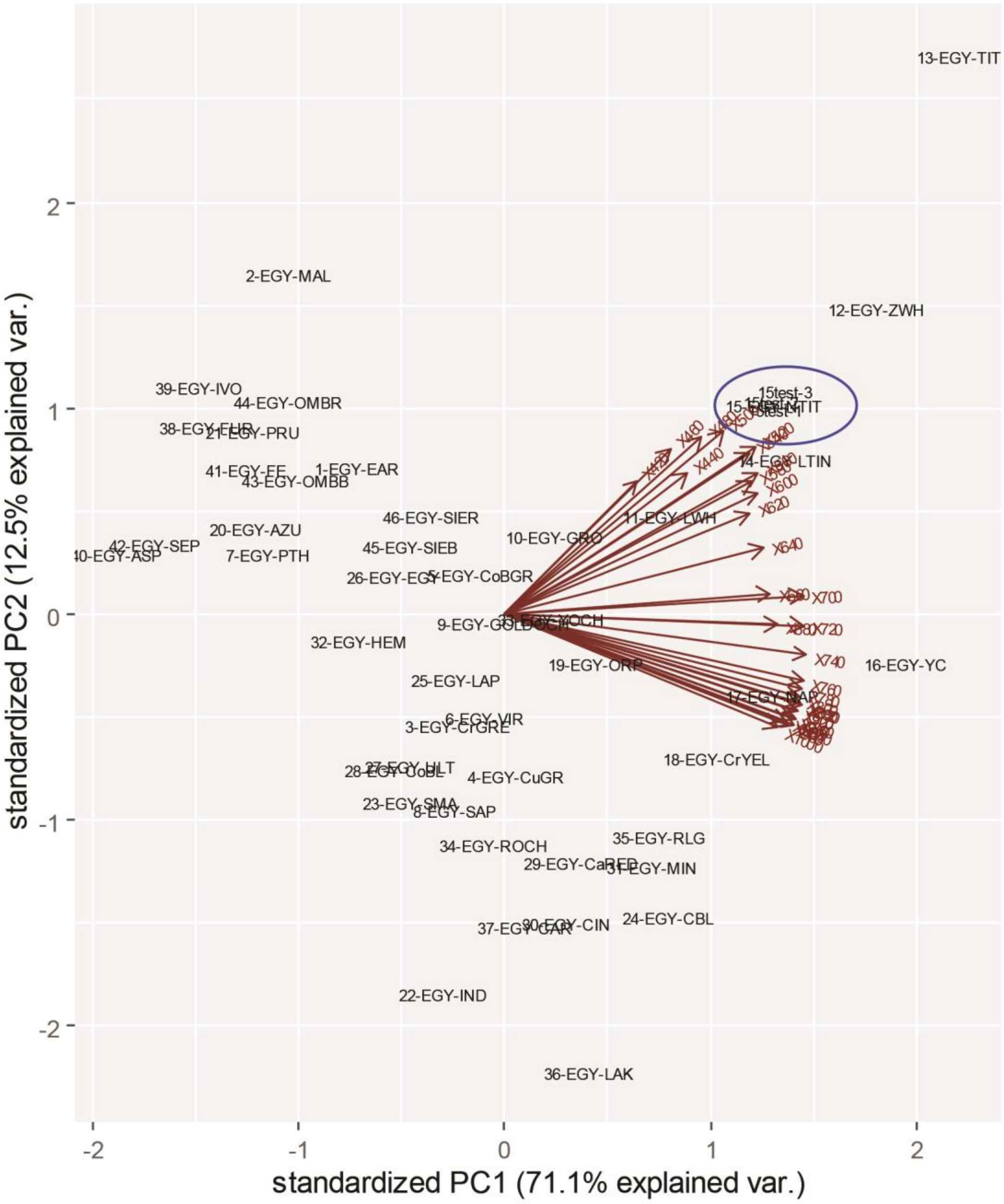

Figure S9: Biplot showing the structure of the loadings from PCA for Comp 1 and 2. The large positive loadings of lower group of variables 420-640nm on component 1 that is the most spectral part of spectra have a strong influence in this component. The upper group of vectors loadings close to 0 indicate that the variable of respective wavelength 660-740nm has a weak influence on the component.

Figure S10: K-means clustering result for K=4, plotted on the first two PCs.

<u>Set 1: K-means Set 1</u>

The k-means method in the present study with k=4, indeed, has resulted to four groups with the group of interest to contain exactly the same samples as in Ward's.

<u>Set 1: Wilks test</u>

Next is the Wilks value, the smaller the value, the better the separation. Average: 0.045395, Complete: 0.030659, Wards: 0.092423, K-means: 0.045395. We notice that the lowest value is given by K-means but the highest by Wards.

<u>Statistical Analysis Set 2</u>

Complete Linkage into 4 groups (Fig.11), and for Ward the division into 4 (Fig.12). The group which includes the tests is highlighted in cyan.

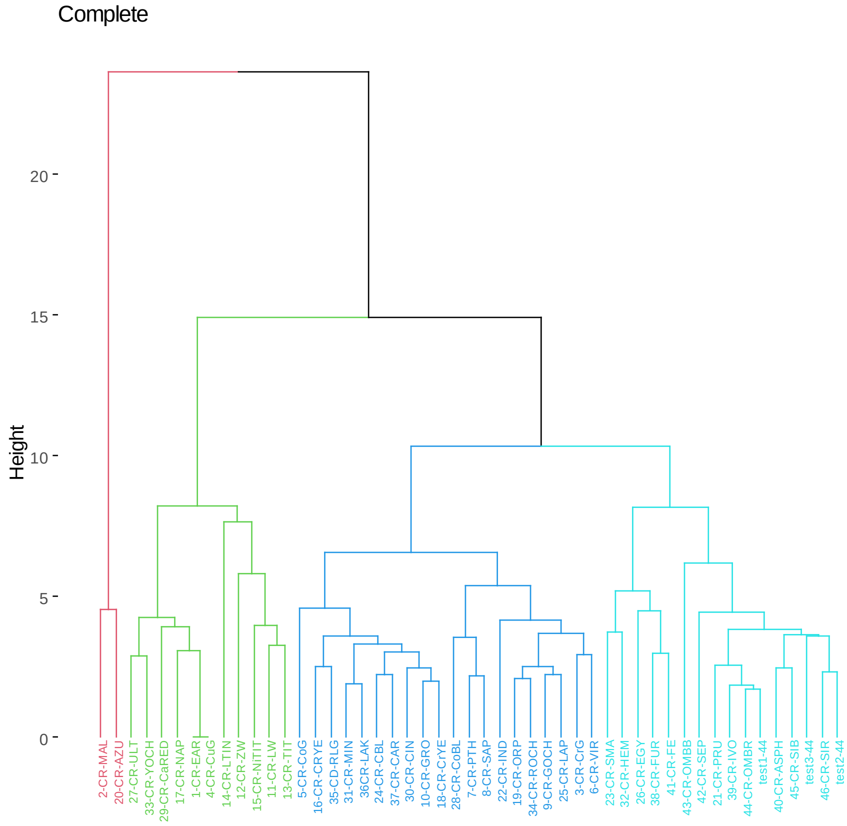

Figure S11: Complete Linkage with 4 groups

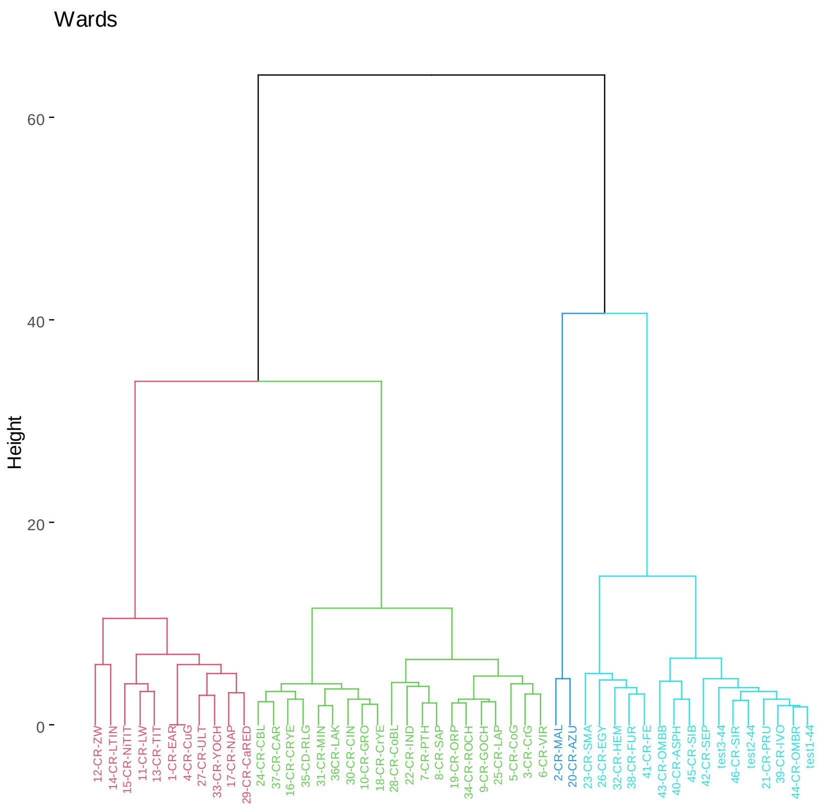

Figure S12: Ward in 4 groups

Below are included the Silhouette values, box plots of the different methods that were used and they concern the order Average and Complete Linkage, Wards, Wards-D2.

Silhouette values Set 2

The Silhouette values for each group by method as well as the average value for each case, all of which are comparable. In Fig.S13 these are shown for the Average and Complete Linkage and Ward's method.

The following Table (Table S4) shows the average values of the 4 groups and Fig.S14 the box plot for the 4 clustering methods. Fig.S15 is the same plot, as in Fig.7 main article but using as a label the upper color (left graph) and the lower color (right graph). The sample points for both graphs are colored with accordance to the Average clustering group.

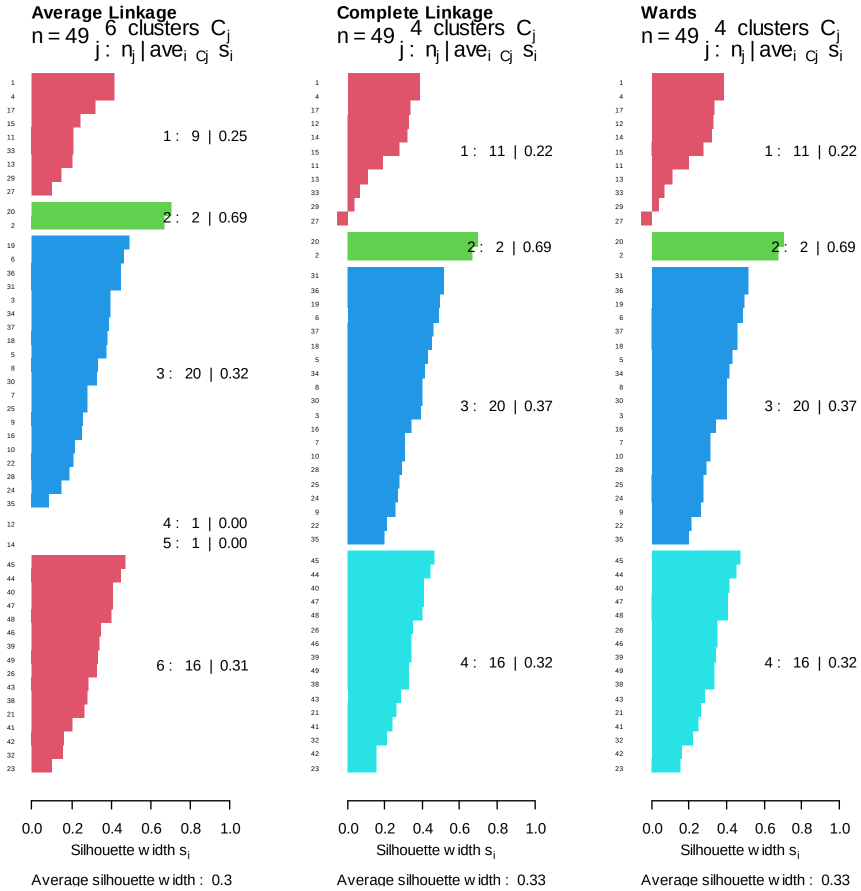

Figure S13: Plots of Silhouettes scores for Average (average 0.30), Complete Linkage (average 0.33) and Ward's (average 0.33) respectively.

TABLE S4 The average values of the 4 groups per wavelength

Spectrum	[1st]	[2nd]	[3rd]	[4th]
620	127.0909	72.5	122.15	120.2500
640	169.8182	80.5	159.70	152.9375
660	183.0000	86.0	172.60	161.6875
680	185.8182	85.0	182.15	164.8125
700	193.0000	83.0	189.25	170.6875
720	199.5455	88.0	190.65	167.6250
740	198.8182	83.0	190.85	166.6250
760	201.8182	85.0	195.00	167.5000
780	204.0909	78.5	198.00	166.3125
800	206.1818	82.0	200.70	167.7500
820	204.5455	77.5	201.60	166.5625
840	206.0000	79.0	201.35	164.0625
860	209.0909	75.5	206.50	167.1250
880	209.3636	75.0	205.50	163.0000
900	208.8182	73.0	208.60	163.0000
920	210.2727	73.0	210.55	166.2500
940	209.1818	69.0	207.90	163.8750
960	209.5455	72.0	207.95	162.9375
980	210.8182	65.0	210.70	162.6875
1000	207.5455	63.0	206.15	155.4375

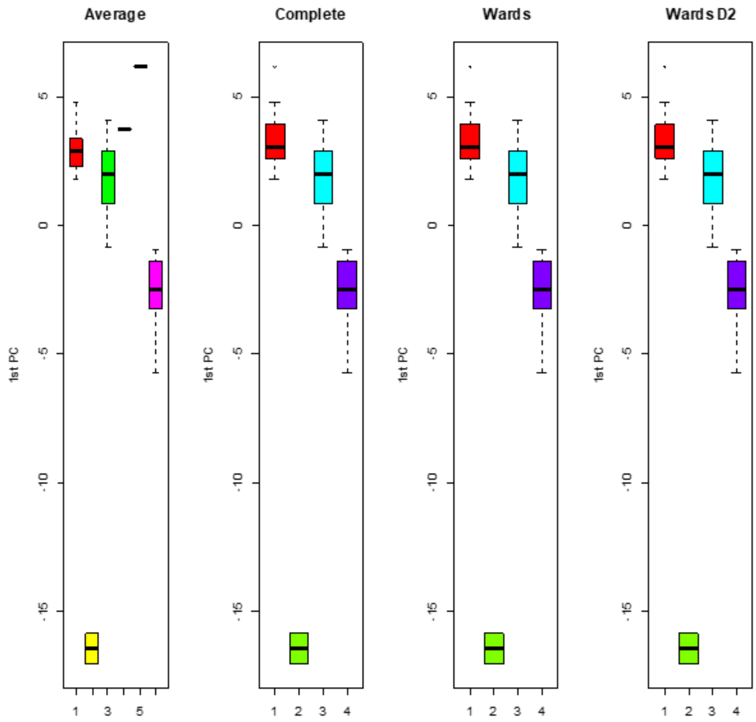

Figure S14: Box plot for: average 6 groups and Complete with 4 groups, Wards with 4 groups, Wards-2 with 4 groups

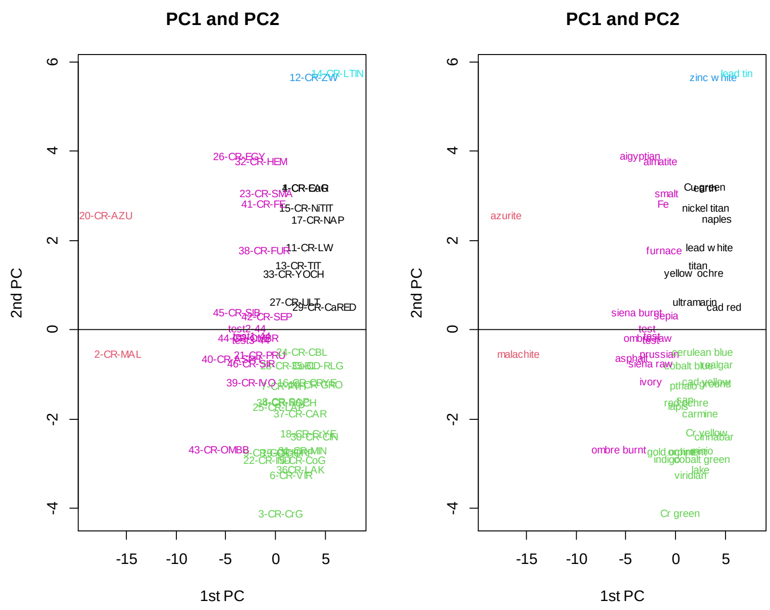

Figure S15: Left: PCA score plots of the samples on the first two principal components. The color in sample points is according to grouping suggested from the Average Linkage. Right: The same plot when using as label for the sample points the lower underpainted color.

The clustering for data set with k-means algorithm gives exactly the same clustering that includes all 3 tests, just like with dendrograms (Fig.S16).

Statistical analysis of Set 3

Sample No 38-YC-MAL (underlying red malachite) has been indicated from cluster analysis to be an outlier. This is also confirmed from from PCA in Figure S17 where No 38-YC-MAL scores very low in the first PC, around -20 while all other samples score above -10.

We next remove the sample 38-YC-MAL from the data set, as confirmed outlier, and repeat the analysis for the remaining 48 samples. Hierarchical clustering for the four linkages lead to dendrograms presented in Figs S18, S19.

The grouping of all samples of the set 3 is also confirmed by the Silhouette values for each group per method as well as their average value as are shown below in Fig.S20. A graphical representation of the clustering results using PCA as a projection method also supports the above result and produces Fig. S21.

The group we are interested in is group 2 for the average and ward's method and is group 3 for complete linkage.

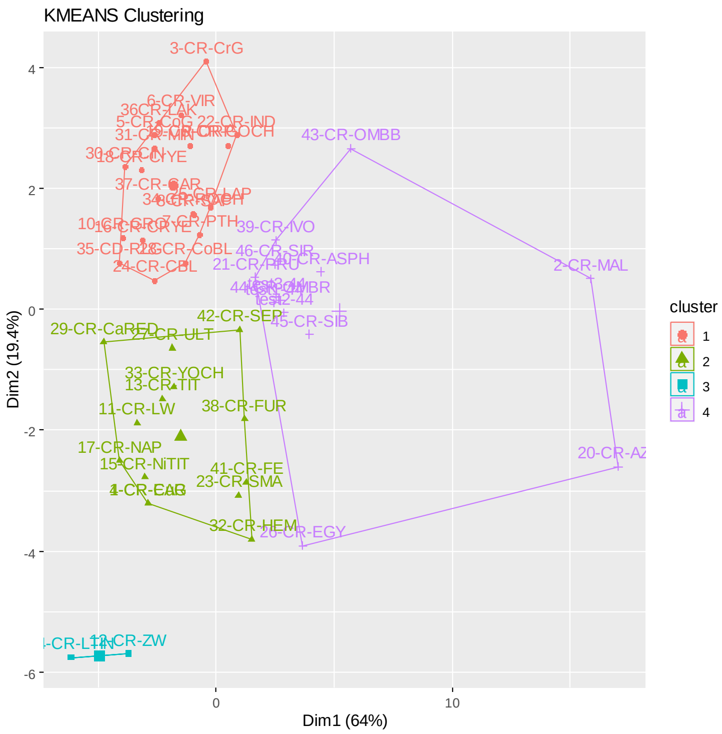

Figure S16: K-Means for 4 groups

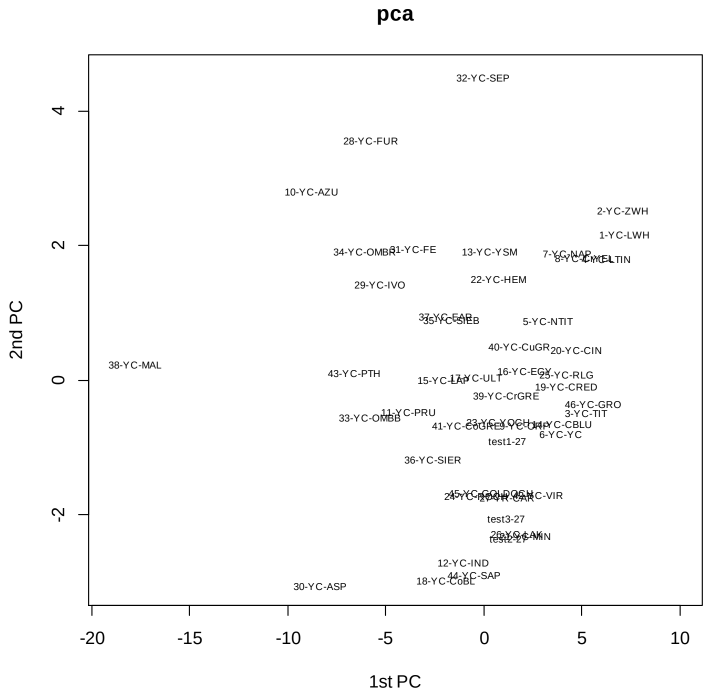

Figure S17: A scatter plot of the set 3 data scores in the first two principal components.

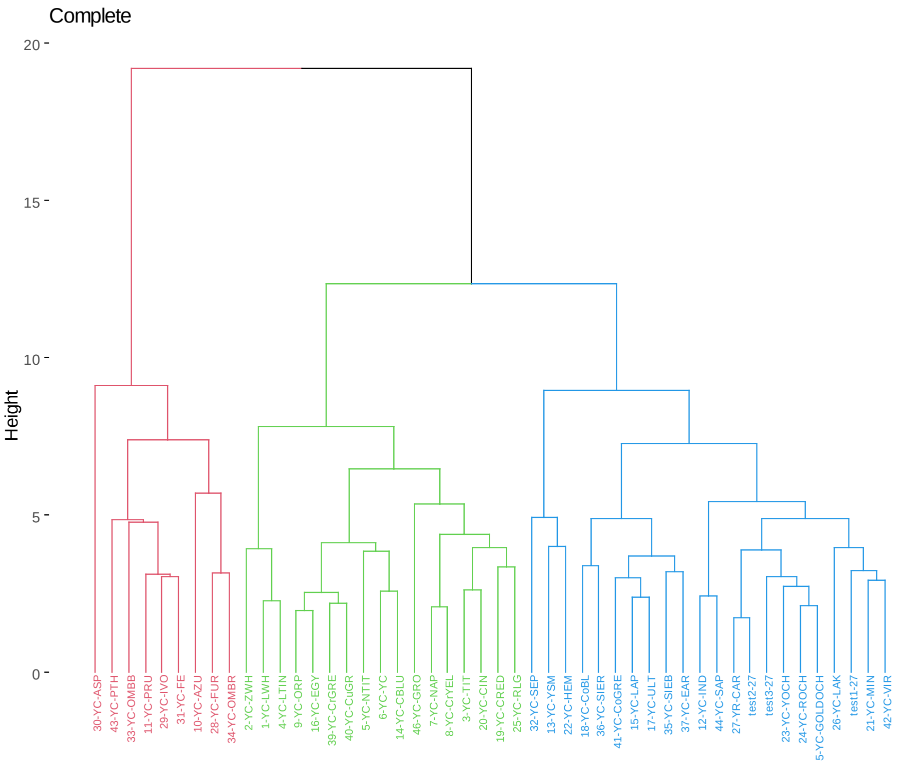

Figure S18: Complete linkage with 3 groups

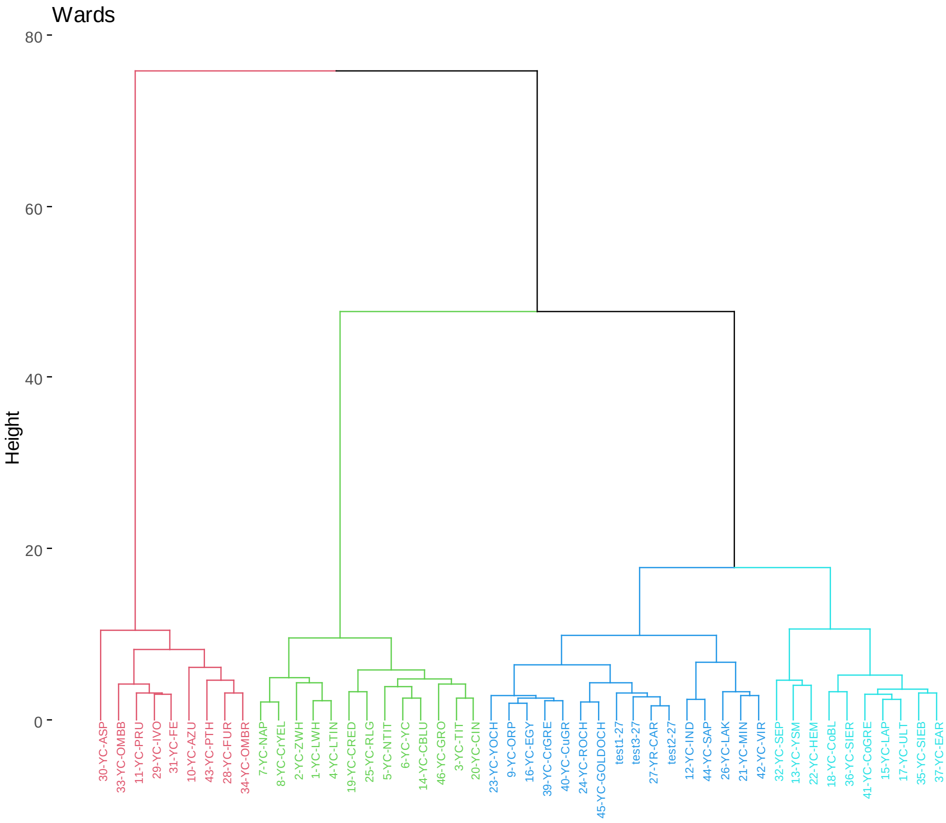

Figure S19: Ward with 4 groups.

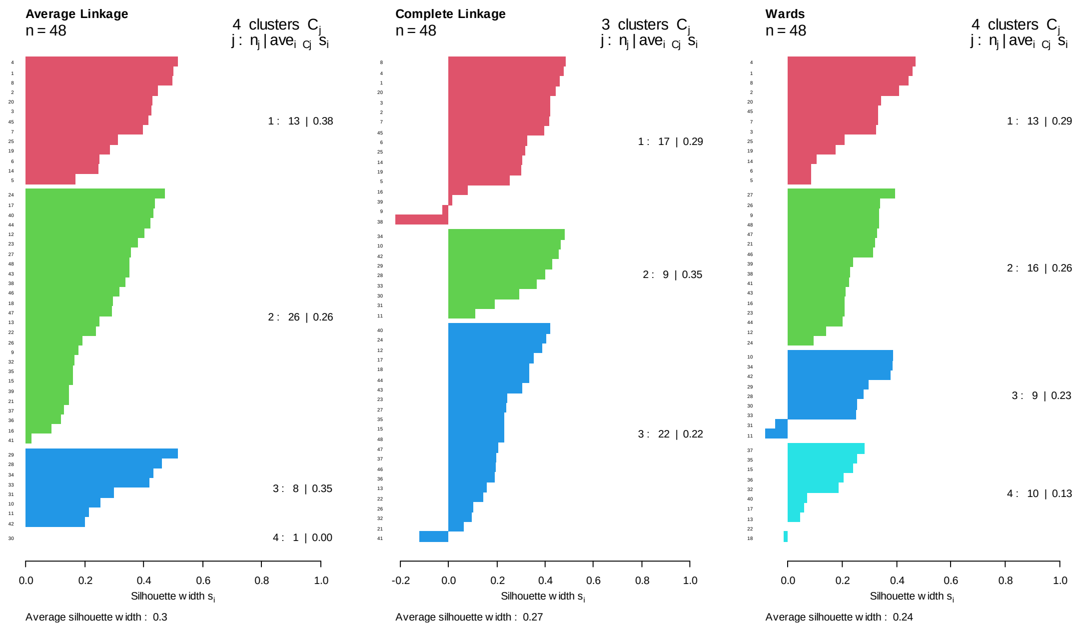

Figure S20: Silhouette scores for average, complete and ward with average ranging between 0.24-0.30.

A graphical representation of the clustering results can be seen using PCA as a projection method and produces Fig.21.

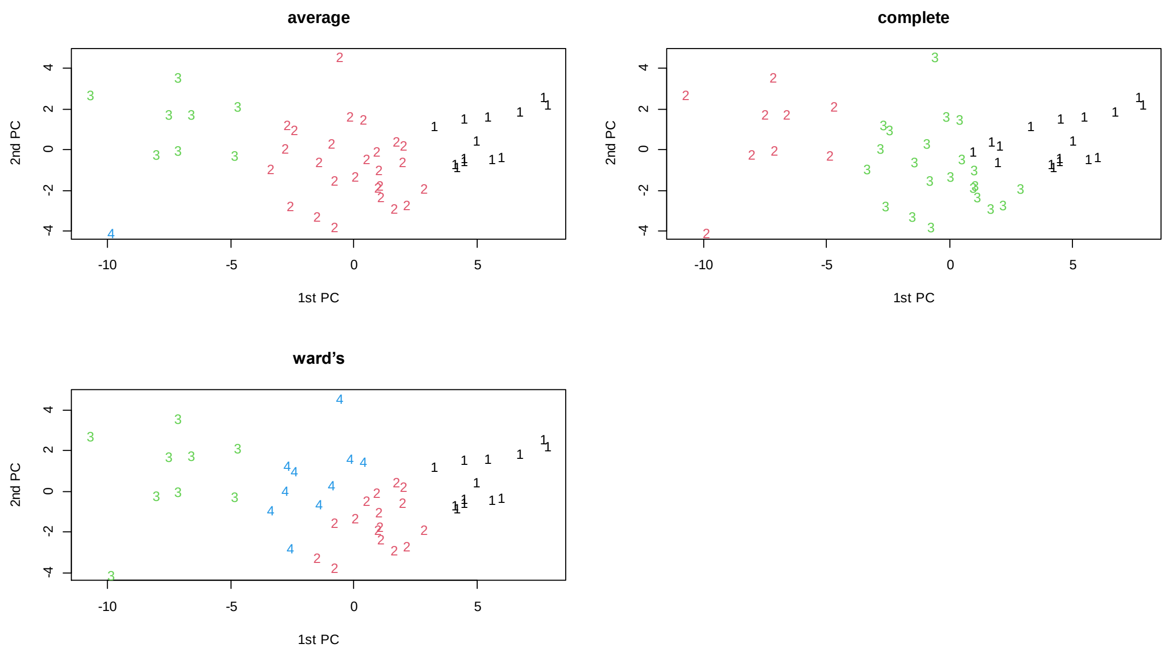

Figure S21: PCA for average, complete and ward.

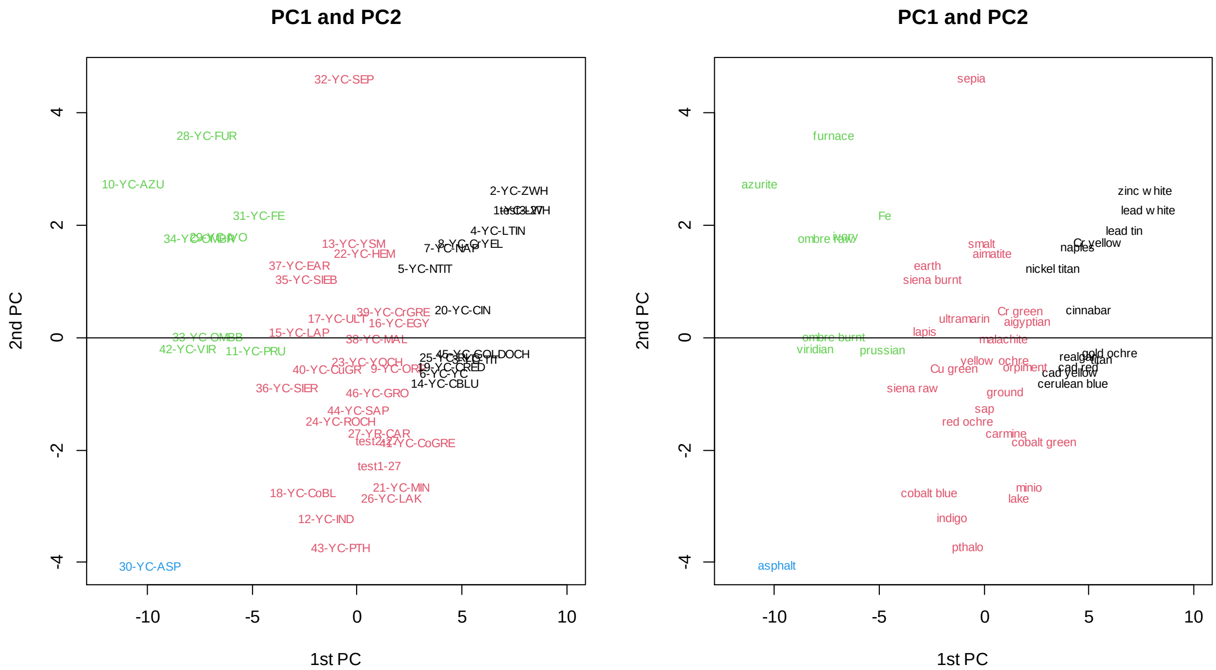

Figure S22: Left: PCA score plots of the samples on the first two principal components. The color in sample points (numerical codes) is according to grouping suggested from the Average Linkage (Fig.8 main article). Right: The same plot when using as label for the sample points the lower underpainted color with their pigment name.

Fig.S22 is the same plot of Fig.10 (main article) but using as a label of the upper color (left graph). The sample points for both graphs are colored with accordance to the Average clustering group.

Finally, the k-Means method below also agrees with the group containing the 3-test close to the expected No 27 and is shown in blue in Fig.S23 below.

Complex Analysis indices plots

Notes: a) not all data were suitable for analyses by some of the 14 indices, b) in all plots the X axis gives the samples on an ordered increasing number (1-49). The last three points are the 3 tests, c) All plots are Fig.S24 – S61.

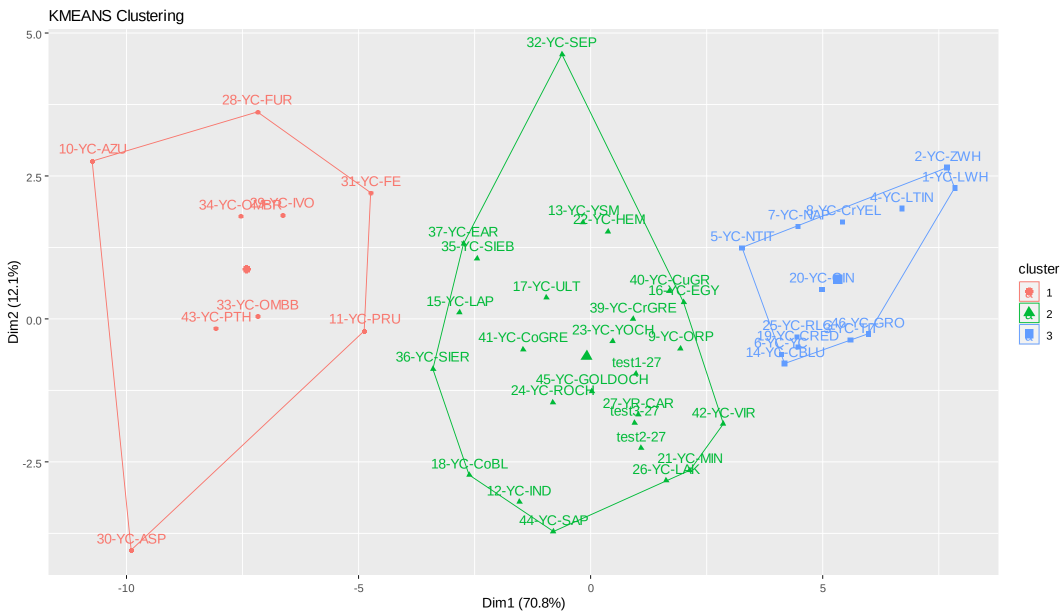

Figure S23: K-Means clustering, where group in green is the group with the 3 tests and concur with previous methods.

1. SET 1: EGYPTIAN BLUE

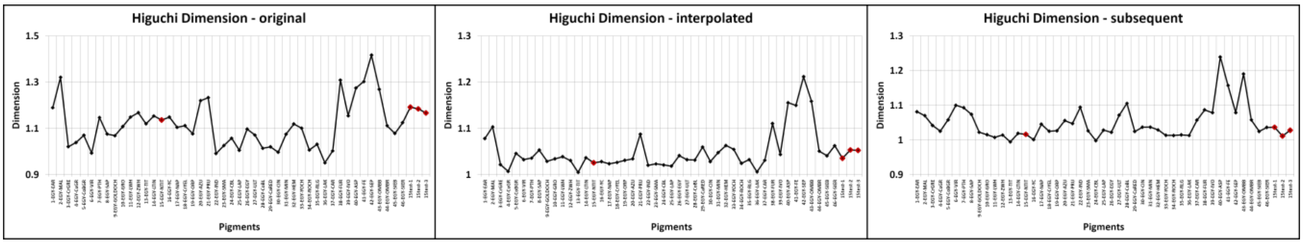

Figure S24: Egyptian Blue Higuchi Dimension without and with interpolation and subsequent boxes.

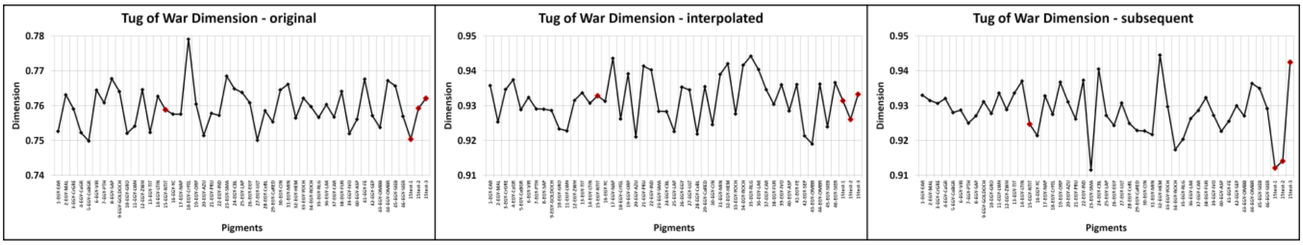

Figure S25: Egyptian Blue Tug of war Dimension without, with interpolation and with subsequent boxes

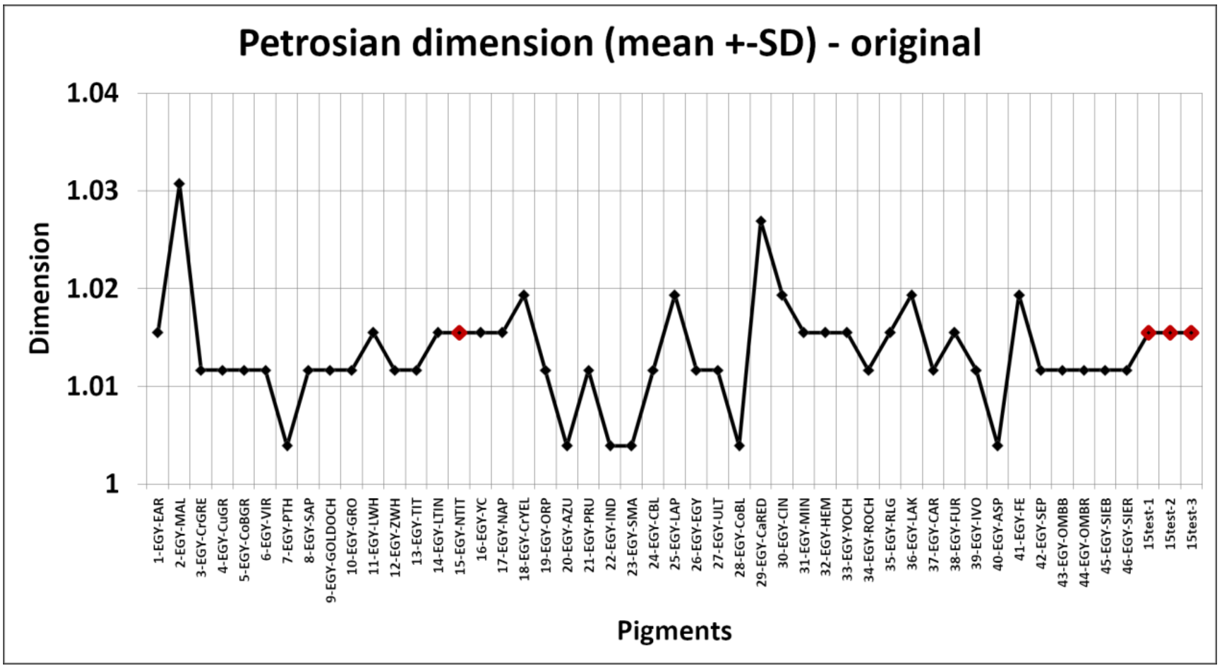

Figure S26: Egyptian Blue Petrosian Dimension without interpolation

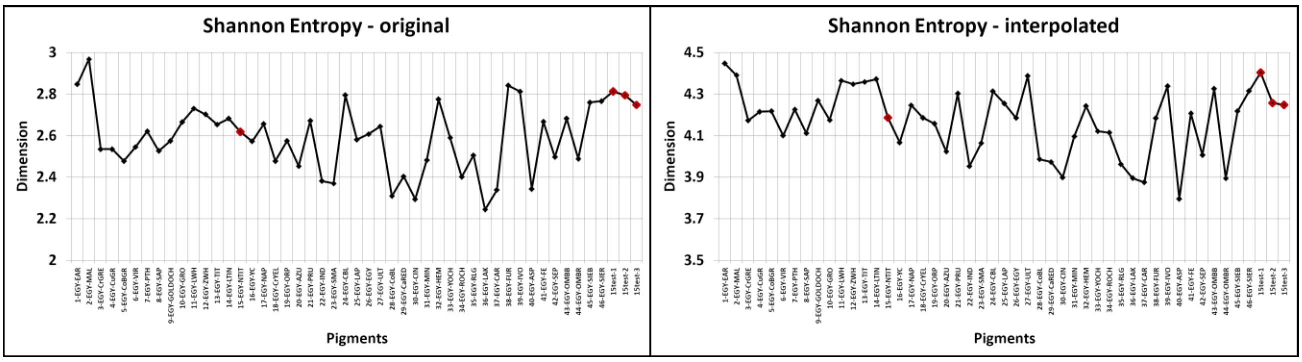

Figure S27: Egyptian Blue Shannon Entropy without and with interpolation

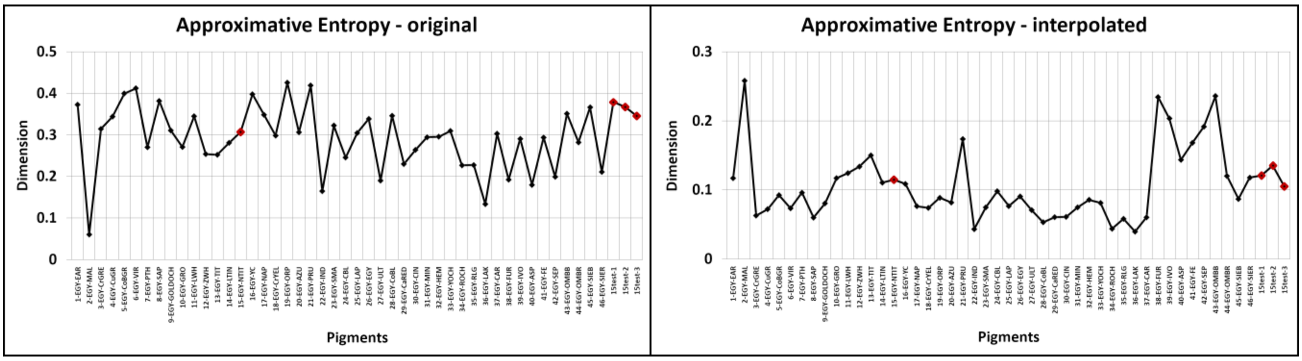

Figure S28: Egyptian Blue Approximative entropy without and with interpolation

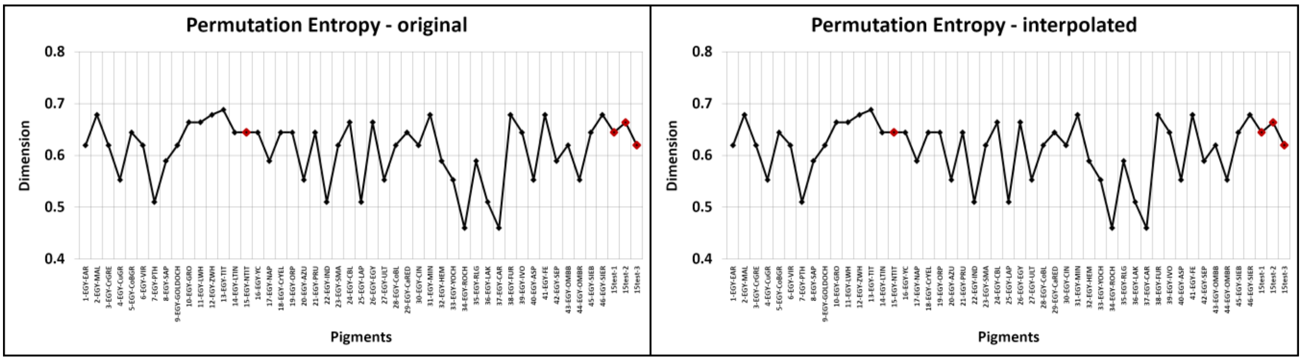

Figure S29: Egyptian Blue Permutation entropy without and with interpolation

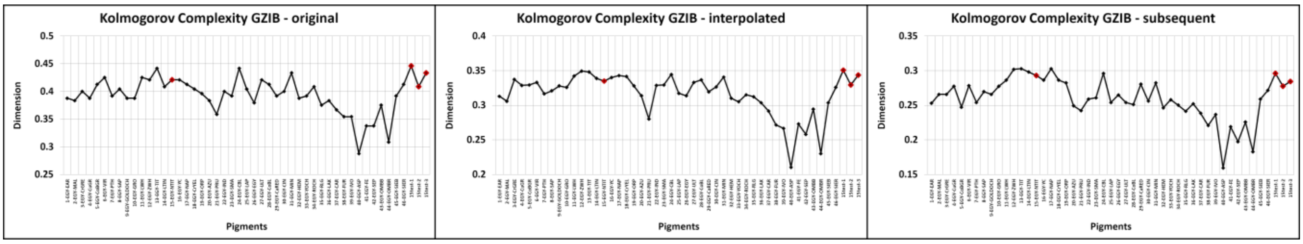

Figure S30: Egyptian Blue Kolmogorov complexity GZIB without, with interpolation and with subsequent boxes

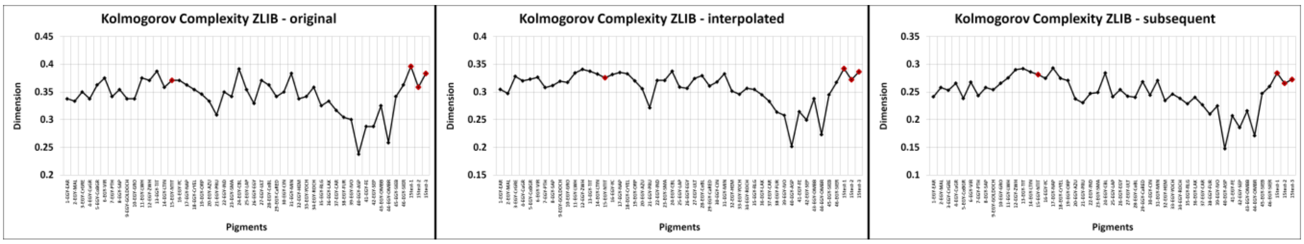

Figure S31: Egyptian Blue Kolmogorov complexity ZLIB without, with interpolation and with subsequent boxes

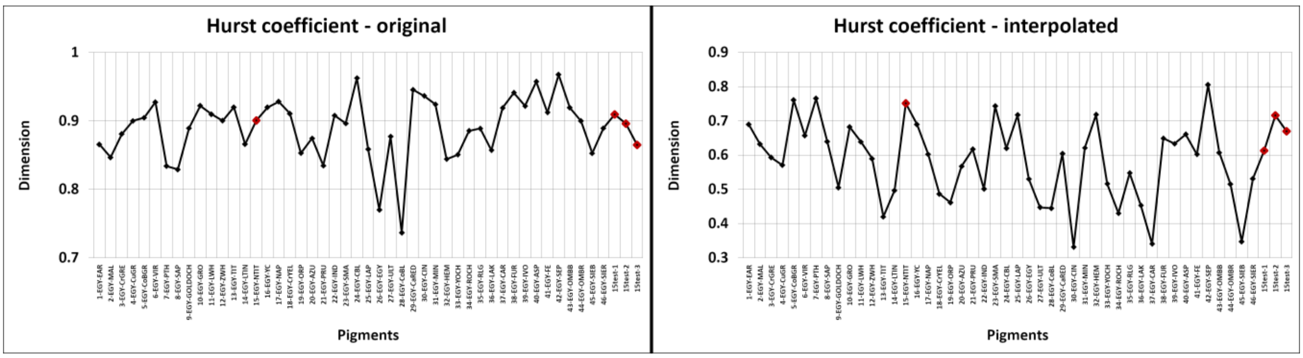

Figure S32: Egyptian Blue Hurst coefficient without and with interpolation.

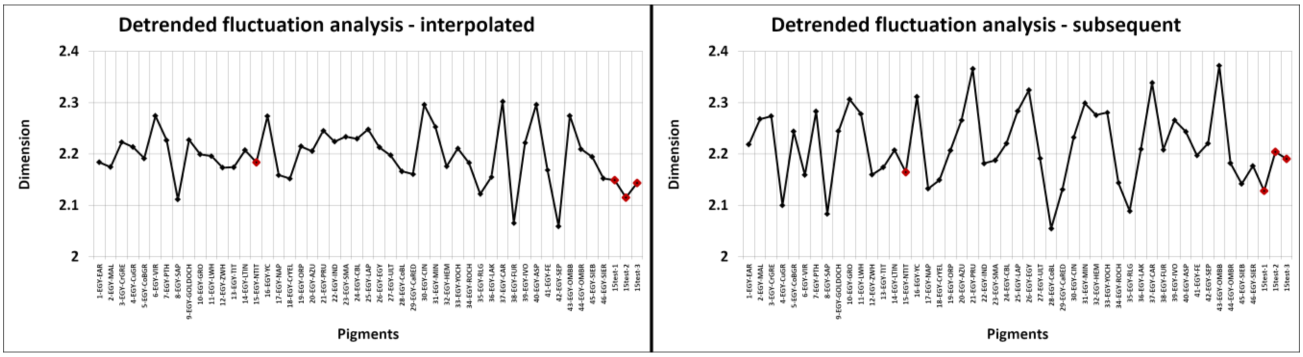

Figure S33: Egyptian Blue Detrended fluctuation analysis without, with interpolation and with subsequent boxes

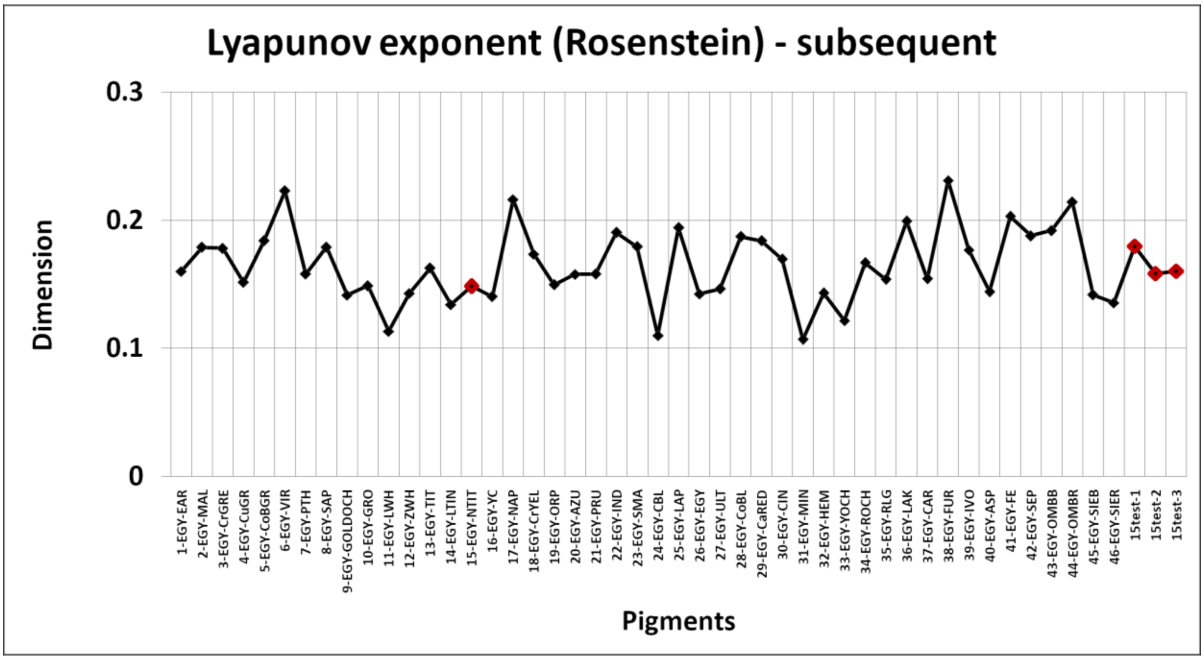

Figure S34: Egyptian Blue Lyapunov exponent with subsequent boxes

2. SET 2: RED Cadmium

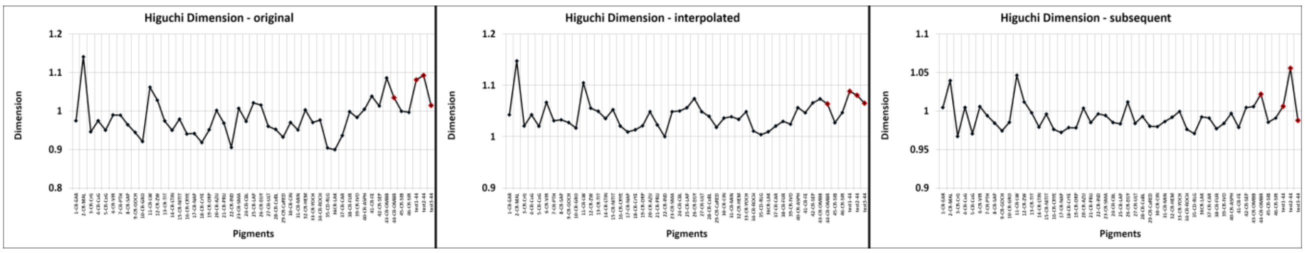

Figure S35: Red cadmium Higuchi dimension without, with interpolation and with subsequent boxes

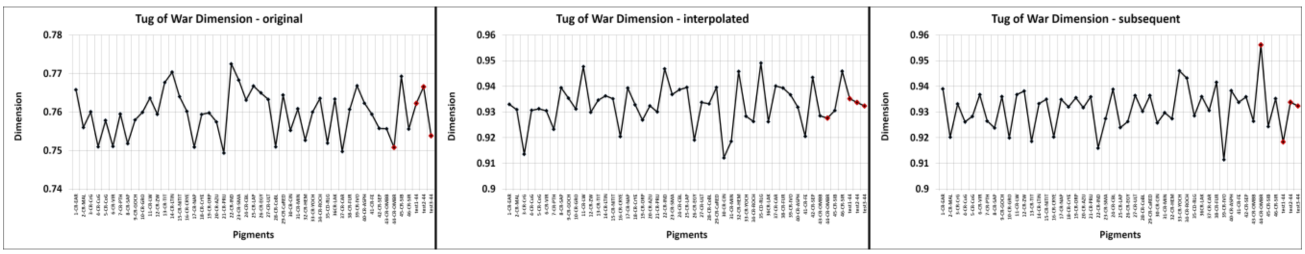

Figure S36: Red cadmium Tug of war dimension without, with interpolation and with subsequent boxes

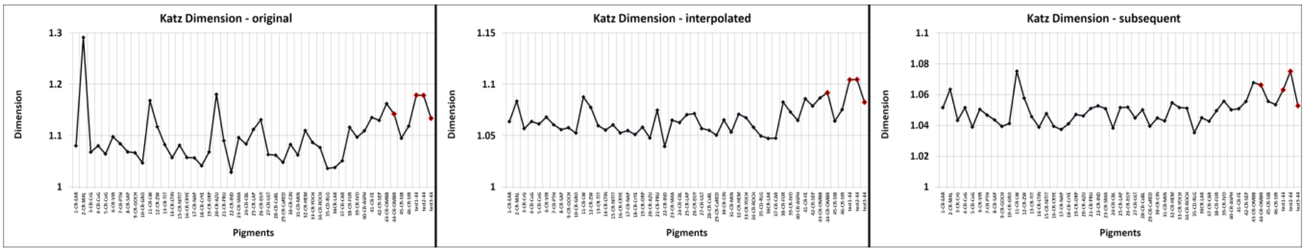

Figure S37: Red cadmium Katz dimension without, with interpolation and with subsequent boxes

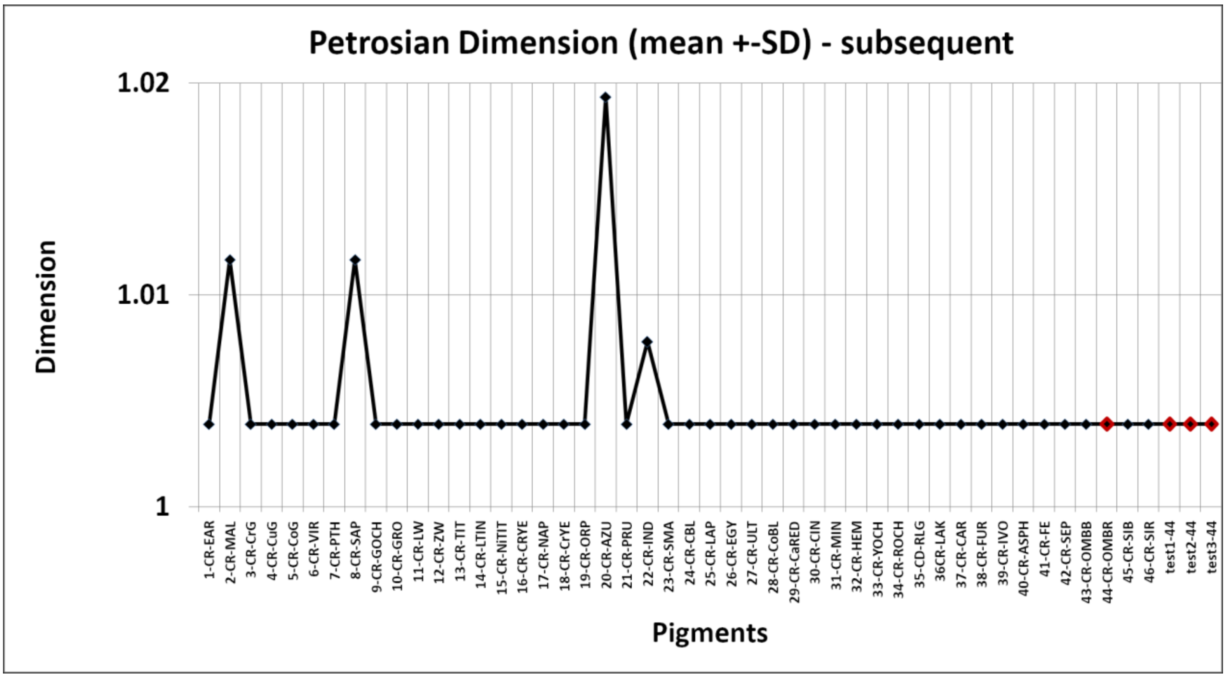

Figure S38: Red cadmium Petrosian dimension without interpolation

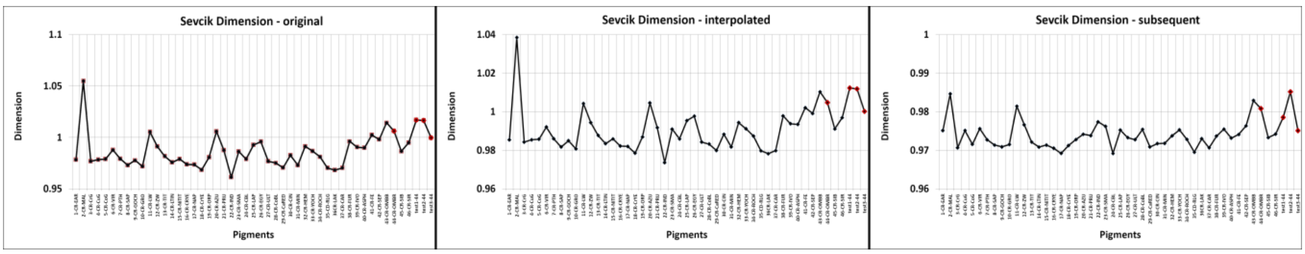

Figure S39: Red cadmium Sevcik dimension without, with interpolation and with subsequent boxes

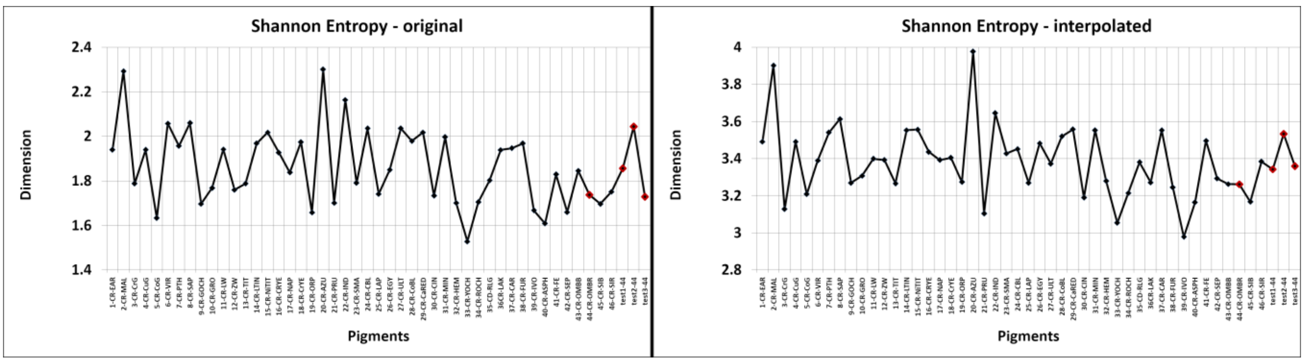

Figure S40: Red cadmium Shannon Entropy without and with interpolation

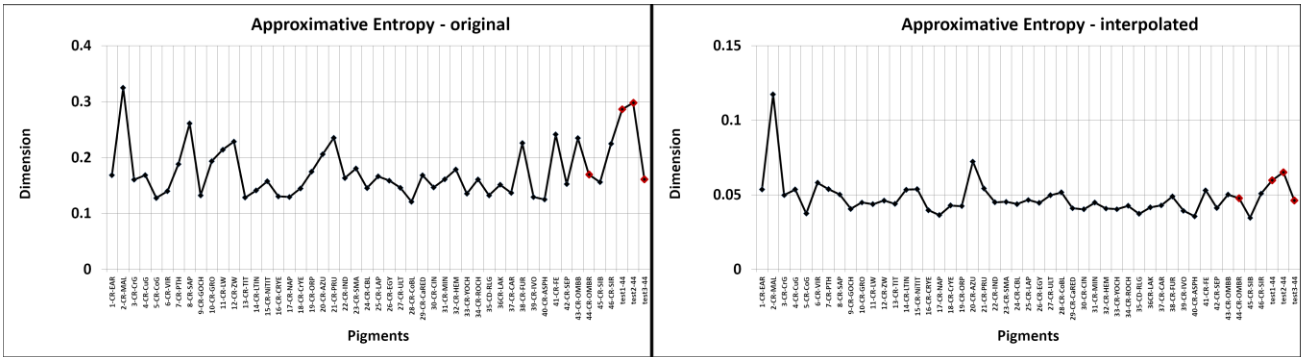

Figure S41: Red cadmium Approximative entropy without and with interpolation.

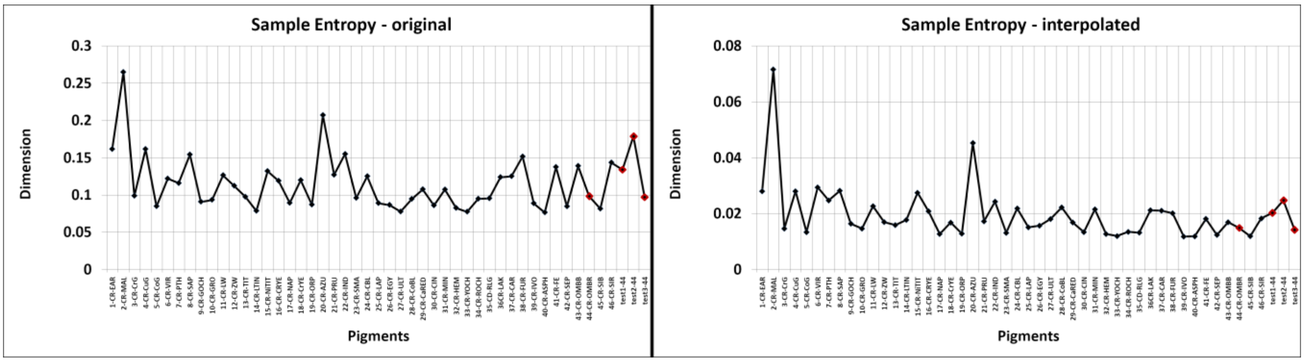

Figure S42: Red cadmium Sample Entropy without and with interpolation

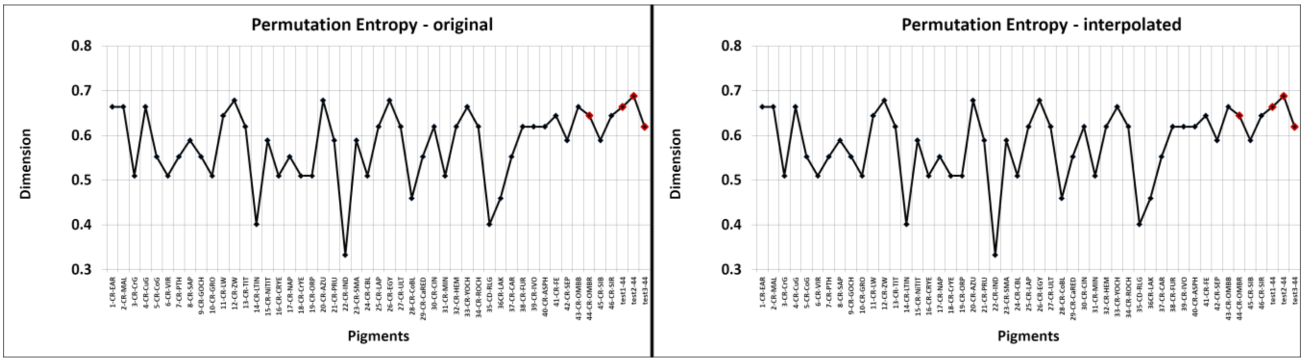

Figure S43: Red cadmium Permutation entropy without and with interpolation

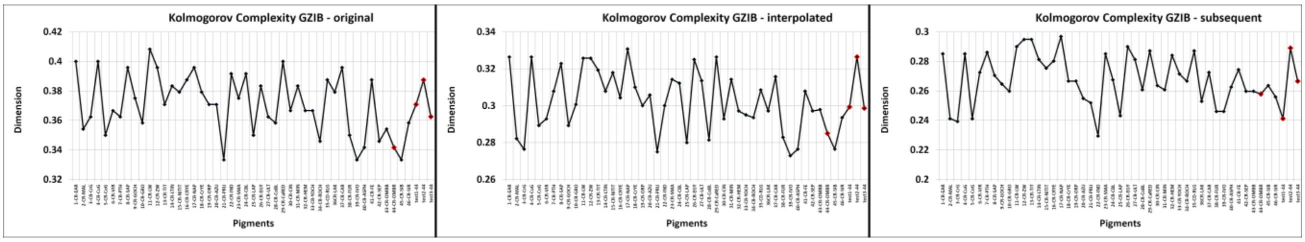

Figure S44: Red cadmium Komogorov complexity - GZIB without, with interpolation and with subsequent boxes

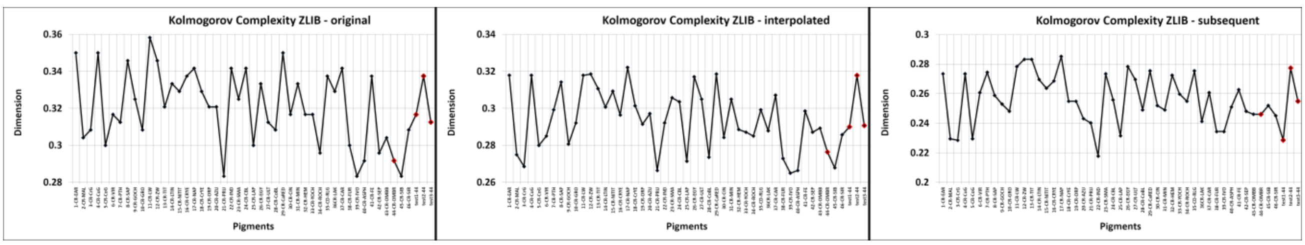

Figure S45: Red cadmium Kolmogorov complexity - ZLIB without, with interpolation and with subsequent boxes

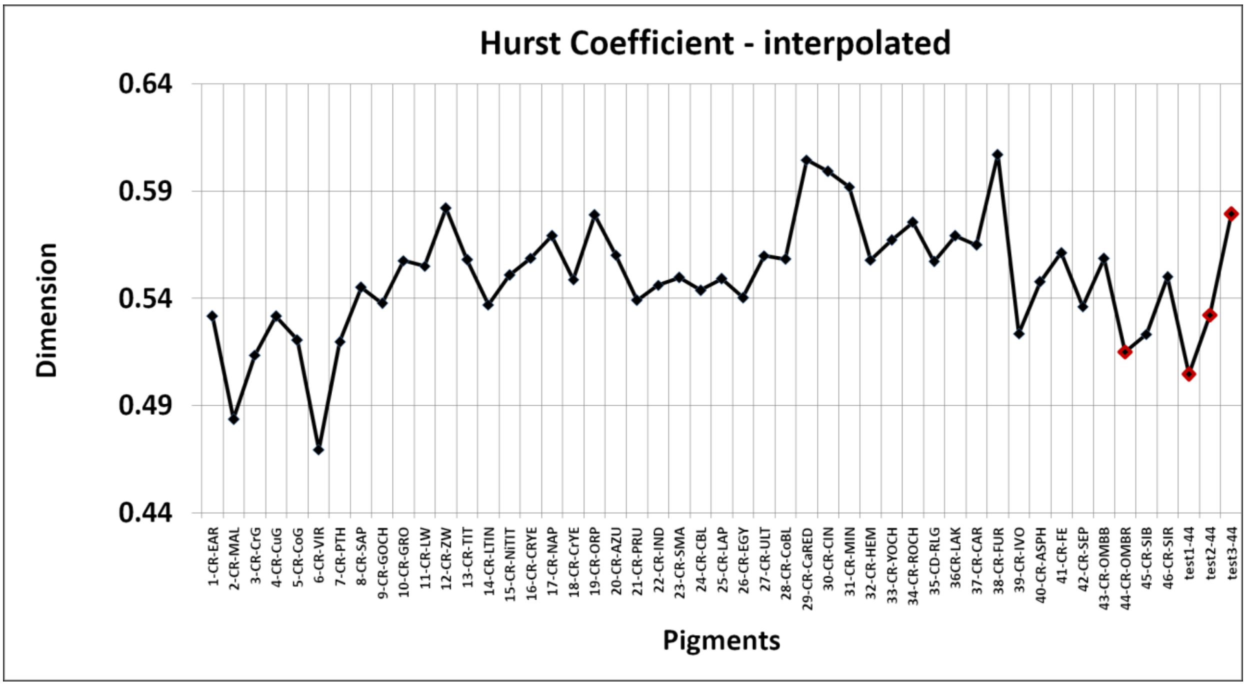

Figure S46: Red Cadmium: Hurst without and with interpolation

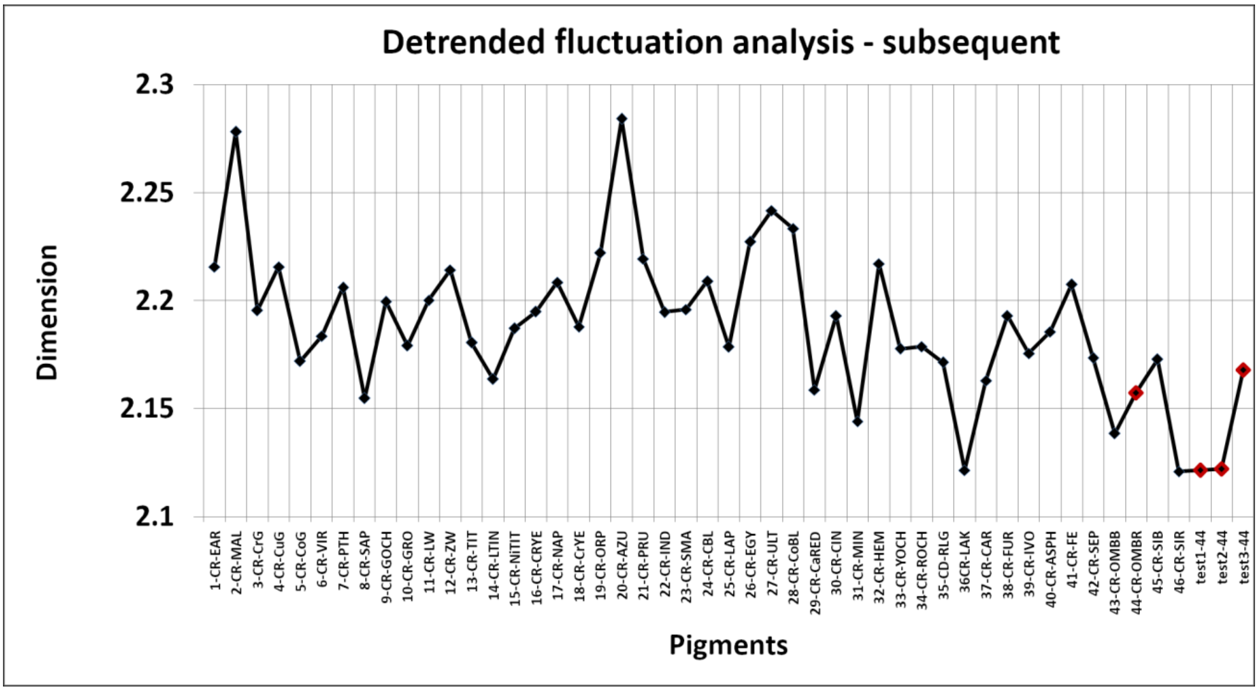

Figure S47: Red cadmium Detrended fluctuation analysis without, with interpolation and with subsequent boxes

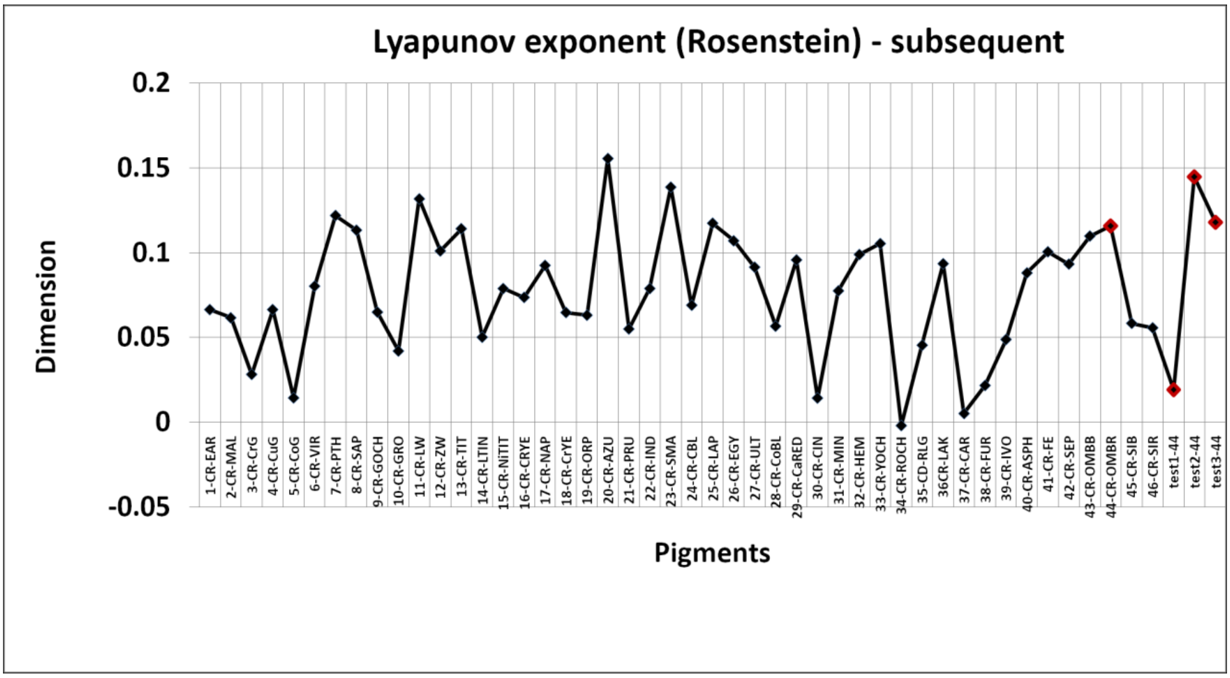

Figure S48: Red cadmium Lyapunov exponent for interpolated and subsequent boxes.

3. SET 3: CADMIUM YELLOW

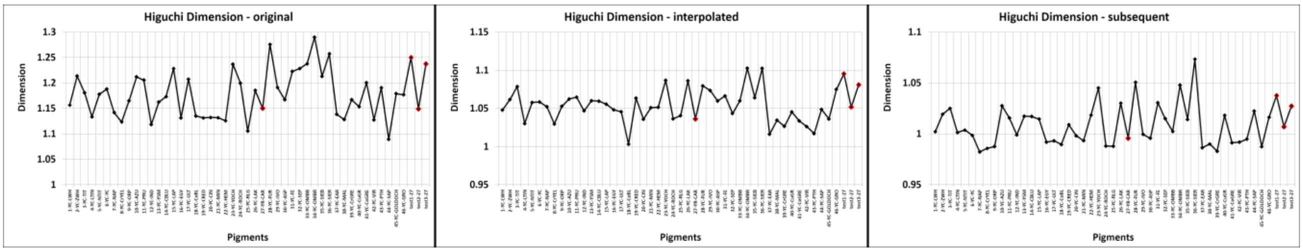

Figure S49: Cadmium Yellow Higuchi dimension without, with interpolation and with subsequent boxes

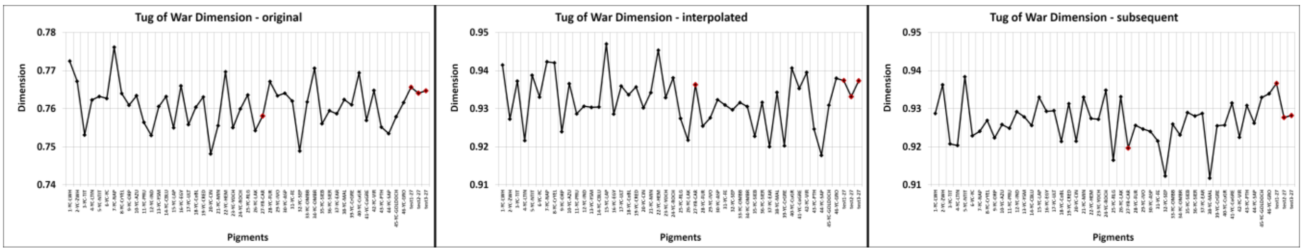

Figure S50: Cadmium Yellow Tug of war dimension without, with interpolation and with subsequent boxes

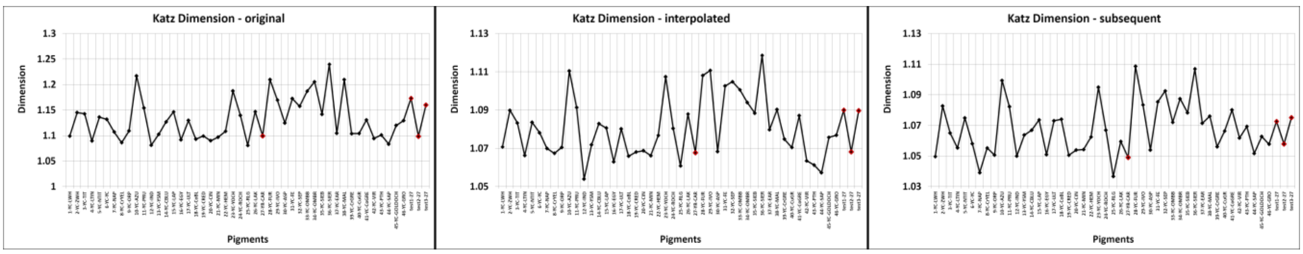

Figure S51: Cadmium Yellow Katz dimension without, with interpolation and with subsequent boxes

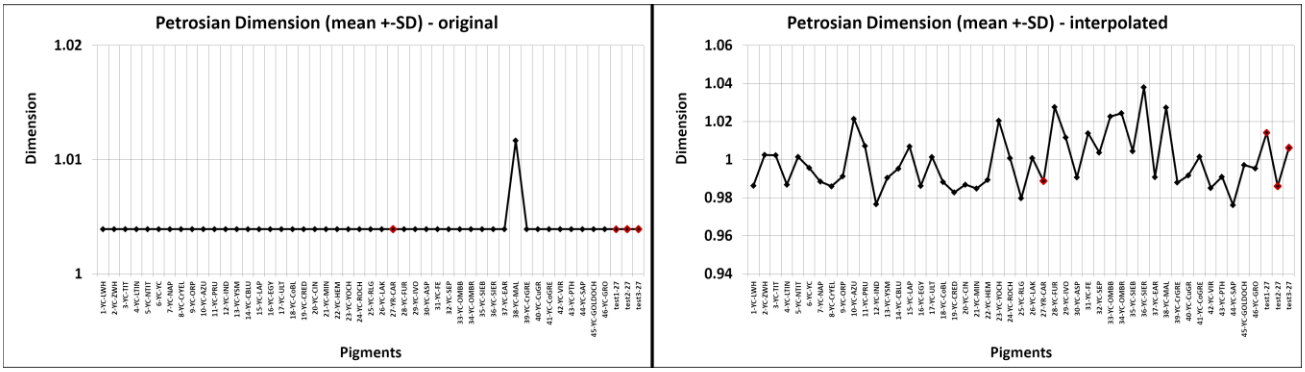

Figure S52: Cadmium Yellow Petrosian dimension without and with interpolation

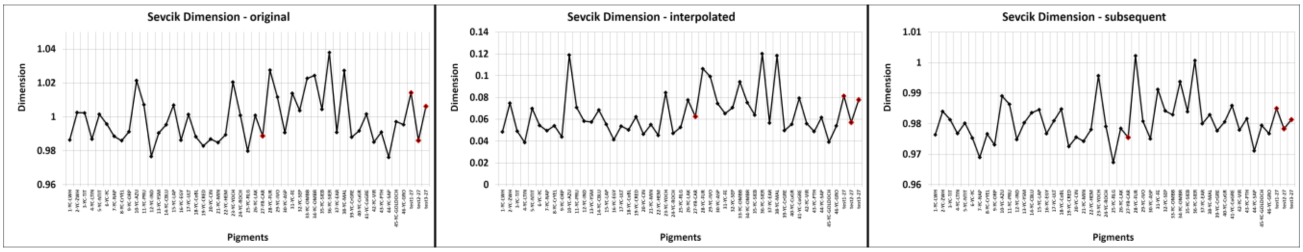

Figure S53: Cadmium Yellow Sevcik dimension without, with interpolation and with subsequent boxes

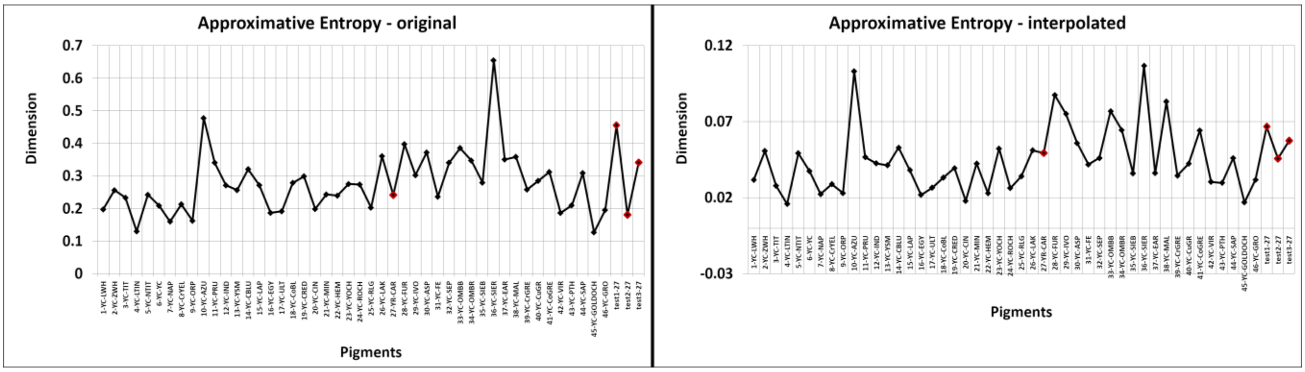

Figure S54: Cadmium Yellow Approximative entropy without and with interpolation

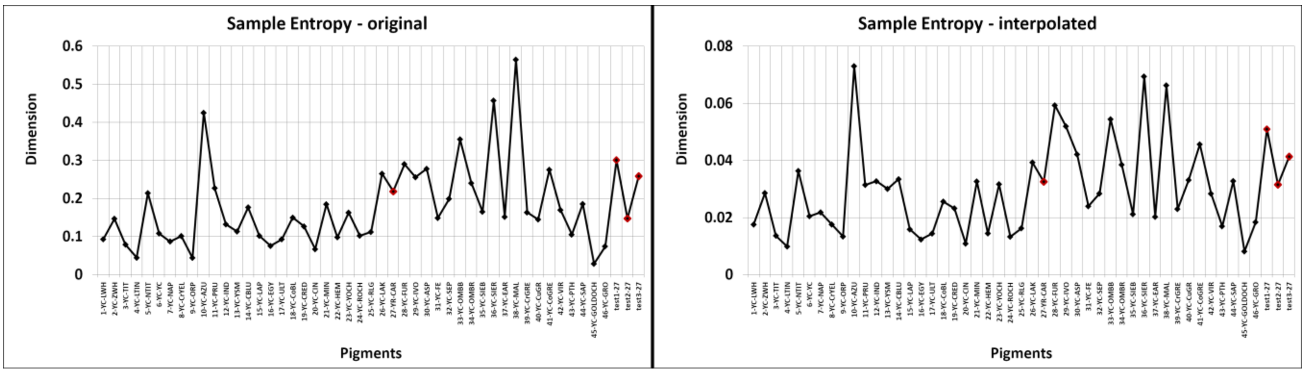

Figure S55: Cadmium Yellow Sample entropy without and with interpolation

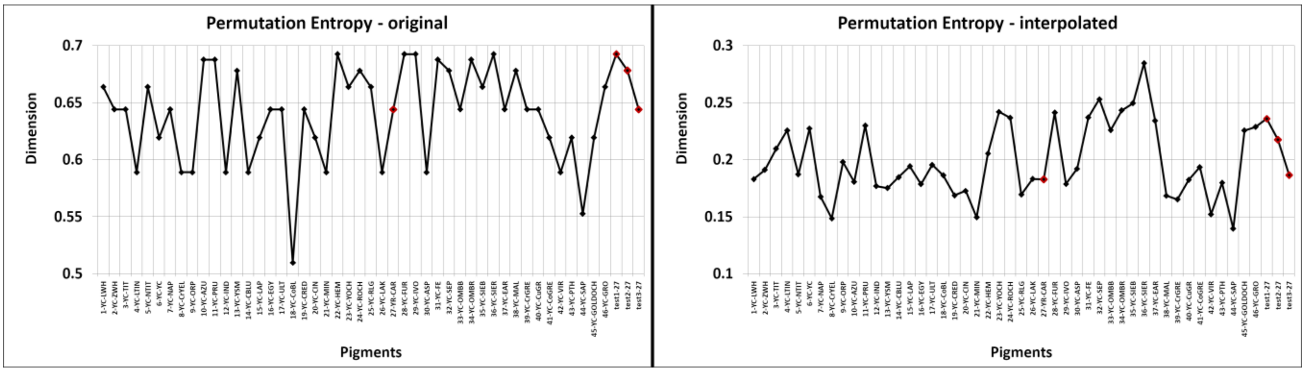

Figure S56: Cadmium Yellow Permutation entropy without and with interpolation

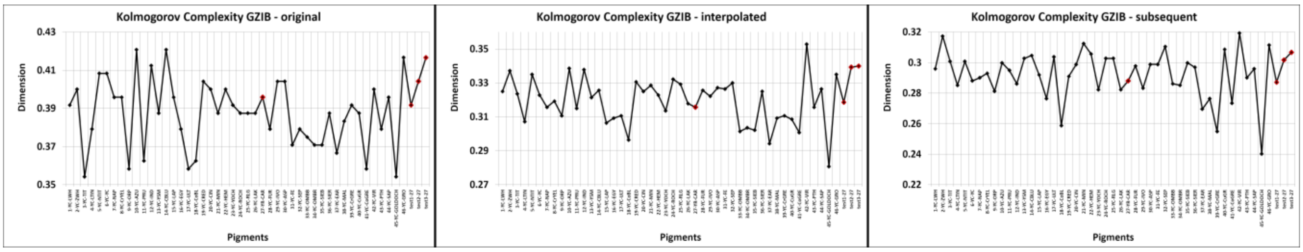

Figure S57: Cadmium Yellow KC GZIB without, with interpolation and with subsequent boxes

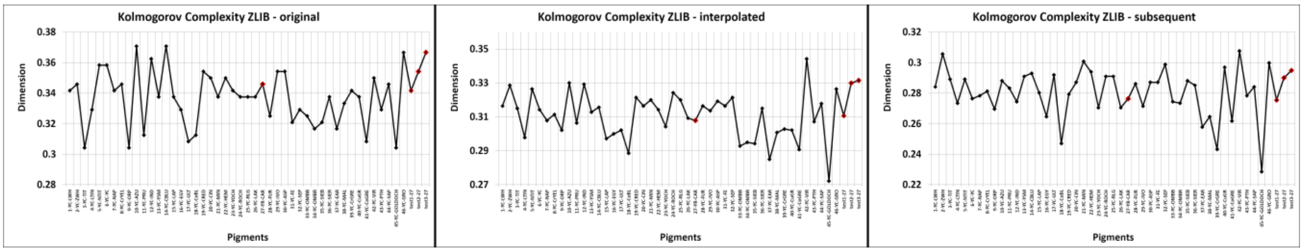

Figure S58: Cadmium Yellow KC ZLIB without, with interpolation and with subsequent boxes

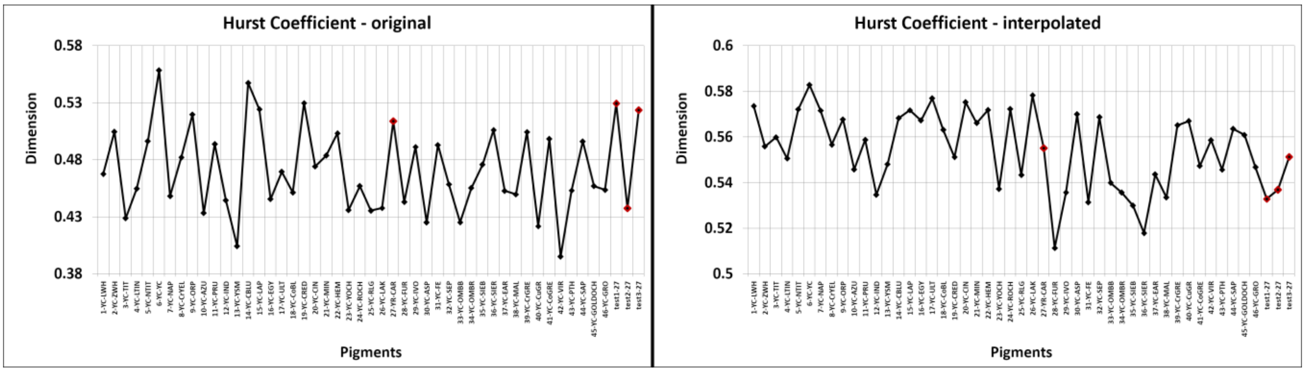

Figure S59: Cadmium Yellow Hurst coefficient without and with interpolation

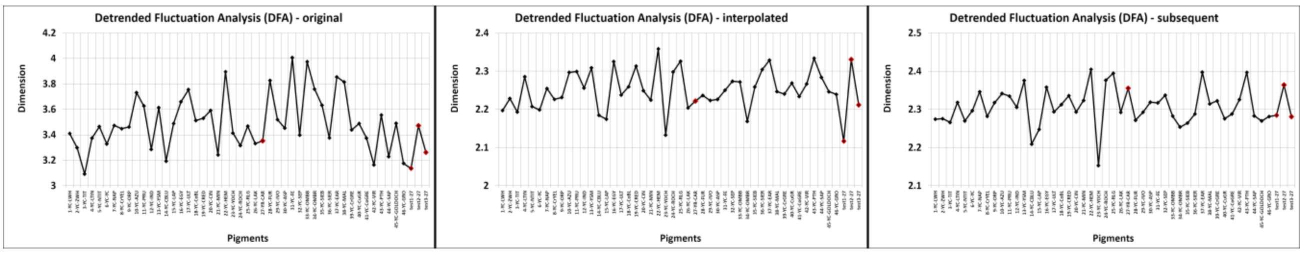

Figure S60: Cadmium Yellow DFA without, with interpolation and with subsequent boxes

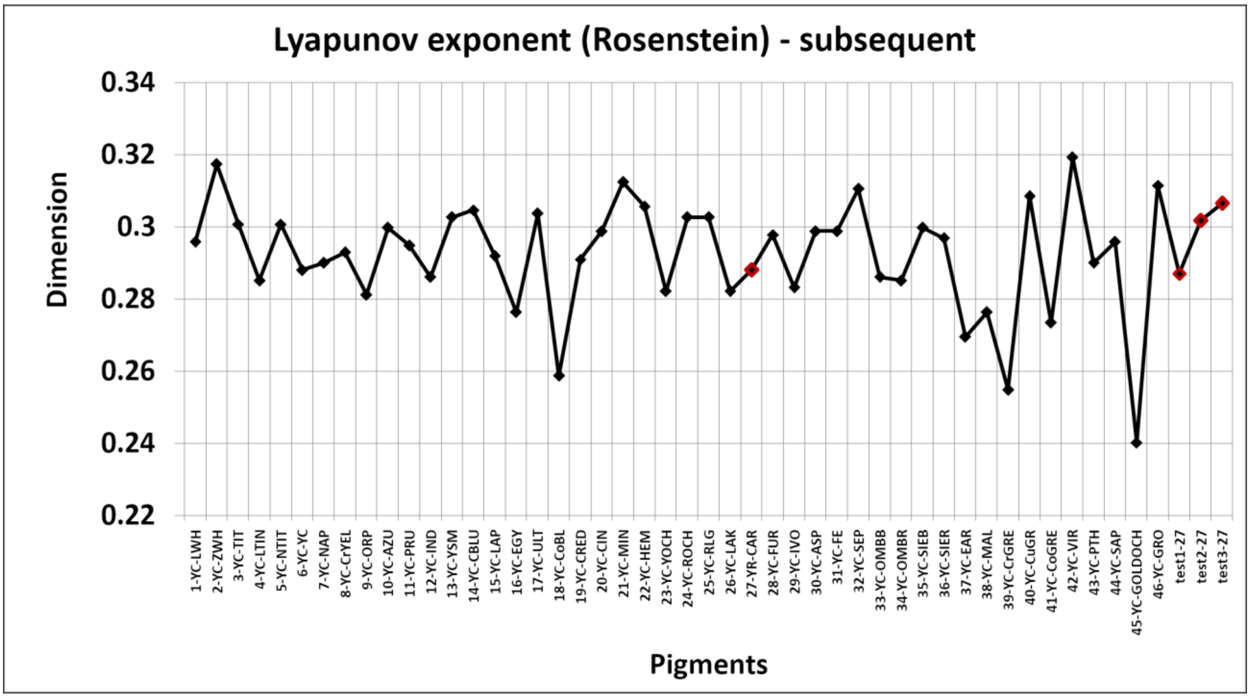

Figure S61: cadmium yellow Lyapunov exponent with interpolation and with subsequent boxes

Example of computing allometric scaling fractal dimension and other complexity measures

For all indices these part are similar:
1. Download Fiji version 20230801-1717 (https://downloads.imagej.net/fiji/archive/20230801-1717/)
2. Download ComsystanJ plugin (https://github.com/comsystan/comsystanj/releases)
3. Unzip the ComsystanJ zip file and copy the folder to the Fiji's plugins folder.
4. Fiji - Plugins - Comsystanj - 1D sequence(s) - Sequence opener
Dataset must to be in cvs format.

Only point 5 will differ. Instead of Allometric scaling, select from the list the desired index (Katz, Petrosian, etc).
Ex:
5. Fiji - Plugins - Comsystanj - 1D sequence(s) - Allometric scaling
or
5. Fiji - Plugins - Comsystanj - 1D sequence(s) - Katz dimension
or
5. Fiji - Plugins - Comsystanj - 1D sequence(s) - Petrosian dimension
etc.

REFERENCES OF SUPPLEMENTARY

Adamson, P. (2006). Vision, light and color in al-kindī, Ptolemy and the ancient commentators. *Arabic Sciences and Philosophy*, Vol. 16/2, 207–236. https://doi.org/10.1017/S0957423906000312

Alexopoulou, A., & Kaminari, A. (2008). Study and documentation of an icon of Saint George by Angelos using infrared reflectography. *Icons by the Hand of Angelos: The Painting Method of a Fifteenth-Century Cretan Painter*, 151–162.

Arroyo, E., Zetina, S., Hernández, E., Falcón, T., Ruvalcaba, J., Mancilla, L., & Nieto, A. (2008). *XVI Century Colonial Panel Paintings from New Spain: Material Reference Standards and Non-Destructive Analysis for Mexican Retablos*. 9th Int. Conference on NDT of Art 2008 Jerusalem, Israel, May 2008. https://www.ndt.net/?id=6068

Balas, C., Epitropou, G., Tsapras, A., & Hadjinicolaou, N. (2018). Hyperspectral imaging and spectral classification for pigment identification and mapping in paintings by El Greco and his workshop. *Multimedia Tools and Applications*, Vol. 77/8, 9737–9751. https://doi.org/10.1007/s11042-017-5564-2

Bandt, C., & Pompe, B. (2002). Permutation Entropy: A Natural Complexity Measure for Time Series. *Physical Review Letters*, Vol. 88/17, 174102. https://doi.org/10.1103/PhysRevLett.88.174102.

Bengin Bilici-Genç, Cem Gök, Evin Caner and Yusuf Özcan (2023) An Archaeometric Investigation on the Pigments Used in the Wall Paintings of Post-Byzantine (XIX. century) Churches in Cappadocia. *Lycus Journal*, June 2023, Issue 7, 41-57, DOI: 10.54577/lycus.1117155

Berns, R. S. (2005). *Rejuvenating the Appearance of Cultural Heritage Using Color and Imaging Science Techniques*. 369–374.

Caley, E. R., & Richards, J. F. (1956). *Theophrastus on stones: Introduction, greek text, english translation, and commentary*. Ohio State University.

Daniilia, S., Minopoulou, E., Demosthenous, Fr. D., & Karagiannis, G. (2008). A comparative study of wall paintings at the Cypriot monastery of Christ Antiphonitis: One artist or two? *Journal of Archaeological Science*, Vol. 35/6, 1695–1707. https://doi.org/10.1016/j.jas.2007.11.011

Dardes, K., & Rothe, A. (1998). *The Structural Conservation of Panel Paintings: Proceedings of a Symposium at the J. Paul Getty Museum, 24-28 April 1995* (K. Dardes & A. Rothe, Eds.). Getty Conservation Institute. http://hdl.handle.net/10020/gci_pubs/panelpaintings

Degano, I., Ribechini, E., Modugno, F., & Colombini, M. P. (2009). Analytical Methods for the Characterization of Organic Dyes in Artworks and in Historical Textiles. *Applied Spectroscopy Reviews*, Vol. 44/5, 363–410. https://doi.org/10.1080/05704920902937876

Eke, A., Hermán, P., Bassingthwaighte, J., Raymond, G., Percival, D., Cannon, M., Balla, I., & Ikrényi, C. (2000). Physiological time series: Distinguishing fractal noises from motions. *Pflügers Archiv*, Vol. 439/4, 403–415. https://doi.org/10.1007/s004249900135

Fairchild, M. D. (2005). *Color appearance models* (2nd ed). J. Wiley.

Gauch, H. G., & Whittaker, R. H. (1981). Hierarchical Classification of Community Data. *The Journal of Ecology*, Vol. 69/2, 537. https://doi.org/10.2307/2259682

Gehad, B., Aly, M. F., & Marey, H. (2015). Identification Of The Byzantine Encaustic Mural Painting In Egypt. *Mediterranean Archaeology and Archaeometry*, Vol. 15/2, 243–256. https://doi.org/10.5281/ZENODO.18057

Healy, J. F. (1999). *Pliny the Elder on science and technology*. Oxford University Press.

Higuchi, T. (1988). Approach to an irregular time series on the basis of the fractal theory. *Physica D: Nonlinear Phenomena*, Vol. 31/2, 277–283. https://doi.org/10.1016/0167-2789(88)90081-4

Iordanidis, A., Garcia-Guinea, J., Strati, A., & Gkimourtzina, A. (2013). Gold Gilding and Pigment Identification on a Post-Byzantine Icon from Kastoria, Northern Greece. *Analytical Letters*, Vol. 46/6, 936–945. https://doi.org/10.1080/00032719.2012.739228

Janssens, K., Van Der Snickt, G., Vanmeert, F., Legrand, S., Nuyts, G., Alfeld, M., Monico, L., Anaf, W., De Nolf, W., Vermeulen, M., Verbeeck, J., & De Wael, K. (2017). Non-Invasive and Non-Destructive Examination of Artistic Pigments, Paints, and Paintings by Means of X-Ray Methods. In R. Mazzeo (Ed.), *Analytical Chemistry for Cultural Heritage* (pp. 77–128). Springer International Publishing. https://doi.org/10.1007/978-3-319-52804-5_3

Karapanagiotis, I., Lampakis D., Konstanta A., Farmakalidis H. (2013). *Identification of Colourants in Icons of the Cretan School of Iconography Using Raman Spectroscopy and Liquid Chromatography,* Journal of Archaeological Science, Vol. 40/3, 1471–1478. https://doi.org/10.1016/j.jas.2012.11.004.

Karapanagiotis, I., Valianou, L. Sister Daniilia, Chryssoulakis, Y. (2007). *Organic Dyes in Byzantine and Post-Byzantine Icons from Chalkidiki (Greece),* Journal of Cultural Heritage, Vol. 8/3, 294–298. https://doi.org/10.1016/j.culher.2007.04.003.

Karydis, Ch., Kyriazi, E., Redina, M.-O., Panagopoulou, A., & Kousouni, C.-K. (2019). Identification of fibres from byzantine and post-byzantine icons of the museum of Byzantine Culture in Thessaloniki: Use of OM, SEM and SPSS analysis. *Mediterranean Archaeology and Archaeometry*, Vol. 19/2, 105–117. https://doi.org/10.5281/ZENODO.3066017

Katsaros, T., Liritzis, I., & Laskaris, N. (2010). Identification of Theophrastus' pigments egyptios yanos and psimythion from archaeological excavations: A case study. *ArchéoSciences*, Vol. 34, 69–80. https://doi.org/10.4000/archeosciences.2632

Katsaros, Th., Liritzis, I., & Laskaris, N. (2009). Is White Pigmnet On Appeles Palette A TiO2 Rich Kaolin? New Analytical Results On The Case of Melian—Earth. *Mediterranean Archaeology and Archaeometry*, Vol. 9/1, 29–35.

Katz, M.J. (1988). Fractals and the analysis of waveforms. *Computers in Biology and Medicine*, Vol. 18/3, 145–156. https://doi.org/10.1016/0010-4825(88)90041-8

Khasawneh, S. A., & Elserogy, A. (2019). Conservation and restoration of church icon from baptism museum, Jordan: Case study. *Mediterranean Archaeology and Archaeometry*, Vol. 19/1, 85–91. https://doi.org/10.5281/ZENODO.2585977

Lazidou, D., Lampakis, D., Karapanagiotis, I., Panayiotou, C. (2018). *Investigation of the Cross Section Stratifications of Icons Using Micro-Raman and Micro-FTIR Spectroscopy*. Applied Spectroscopy, Vol. 72, 1258. https://doi.org/10.1177/000370281877777

Legnaioli, S., Grifoni, E., Lorenzetti, G., Marras, L., Pardini, L., Palleschi, V., Salerno, E., & Tonazzini, A. (2013). Enhancement of hidden patterns in paintings using statistical analysis. *Science and Technology for the Safeguard of Cultural Heritage in the Mediterranean Basin*, Vol. 14/3 Supplement, S66–S70. https://doi.org/10.1016/j.culher.2012.11.013

Legnaioli, S., Lorenzetti, G., Cavalcanti, G. H., Grifoni, E., Marras, L., Tonazzini, A., Salerno, E., Pallecchi, P., Giachi, G., & Palleschi, V. (2013). Recovery of archaeological wall paintings using novel multispectral imaging approaches. *Heritage Science*, Vol. 1/1, 33. https://doi.org/10.1186/2050-7445-1-33

Loeb, J., & Henderson, J. (1970, January 1). *Aristotle, "On Colours."* Loeb Classical Library. https://www.loebclassics.com/view/aristotle-colours/1936/pb_LCL307.5.xml

Mastrotheodoros, G.P., & Beltsios, K.G. (2022). Recipes for pigment manufacturing in greek post-byzantine painting manuals. *Scientific Culture*, Vol. 8/1, 147–159. https://doi.org/10.5281/ZENODO.5772478

Mastrotheodoros, G.P., Asvestas. A., Gerodimos, T. and Anagnostopoulos, D.F. (2023) *Revealing the Materials, Painting Techniques, and State of Preservation of a Heavily Altered Early 19th Century Greek Icon through MA-XRF*. Heritage, 903–1920. https://doi.org/10.3390/heritage6020102

Papageorgiou, I. (2020). Ceramic investigation: How to perform statistical analyses. *Archaeological and Anthropological Sciences*, Vol. 12/9, 210. https://doi.org/10.1007/s12520-020-01142-x

Peng, C.-K., Buldyrev, S. V., Havlin, S., Simons, M., Stanley, H. E., & Goldberger, A. L. (1994). Mosaic organization of DNA nucleotides. *Physical Review E*, Vol. 49/2, 1685–1689. https://doi.org/10.1103/PhysRevE.49.1685

Petrosian, A. (1995). Kolmogorov complexity of finite sequences and recognition of different preictal EEG patterns. *Proceedings Eighth IEEE Symposium on Computer-Based Medical Systems*, 212–217. https://doi.org/10.1109/CBMS.1995.465426

Richman, J. S., & Moorman, J. R. (2000). Physiological time-series analysis using approximate entropy and sample entropy. *American Journal of Physiology-Heart and Circulatory Physiology*, Vol. 278/6, H2039–H2049. https://doi.org/10.1152/ajpheart.2000.278.6.H2039

Rosenstein, M. T., Collins, J. J., & De Luca, C. J. (1993). A practical method for calculating largest Lyapunov exponents from small data sets. *Physica D: Nonlinear Phenomena*, Vol. 65/1, 117–134. https://doi.org/10.1016/0167-2789(93)90009-P

Saunders, D., Billinge, R., Cupitt, J., Atkinson, N., & Liang, H. (2006). A New Camera for High-Resolution Infrared Imaging of Works of Art. *Studies in Conservation*, Vol. 51/4, 277–290. https://doi.org/10.1179/sic.2006.51.4.277

Sevcik, C. (2010). A procedure to Estimate the Fractal Dimension of Waveforms. *Complexity International*, Vol. 5, 1–10. https://doi.org/10.48550/ARXIV.1003.5266

Shannon, C. E. (1948). A Mathematical Theory of Communication. *Bell System Technical Journal*, Vol. 27/3, 379–423. https://doi.org/10.1002/j.1538-7305.1948.tb01338.x

Sotiropoulou, S., Sister Daniilia (2010). *Material Aspects of Icons. A Review on Physicochemical Studies of Greek Icons,* Acc. Chem. Res. Vol. 43/6, 877–887. https://doi.org/10.1021/ar1000082.

Taylor, J. (1979). *Icon painting*. Phaidon Press.

Theodoropoulou, O., & Tsairis, G. (2000). Non-Destructive Analysis of Two Post-Byzantine Icons by Use of the Multi Spectral Imaging System (MU.S.I.S 2007). In C. Fotakis, T. G. Papazoglou, & C. Kalpouzos (Eds.), *Optics and Lasers in Biomedicine and Culture* (pp. 218–222). Springer Berlin Heidelberg. https://doi.org/10.1007/978-3-642-56965-4_43

Valianou, L., Wei, S., Mubarak, M. S., Farmakalidis, H., Rosenberg, E., Stassinopoulos, S., & Karapanagiotis, I. (2011). Identification of organic materials in icons of the Cretan School of iconography. *Journal of Archaeological Science*, Vol. 38/2, 246–254. https://doi.org/10.1016/j.jas.2010.08.025

Walmsley, E., Metzger, C., Delaney, J. K., & Fletcher, C. (1994). Improved visualization of underdrawings with solid-state detectors operating in the infrared. *Studies in Conservation*, Vol. 39/4, 217–231. https://doi.org/10.1179/sic.1994.39.4.217

West, G. B., Brown, J. H., & Enquist, B. J. (1999). A general model for the structure and allometry of plant vascular systems. *Nature*, Vol. 400/6745, 664–667. https://doi.org/10.1038/23251

Wong, A., Wu, L., Gibbons, P. B., & Faloutsos, C. (2005). Fast estimation of fractal dimension and correlation integral on stream data. *Information Processing Letters*, Vol. 93/2, 91–97. https://doi.org/10.1016/j.ipl.2004.09.018

Yu-Ichi, O. (1980). A Region-Oriented Image-Analysis System by Computer. *PhD Dissertation, Department of Information Science, Kyoto University, Japan*.

Zenil, H. (2020). A Review of Methods for Estimating Algorithmic Complexity: Options, Challenges, and New Directions. *Entropy*, Vol. 22/6, 612. https://doi.org/10.3390/e22060612